V. Stefanovici

REMOVE BEFORE FLIGHT

Navigation through terrain recognition for on-boardradar systems

TU Delft

Navigation through terrain recognition for on-board radar systems

by

Vlad Stefanovici

to obtain the degree of Master of Science
at the Delft University of Technology,
to be defended publicly on Friday December 13, 2019 at 09:30 AM.

Student number: 4423682
Project duration: November 1, 2018 – December 13, 2019
Thesis committee: Prof. Dr. Ir. J. Hoekstra,   TU Delft, Supervisor
                    Ir. J. Maas Brown,   TU Delft, Daily supervisor
                    Ir. R. van Gent,   TU Delft, Daily supervisor
                    Prof. Dr. Ir. A. Gangoli Rao,   TU Delft, Examiner

This thesis is confidential and cannot be made public until December 31, 2020.

An electronic version of this thesis is available at `http://repository.tudelft.nl/`.

TUDelft

Preface

Through finishing this report, I finish my master thesis as well as my time as a student at TU Delft. During this time, I better developed my knowledge, defined my interests and refined my scope as a professional. I humbly look back and welcome this finish like a rewarding end.

This thesis would not have been possible without the help of my supervisors, Dr.Ing. Jacco Hoekstra, Ir. Jerom Mass and Ir. Ronald Gent whom I would like to acknowledge their invaluable guidance and patience throughout the thesis. Furthermore, I would like to offer my appreciation to Ir. Jerom Maas for sharing his experience with me to conduct my research and to Ir. Ronald van Gent for offering a peek within the industry, along with the necessary feedback and help to get me closer towards becoming a professional.

Finally, I would like to express my gratitude to my parents and their inexhaustible support, my girlfriend who pushed me forward and stood by my side to make sure I succeed every step of the way, as well as my friends whom made sure I had fun learning.

Vlad Stefanovici
Delft, December 2019

List of Abbreviations

ACAS Airborne Collision Avoidance Systems

ANSP Air Navigation Service Providers

CAE-TVL Convolutional Autoencode with Total Variation Loss

CAR Collision Avoidance Radar

CGAN Conditional Generative Adversarial Nets

CNN Convolutionl Neural Networks

CRF Conditional Random Fields

DAE Direction of Arrival Estimation

DL Deep Learning

DOG Difference of Gaussian

DOG Determinant of Hessian

ED Entropy Detection

ESA European Space Agency

FCNN Fully Convoluted Neural Networks

FMCW Frequency Modulated Continuous Waves

GA General Aviation

GC Gamma Correction

GPS Global Positioning Systems

IMC Instrument Meteorological Conditions

INS Inertial Navigation Systems

LoG Laplacian of the Gaussian

Me-F Mean Filter

MIMO Multi Input Multi Output

ML Machine Learning

MSE Mean Square Error

NDB Non-Directional Beacons

PSNR Peak Signal to Noise Ratio

RD Ridge Detection

SAR Synthetic Aperture Radars

SLAR Side Looking Airborne Radar

SLHT Straight Line Hough Transform

SSIM Structural Similarity Index Measure

SNAP Sentinel Application Platform

VFR Visual Flight Rules

VOR VHF Omnidirectional Range

List of Figures

List of Tables

Contents

1

Report outline

The outline of this report will be broken down into three parts. First, the research paper will be introduced. Within this paper the main points of research are presented along with the results. Most concepts are considered known by the reader, giving importance to setting up the experiment along with all contributing factors and parameters. The methodology is presented with only the most important aspects needed to understand the experiment setup. The used algorithms are also shortly presented and results will focus mostly on the top two performing algorithms. An in-depth discussion is delivered with regards to the performance of all algorithms.

Following, the preliminary report will be included to provide additional steps that preceded the creation of the research paper as well as presenting additional information about the chosen algorithms. The preliminary report is a support document to the research paper that starts by presenting radar theory that is necessary to understand how the databases used in the experiment are recorded and applied. This is followed by the identification of limitations of participating databases with a focus on the air-born radar database. After the discussion of how the radar map is obtained, the methodology is introduced with a complete view that includes the hypothesis and the metric chosen to compare two different image candidates. Following, every candidate is introduced in more detail in order to understand exactly the advantages and limitations for each and why a two tier system for image transformation was chosen. The experiment setup is reiterated with additional information, and results are presented with additional figures that completely visualizes the whole process of conducting the two part experiment. Finally, the conclusion provides an overview over all items presented along with a discussion over the results.

The last chapter includes the appendices with additional information relating to the research paper especially with regards to statistical results. This includes information that covers all results and shows the complete process, with a focus on the image database as well as results for all other experiments.

2
Research paper

Navigation through terrain recognition for on-board radar systems

Vlad Stefanovici, Ir. Jerom Maas and Prof.dr.ir. Jacco Hoekstra

TU Delft Faculty of Aerospace Engineering

Abstract— **Radar technique advancements have made it possible to equip lightweight aircraft with radar systems. These systems can help determine the relative position of the world around the aircraft. Performing calculations on the incoming radar signals, it is possible to determine the locations of the ground elements in the aircraft body of reference, which can be done using Direction of Arrival Estimation (DAE) in a lateral setting, as a Side Looking Airborne Radar (SLAR). Using traditional computing techniques for image processing as well as two pre-trained image segmentation machine learning algorithms, it is possible to identify the aforementioned structural elements onto a satellite image to determine the actual position of the aircraft. As a consequence, navigation may be possible alongside Global Positioning Systems (GPS) methods, through obtaining the coordinates of the aircraft based on radar images. Experiment results show that a high accuracy identification rate is possible, based on large features, such as highways, within the radar image.**

I. INTRODUCTION

Current developments on radar techniques have made it possible to create lightweight radar systems that can be carried on board of an aircraft and are now becoming available to General Aviation (GA). When such a system is carried on board, it may be used for in-flight surveillance of neighbouring aircraft and the environment. A radar installation can alert the pilot if proximity with other participants or terrain poses a hazard to the safety of the aircraft. Additionally, radar installations are especially useful for VFR flights that might enter Instrument Meteorologic Conditions (IMC), as their sensing capabilities are not completely infringed by adverse weather[1].

In the near future, Frequency Modulated Continuous Waves (FMCW) radars for on-board aircraft will be small, lightweight and could be mounted almost anywhere on the aircraft. This makes them an ideal test case to obtain radar imagery that may be used to determine the aircrafts position. The current proposal has the aim to assess whether within the data provided by the on-board radar, a set of information can be derived, which leads to a strategy that analyses and deduces coordinate information of the aircraft. This will allow the aircraft to obtain location information alongside GPS, acting as a self-contained system.

A consequence for on-board radar systems is that they may also be used to provide assistance in navigation and attitude determination. Clear reflections of the ground can be observed from radar images taken mid-flight, in which structural reflections are distinguishable. These reflections originate from ground elements, such as rivers, highways, lakes, forests etc. It would be possible to determine the locations of these ground structural elements by using Direction

of Arrival Estimation (DAE), algorithm which makes use of the propagating wave arriving at a certain point [1]. This provides the basis for creating a new radar map, a translation from the radar distance and Doppler velocity reflections to their positions on a 2D plane depicting the distance from the antenna. Within this radar map, certain features become apparent. These features either present geometrical or intensity consistency and together can be used as a unique template. The task of image processing algorithms is to segment the image in a robust way to ensure the same template identification in both the radar and satellite databases. Due to radar noise, as well as the absence of a ground reference, the use of additional information from GPS and flight parameters becomes of paramount importance.

Furthermore, the process needs to be conducted in a timely manner and with the advances in machine learning and computer vision, more specifically with the almost complete dominance of systems built on top of Convolutional Neural Networks, deep learning will also be considered. However, due to the lack of a solid database upon which a deep learning algorithms can be trained, only pre-trained algorithms will be treated. These algorithms will mainly focus on image segmentation within Synthetic Aperture Radar (SAR) imagery, in order to offer a suitable comparison for future research.

II. RADAR PRINCIPLES AND TECHNOLOGY

A radar system can determine the relative position of the world around the aircraft, and this information can be used to find the actual aircraft state information. The main working principle is the emission of electromagnetic energy and the analysis of the reflected energy by the environment, or echo of a reflecting object. The echo can be used to determine the direction and distance and based on the radar frequency, the Doppler speed. Based on the type of technology, radars can be categorized into multiple sets. A focus will be given to Frequency Modulated Continous Wave (FMCW) radars, Side Looking Airborne Radars (SLAR), as well as databases based on Synthetic Aperture Radars (SAR). This is due to the radar database being recorded in FMCW radar in SLAR conditions. Most databases that encode geographical information are captured using SAR technology and that will be used for comparison purposes.

A. Frequency Modulated Continous Wave Radar

Frequency Modulated Continous Wave (FMCW) radars have arguably become compact and low cost. Due to their relatively low power consumption and continuous operation

transmitting modest power, they have become of interest to GA. The FMCW radar emits constant transmitted waves, with the possibility of modulating the operating frequency during the measurement in frequency or phase. This allows for the necessary timing to accurately transmit and receive increasing or decreasing frequency cycles and convert them into range. Maintaining the frequency linear over a wide range allows for range determination through frequency comparisons, making the frequency difference Δf proportional to the slant distance R from the antenna. Furthermore, without Doppler effects, the absolute magnitude of Δf becomes linearly dependent on the decreasing frequency [2].

Should the reflecting object also have radial speed with regards to the receiving antenna, a Doppler frequency Δ_f that is added or subtracted from the received echo frequency, depending on the type of movement the object has in relation to the antenna. Furthermore, for a FMCW radar to be used as a imaging radar, two problems emerge. Namely, the ambiguity and a stationary assumption problems. The first one is with regards to placement on the airborne platform.

Unlike optical systems that look forward, radars need to take into account the geometry of acquisition in order to properly interpret radar data[2]. Two returns at an equal distance from the aircraft arrive at the antenna simultaneously. This leads to the ambiguity problem in right/left symmetry, that forces the radar position to one side of the platform, to detect all points in the environment at different times and be able to distinguish all points from each other. As it can be seen in Fig. 1, all detected points within the Doppler cone will have a different angle, effectively solving this ambiguity. The aforementioned restriction effectively transforms the radar intro a Side Looking Aperture Radar (SLAR)[3].

The second problem worth discussing relates to the stationary assumption that all aperture radars require in order to deduce radar images. As FMCW radars work continuously to produce information, frequency non-linearities appear in data-acquisition. This has been enhanced by correcting the whole range of frequencies to a comprehensive and successful extent [4]. It is assumed that the received radar database takes this into account to a degree that will not affect the experiment.

Another important aspect of radar principles is the Direction of Arrival Estimation (DAE). DAE refers to the ability to process the direction information of several electromagnetic waves from received outputs onto a sensor array. The literature offers multiple possibilities for conducting DAE on to a successful extent. The echos in the image are considered to be stationary and captured by a Multi Input Multi Output (MIMO) FMCW radar[4].

B. Side Looking Airborne Radar

In a SLAR, the aircraft behaves like a platform that travels forward with the radar antenna projected perpendicular to the flight direction[3]. The nadir, or the projection of the radar antenna onto the 2D surface lies directly beneath the platform. The radar beam is thus transmitted obliquely at right angles to the flight path, creating a swath. Range

is taken as a reference across-track, perpendicular to the flight direction. Azimuth here directly refers to the parallel along-track to the flight direction. Fig. 1 illustrates the imaging geometry for a SLAR.
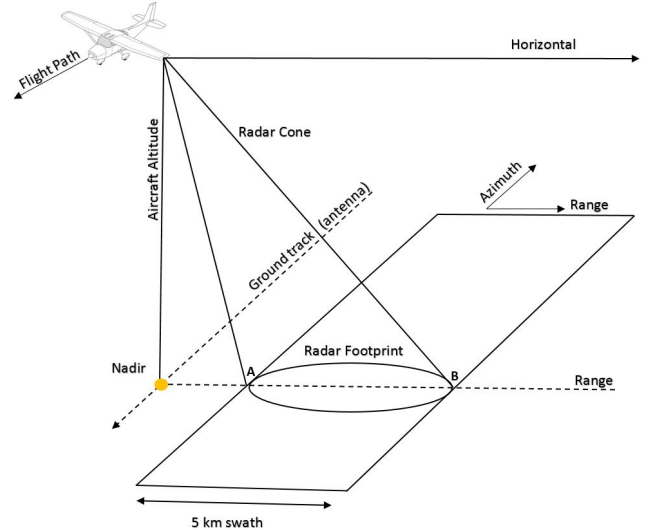
Fig.1: FMCW side looking radar concept

Using the geometry in Fig. 1, the SLAR translation to a 2D map and consequently the resolution, ca be expressed in terms of system and flight parameters. Due to measuring the slant range, side-looking radars create several distortions, with regards to elevation and range, as well as with occlusion. These conflicts are usually avoided when using a Synthetic Aperture Radar (SAR), that removes the dependence of the azimuth resolution on the incidence angle.A Synthetic Aperture Radar (SAR), is a type of SLAR that electronically reproduces a large antenna aperture by using the aircraft flight path. The magnitude and the phase of the signal is used to store data and create a high-resolution image of the terrain[3].

III. AVAILABLE DATA

A test flight using Metasensings FMCW radar was conducted on Teuge (ICAO: EHTE) airport, conducting one flight with one touch and go, between cities Apeldoorn and Twello, the Netherlands. The radar data was recorded as a range and Doppler velocity matrix of all points detected in a 5 km^2 range. This also represents the maximum mathematical constraint of the radar data, i.e. all maps created for comparison purposes will remain within this window. As presented in the aforementioned chapter, information with regards to altitude, velocity and flight path angle are also necessary. This is provided for each GPS coordinate recorded during the flight, with a one second increment. Heading measurements were deduced via interpolation of GPS coordinates. It should be noted that these heading measurements do not take into account wind.

Fig.2: Teuge Airport Satellite View, Apledoorn (left) and Twello (right).

Synchronizing the radar and flight data yields a linear function for parameter matching. This allows for all the necessary values to translate the range Doppler-velocity matrix onto a 2D radar map each second of the flight.

A. Comparison Databases

Having computed the radar map, it becomes increasingly useful to have an equivalent map for comparison purposes. Google maps allows the visualization of either a satellite or a vectored depiction of the roads for a certain central coordinate. The radar region is overlapped onto a Google image to show what the radar can detect. This will also provide a direct link between SAR and FMCW intensity reflections. It is acknowledged that as the two databases are in taken in different light spectrum, photography and magnetic, this will have an effect on the intensity of each presented point. However, geometrical features such as roads or rivers in the image should remain constant. The Google maps database will mostly be used within the comparison due to its ease of access and filter.

The European Space Agency's Sentinel 1 database will be used, to have the similar spectrum comparison in the experiment. The Sentinel 1 database [5] was chosen to be vertically polarized, to ensure a close match to the radar images. Fig.3 shows the databases used.

It becomes apparent that the vectored Google maps can be used for road detection, while the Sentinel 1 database [5] for highly reflective points, such as industrial buildings. It should be noted that these are the only types of features that can be identified in the radar image, i.e. geometrical features from roads or highways and high intensity points from highly reflective objects in the environment.

Fig.3: Radar map (left), Google road vectored map (center), Sentinel I - Vertically polarized - SAR map(right) at second 1000 of radar recording.

IV. METHODOLOGY

The available data offers the possibility to test various filtering techniques and assess whether they are effective in determining the scope of the research. The starting hypothesis is that it is possible to recognize features within airborne radar images that can assert the possibility of matching to Google maps or satellite SAR maps. Given certain conditions, GPS fails to provide a correct reading with little or no systems put in place to aid [6]. Thus the ability to easily and timely confirm the validity of GPS coordinates becomes of paramount importance. The methodological approach thus becomes to find a technique or composition of techniques that robustly compares two images, one produced by the radar antenna and one indicated by GPS coordinates onto a satellite database. As all considered databases essentially produce a gray-scale image of the information contained, a computer vision approach can be easily implemented for the comparison. The presence of noise and the quality of the radar images excludes the possibility of using point detection algorithms[7]. As such, image transformation algorithms that are robust to noise is desired, as well as the effects presented in the previous chapter. As such a list of the used algorithms is shortly presented and explained below.

A. Experiment candidates

- **Gamma Correction** - Also known as Power Law Transform. This function transforms the input image pixel-wise as a power of gamma, after scaling each pixel to the range 0 to 1 [8].
- **Thresholding** - The creation of a new binary containing the pixel positions of all intensities that are above a certain threshold.
- **Local Histogram Equalization** - A method which modifies contrast, to stretch out the intensity range, reducing any non-linearity within pixel intensities [9].
- **Contour Finding** - A curve joining all the continuous points (along the borders) that have the same intensity and or color. The contours are a useful for shape analysis and object detection [10].
- **Ridge Operators** - Algorithm that relies on the eigen-values of the Hessian matrix, calculated from intensities within the image in order to detect ridge structures where the intensity changes horizontal, but not along the structure [11].

3

- **Straight Line Hough Transform** - A common algorithm that assigns pixels to the existence of a line that meets width, length and direction properties [12].
- **Blob Detection** - A group of pixels that share some a common property, for example intensity in this experiment or colour [13].
- **Entropy Detection** - The entropy filter is capable of detecting slight variations in the local gray level distribution [14].
- **Watershed** - A marker controlled Watershed is an image transformation algorithm that interacts for a grayscale image and considers the image as a topographic surface, calculating the energy gradient of a higher altitude (higher intensity) towards a smaller altitude (lower intensity value)[15].
- **CGAN - CRF** - Unsupervised learning algorithm based on hierarchical Conditional Generative Adversarial Nets (CGAN) and Conditional Random Fields (CRF) Geo Land sensing - categorizing each pixel in satellite images into a category such that we can track the land cover of each area [16].
- **CAE-TVL** - A pre-trained Convolutional Autoencoder with Total Variation Loss (CAE-TVL) for satellite image segmentation as well as generic images [17].

Due to the power capabilities of the radar, a non-linearity for all intensities was observed, that could not be fixed via multiplication with a range function. This non-linearity is kept even with different range multiplications, whether it is with regards to range squared, cubed or fourth. This implies that local changes in intensities are required to obtain a clear image. This can be easily obtained from using image modification algorithms such as Gamma Correction, Threshold setting or Local Histogram Equalization. These algorithms become the corner stone for a first filter within the image to attempt a linear equalization of all intensities and assure that any transformation conducted by following algorithms would work correctly over the whole considered area.

It can be observed that both image transformations focus on filtering certain features within the radar image. These features can be any combination between high intensity points and shape features, such as roads or highways. In order to correctly compare to a database, a one-to-one comparison is preferable. This means that vectored shape information contained in Google images can only be compared to radar images filtered by methods that focus on filtering for shapes. It is possible to compare both within the same light spectrum, however, the vertical polarized nature of the provided information, makes filtering for intensity more favourable. Only Methods 2 and 7 that use Blob Detection will compare with Sentinel 1 database. As all other methods only filter mostly for geometric shapes which represent roads or highways, it is easier to use the Google database.

TABLE I

IMAGE TRANSFORMATION SEQUENCE

Method #	1st Image Transformation	2nd Image Transformation
1	Gamma Correction	None
2	Gamma Correction	Blob Detection
3	Gamma Correction	Threshold
4	Threshold	Contour Finding
5	Threshold	Entropy Detection
6	Threshold	Hough Line Transform
7	Threshold	Blob Detection
8	Histogram Equalization	Ridge Operators
9	Histogram Equalization	Entropy Detection
10	Histogram Equalization	Watershed marker
11	Histogram Equalization	Contour Finding
12	CGAN - CRF	None
13	CAE - TVL	None
14	Histogram Equalization	CGAN - CRF
15	Histogram Equalization	CAE - TVL

B. Experiment setup

The output of the presented algorithms or set of algorithms onto the radar is a template, in the sense of this paper, a shape used as a pattern for matching. In order to compare two templates from their designated radio or Google/SAR databases, a comparison metric is necessary. The used comparison metric is the Structural Similarity Index Measure (SSIM). This is a objective method for assessing perceptual image quality alongside structural components [18]. The SSIM is a metric for measuring the similarity[18], based on luminance, contrast and structural correspondence. Fig. 4 shows how two images are compared using this algorithm. In this case, both images are compared based on luminance, defined as the intensity value found within a certain pixel.
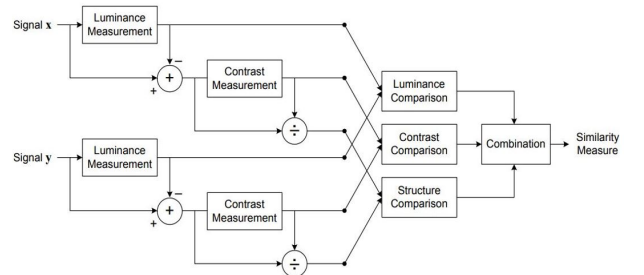
Fig.4: Structure Similarity Index Measure: Flowchart

Contrast, which is defined as the difference in luminance over a certain area and finally structure, or consistent geometrical relations over a index map which provides local image quality over space. The SSIM was compared with other possible comparison metrics such as Mean Square Error (MSE), or Peak Signal to Noise Ratio (PSNR). Of these metrics, only the SSIM analyzes the structure information between the reference and the test images. It is very important that the chosen metric takes into account differences in geometry of detected points, even under heavy noise presented in the image, hence why the SSIM is a valid and desired metric [19]. Furthermore, preliminary tests have concluded

the possibility of SSIM algorithms to detect rotations smaller than 1, given perfect image quality, as well as being able of assessing the quality of the given image[19]. This makes SSIM a desirable candidate for this experiment.

Taking the radar image as the image perfect quality, and a Google/SAR image as the comparison image, yields a certain value for the SSIM. It is to be expected that due to noise and lack of certain features, the value will be small. What is left is to create a pool of randomised candidates in which the original indicated image is to be placed. Ideally, the SSIM will choose the corresponding Google/SAR image to the radar, indicated by GPS coordinates, every time, out of the randomized pool. In order to realistically randomize around the given GPS, we turn to errors in flight, either due to position (GPS) or direction (heading measurement via magnetic compass). Literature shows that GPS can have error measurements as low as 10m [20], while heading measurements range around 1[20]. This means that to be realistic, around the actual GPS position of the aircraft, a radius of around 10m and variation of 1 is to be considered. Due to large number of possible experiment setups, the approach that was followed for the purposes of this research was to devise two experiments. One to test all combination and filter for the best working algorithms and another to test these best algorithms in as realistic situations as possible.

V. EXPERIMENT A - SETUP

Both experiment setups follow the same logic, to create a pool of randomized samples of radar-map pairs. Each pair has an assigned range and heading, along with a calculated SSIM value. Within this pool the original indicated pair is also present, with its own calculated SSIM value.
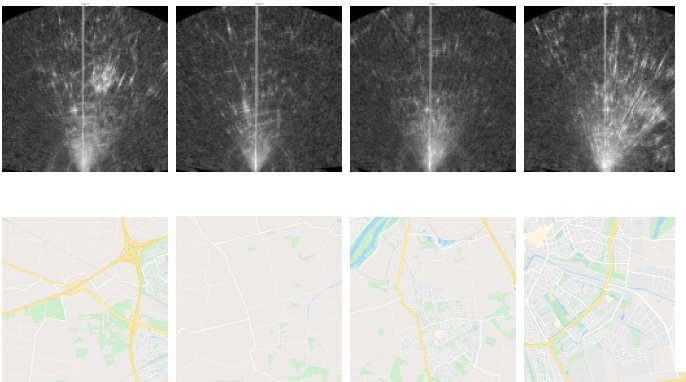
Fig.5: Image pool for Experiment A

The purpose of the first experiment is to filter the best combination of algorithms and choose the best top three. As such, the first experiment will be less strict on the randomization of the radar-map pairs. From the radar data, a representative sample of 4 images were chosen that were then translated to a 2D representation and assigned their corresponding GPS coordinate. Fig. 5 shows a representation

of these images.

Following this step, candidate coordinates are produced in a radius of 150 m around the original coordinate with a modification of +/- 15 around the correct heading, as represented in Fig. 6. The increment for creating randomized values for both radii and heading measurements is always one. The radius and heading measurements can be regarded as the independent variables within the experiment. A total of 300 candidates are created, each with their own SSIM value, which will be regarded as the dependent variable. Fig. 7 shows an example of how a candidate is being created.
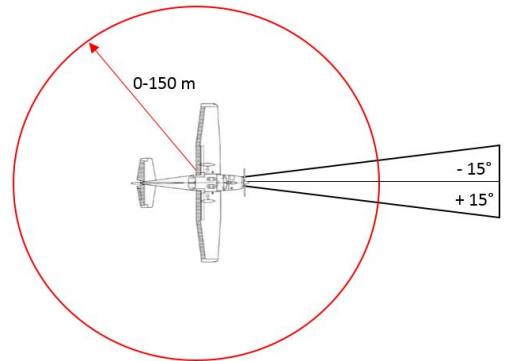
Fig.6: Illustration of radius and heading variations for Experiment A
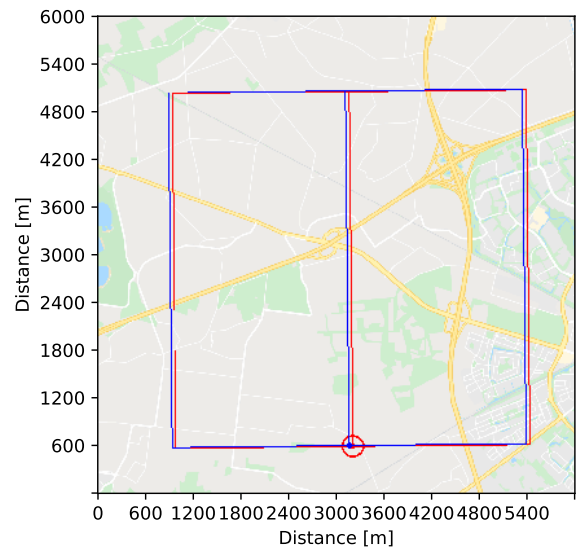
Fig.7: Image pool for Experiment A with two candidates with different radar views, (red) the original coordinate (blue) a randomized candidate within the 150m radius.

A. Experiment A - Results

Following a total of 15 experiments done over 4 flight radar images, Table II shows the average results with regards to heading deviation, position error and the percentage of SSIM that is greater than the original pair. The average of position error, as well as heading values is of interest to show the overall performance of the experiment, not just

the best indicated value. It should be noted that the heading deviation is absolute, between calculated heading and best candidate heading. The position error is the distance from the generated coordinate to the GPS-indicated coordinate. And, finally, of the total randomized positions, a percentage above the original pair is calculated and presented. All averages are taken as integers, calculated by summing the best candidates and dividing by the amount of total candidates. Over all parameters within the results, the lower the value, the better the performance.

Method	Results Experiment A - Average over 4 points		
	Absolute Heading Deviation	Position error	False Positive
1	7	108	53%
2	6	68	52%
3	3	75	50%
4	11	46	39%
5	**5**	**24**	**23%**
6	4	53	67%
7	8	35	28%
8	**0**	**0**	**0%**
9	**0**	**0**	**0%**
10	6	119	38%
11	2	37	89%
12	14	126	55%
13	12	124	53%
14	12	52	45%
15	6	112	35%

B. Discussion upon the results of Experiment A

Table II presents the results for a total of 15 experiments. It should be noted that the performance of all experiments relates directly to the SSIM, i.e. how well do overall transformations relate the radar transformations to comparison databases in terms of contrast, luminance and structure. As such, it is to be expected that the methods that best control all three parameters will provide the best results. A special importance is given to structure, as that will be main parameter used to determine position and rotational differences within each image-pair.

Discussing these results it becomes apparent that overall first image transformations using gamma correction behaves as expected. Prior transformations to the ones based on range had a similar effect on the radar image. Although gamma correction highlights features that normally would be hardly visible, the algorithm equation behaves in a quadratic manner, maintaining a non-linear relation within all values.

Noise is carried forward to the second image transformation by all algorithms, leaving the second image transformation to provide a robust feature identification. This means that first image transformations that filter the image drastically, such as thresholding, do not provide a further attempt to discriminate between noise and actual information. As such, neither a high accuracy with regards to position is expected, nor to rotation.

Of all image transformations, the local histogram equalization was expected to perform, yielding a good start for future algorithms to detect features, only pertaining to structure, such as rivers, roads or highways. At the start of the experiment, there was no specific way of pointing whether a certain geometrical structure within the image was a particular landmark, such as a river or a road. However, it became clear as the experiment progressed that the radar reflected mostly highway or road information. This was verified through observation onto actual satellite images.

Going into detail for second image transformations, each Method will be examined in particular. **Method 1** does not use any second image transformation and was chosen mostly as a baseline to see how well a simple and fast algorithm will behave. As explained above, gamma correction also forwards noise found in the image. Even when the same contrast was found between two comparison images, luminance and especially structural differences rendered the SSIM insignificant to distinguish between images.

Method 2 employed an algorithm called Blob Detection. Reflective buildings, such as industrial warehouses remained in the image when 85% of intensity values were filtered. Computing the laplacian of the gaussian (LoG) with a increasing standard deviation, blobs become local maxims within a cubic representation. Detecting larger blobs requires a larger kernel size that slows down the convolution, however for the purposes of the experiment that was neglected. This methods removes noise by estimating the centre of gravity of nearby bright points and its radius to encompass them. Here a comparison with Sentinel 1 database is more desirable as all features behave in a similar way. The explanation for this comes from how noise contributes to the radar image, changing the properties of the detected objects.

Method 3 attempted to use threshold measures to control for luminance. A binary image will have luminance values between 0 and 1 and before that, contrast changes will bring into view objects that are barely visible in the electromagnetic spectrum. It was found that after gamma correction for both images, high intensity objects were highly visible, as well as roads roads. Via visual inspection, most roads appeared in the image as a function of the maximum intensity value, between 30-50% Unfortunately, that is also where noise was identified, which predictably would skew results. Again, the problem was with noise, as in both transformations forwarded noise.

Method 4, with the aid of threshold and contour finding, attempted to filter most noise and draw the contour of as many features that it found. A visible improvement was seen in the results, where the SSIM values did not seem random. It became clear that contours contributed towards improving the results. Again, noise played a role in distorting the detected shapes. It becomes clear that a noise robust algorithm that uses either the hessian, laplacian or gaussian of the radar image is necessary.

With **Method 5**, the idea of entropy was introduced, or the informational complexity contained in a given neighbourhood that is typically defined by a barrier. Thresholding with

regards to most noise, allows the detection of features within the radar image. With regards to the rest of the noise, an entropy algorithm takes into account the uniform distribution in the neighbourhood area. This yields structuring elements such as roads or highways, even under noise skewing. The reason for its lack of accuracy was that the thresholding algorithm forwarded noise reflections as structuring elements that were taken into account when comparing, yielding a false comparison.

While applying threshold algorithm for roads, it was observed that multiple points appeared in place of where visually a road should be. **Method 6** attempted to unite all points that normally would be a road through the use of the Hough Line Transform. Using multiple settings, alignment of these points was attempted. Unfortunately, the process due to the large amount of settings combinations, a good result was not achieved.

Method 7 attempted to directly adjust the image to then apply the blob detector. Unfortunately, due to noise, the center of gravity of all remaining points was different from what was detected within the Sentinel 1 Database. This is also explained by the difference in power and settings of the two radars that acquire images.

Method 8 moves to using Histogram Equalization as the first image transformation. This algorithm works similarly to gamma correction by improving contrast in images. However, it accomplishes this by effectively spreading the most frequency intensity values and stretching the intensity range withing the image, not through a quadratic equation. Following, ridge operators calculate the eigenvalues of the second order matrix of the image, also known as the hessian matrix. The local maxima or minima of the matrix determines ridges. This method works very well with noisy images, being employed in the medical industry to detect blood vessels in radio images. This is reflected in the excellent results for experiment A, being able to identify the original image overall.

Method 9 as with method 5, entropy detection is better employed using histogram equalization. This provides the necessary accuracy to detect features within the image to an extraordinary effect. The resulting templates allows for changes in range and rotation that better allow the SSIM to discriminate for the original value. This also provided very good results due to the ability to very well discriminate edges under noisy conditions.

Method 10 allows for selecting the ranges of intensities used to segment grayscale images. The higher or custom intensities within an image are considered specific seed points where flooding is simulated, segmenting the image. The algorithm works poorly, even with custom ranges, as noise is not at all filtered. The main advantage of this method is that it can be directly related to intensity values of the radar, allowing for automation.

Method 11 used histogram equalization first to transform the image and attempt to find Contours. New contours were created due to noise and it is impossible to determine whether they are features within the candidate image or not.

Methods 12, 13, 14 and 15 represent a variation on pre-trained neural network algorithms, designed to segment SAR images. The scope was to attempt and segment the image based solely on pixel value and see whether this can be used for a suitable comparison. Local histogram equalization is also used to bring into view features that were otherwise ignored or miss-interpreted by the algorithms. While segmenting the Sentinel 1 SAR databases to an acceptable degree, both algorithms have been trained on high resolution SAR images, or even on multi-spectral information. The radar database does not offer the necessary resolution and noise is not correctly filtered to allow for a correct segmentation. It is possible to train these algorithms, however a bigger database is necessary, as well as more pre-processing to each individual radar image. With the hierarchical CGANs and CRF [12], high resolution imagery are necessary. The concept of superpixel is necessary to reduce burden of performance, i.e. as with watershed markers, pixels need to be pointed out as representative of an area that is to be segmented. The Convolitional Autoencoder with Total Variation Loss [13] is using multi-spectral data in the segmentation process. Additionally, the sensor uses laser scanning to produce the database. This method was selected in the attempt to use ranges of intensities as part of a common feature to segment mostly roads and highways.

VI. EXPERIMENT B

Once the top three most performing combinations of algorithms are chosen, the second experiment can commence. This algorithms are: Experiment 5, Experiment 8 and Experiment 9 as taken from Table I. This time, a more extensive representative sample is chosen, comprising a total of 20 images. In this experiment the independent variables are randomized more strictly, in two steps. The first step assumes the first randomization technique of radius and headings, applied to a larger variation of radar images during the flight. Within Fig. 8 it can be seen that these points are chosen as far apart as possible along the two flights. During landing and take off, the altitude of the aircraft is too low to ensure a good reading of the surrounding area and proper match within the five square kilometer area. As such, only points above 100 m are taken into consideration. The second step greatly increases the realism of the experiment, only varying the heading by +/-15 while assuming a near-perfect reading of the GPS coordinate, at 0 m.

A. Experiment B Results

Following this step, candidate coordinates are produced in a radius of 150 m around the original coordinate with a modification of +/- 15 around the correct heading. The increment for creating randomized values for both radii and heading measurements is always one. The radius and heading measurements can be regarded as the independent variables within the experiment. A total of 300 candidates are created, each with their own SSIM value, which will be regarded as the dependent variable.
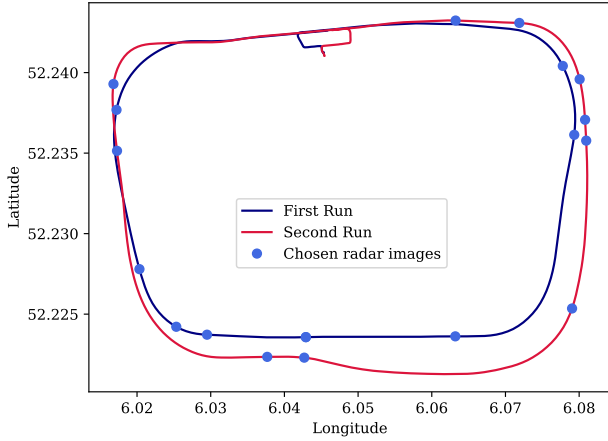
7

Fig.8: Illustration of selected coordinate points for Experiment B

Following the 2 experiments done over 20 flight radar images, Table III shows the average results with regards to average heading deviation, average position error and percentage better candidates with regards to the original SSIM value. The average of position error, as well as heading values is of interest to show the overall performance of the experiment, not just the best indicated value. It should be noted that the heading deviation is absolute, between calculated heading and best candidate heading. The position error is the distance from the generated coordinate to the GPS-indicated coordinate. And, finally, percentage better is the percentage of candidates with a higher value for the SSIM than the one of the indicated pair. All averages are taken as integers, calculated by summing the best candidates and dividing by the amount of total candidates. Again, over all parameters, the lower the value, the better the performance and averages are taken as integers.

TABLE III

AVERAGE RESULTS OVER EXPERIMENT B

| Method | Results with 0:150m range | | |
	Absolute Heading Deviation[]	Position error[m]	False Positive
5	5	45	42%
8	1	1	14%
9	2	5	9%
Method	Results with 0m range		
	Absolute Heading Deviation[]	Position error[m]	False Positive
5	12	N/A	51%
8	2	N/A	2%
9	9	N/A	48%

Through a quick look at the results, it becomes obvious that the average position error is not 0, as in the previous experiment. As such, a direct representation of these variations per image is shown in Fig. 9 and Fig. 10.
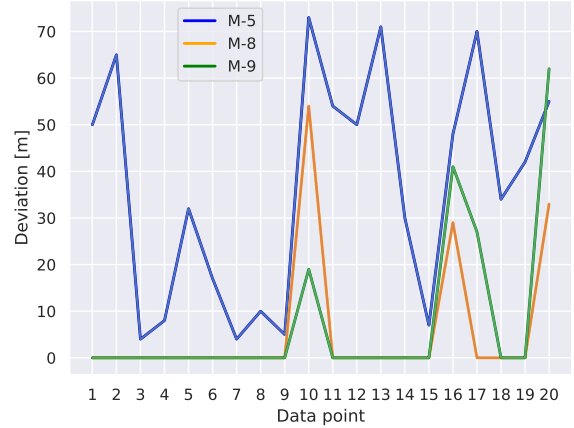
Fig.9: Illustration of radius variations for Experiment B, for all 20 candidate images **with 0:150m range**
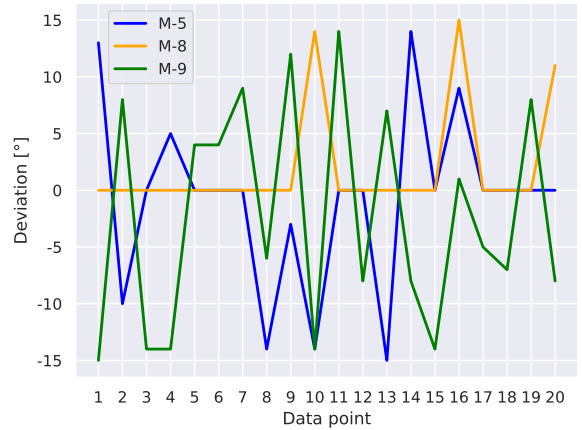
Fig.10: Illustration of heading variations for Experiment B, for all 20 candidate images **with 0m range**

B. Discussion upon the results of Experiment B

Through the virtue of complete randomization at a realistic scale, the employed algorithms were heavily tested, each part of experiment B multiple times, to ensure viability of results.

To begin with, the results of **Method 5** will be discussed. While being the third most promising method, thresholding for road segmentation between 30-50% of the highest intensity and applying entropy detection yielded competitive results. The two image transformations are enough on average to affect the SSIM. The determining factor in this is the first image transformation, which allows for too much noise to be forwarded to the next step. Combining this with the entropy algorithm that slightly blurs the image makes for a increase in error and decrease in reliability, especially under small variations.

Method 8 overall provided the best results. Fig. 11 shows how the algorithm worked in identifying features within both the radar and the google vectored road-map. It is possible through the setup of the method to ignore smaller features within a high quality image, however within the radar image, a lot of noise is taken and cannot be changed. This forces
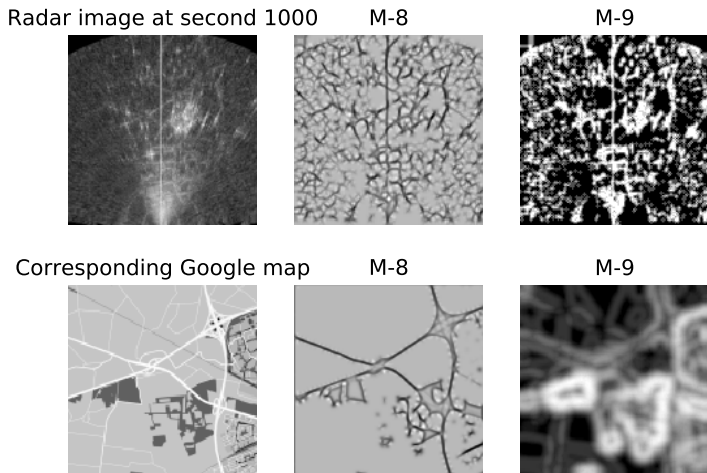
Fig.11: Radar image 6 and its corresponding Google vectored image transformed via Method 8 & 9.

the strategy to focus on identifying bigger structures, which in this case will be highways.

When looking at the average results we can see a slight inconsistency where position and heading errors appear. This is in contrast to what Experiment A showed. When looking at Fig.10, one can see that at image 10, 16 and 20, all algorithms provided an erroneous estimation. Below, in Fig. 12, these radar images are depicted along a typical successful radar image.

Fig.12: Radar images 10 (left), 16 (middle) and 20 (right), present no evident feature to track by any method.

It becomes obvious that these images, although presenting heavy noise capture, do not contain any identifiable features for all algorithms. Image 16 is taken during a turn, heavily skewing the relative position of the reflected points with regards to the aircraft. Image 10 and 20, however are taken during straight, leveled flight. The major difference between these two image sets and for example the ones from experiment A is the absence of highways, i.e large detected f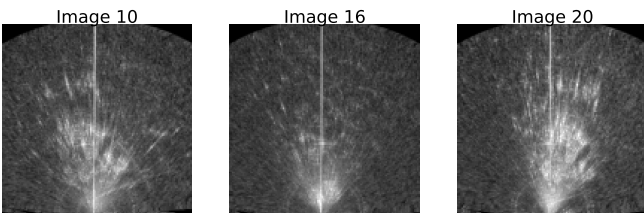eatures. It becomes apparent that in most images used within the experiment, large roads are detected that allow the SSIM to calculate very small changes within candidate images.

Method 9 also did very well compared with other methods in experiment A. When attempting to reduce the range to

0, this method was unable to detect small variations within the candidate pool. This indicates the methods possibility to discriminate based on range and not allow the SSIM to calculate relevant values when the rotation involving up to 5. This is due to a blur effect of the algorithm to the Google database image that does not maintain any identifiable features at small image rotations. Surprisingly, the algorithm managed to identify the correct coordinate at image 16 of the candidates. When looking at the respective image, it can be seen that a large area near the middle of the image may have been taken as the main feature. This could be studied further for entropy algorithm with images that possess heavy noise skewing. Regardless, the performance of Method 9 was lackluster when small variations occurred in all other candidate images.

Overall, both experiment setups had problems with the noise contained within the image. Attempting to smooth the image or apply synthetic aperture radar denoising techniques blurred smaller features. A trade-off to find a common ground became the basis for most employed methods.

Geometrical occlusion due to the altitude of the aircraft may have provided a small source of noise, however negligible with regards to feedback and power noise. The mathematical area in which the antenna detected reflections was invaluable towards the implementation of any method. A continuous estimation based on the aircraft altitude may allow for identification of features at smaller altitudes.

The SSIM is regarded as the most valuable algorithm within this experiment. Given the right conditions, i.e. no noise, approximate electromagnetic spectrum comparison, it may be possible for it to work without any transformations on the radar image. As image transformations changed all candidate images, it normalized luminance and contrast to a high degree. This allowed for the structure comparison part of the algorithm to correctly identify features even in noisy images. However, it affected the overall performance of the SSIM and low scores were obtained.

All considered databases employ different electromagnetic spectrum. This was a main reason why most methods considered shape as the main feature identification. When filtered and thus normalized for color differences, all shapes become similar and thus can be compared. There is no way of identifying features within the radar map as roads, rivers or highways, without comparison to a known database. Of all shape features, highways were the least susceptible to noise and occlusion, due to their size. This also provides a valuable advantage as Google maps offers a vectored roadmap, where highways are highlighted.

VII. CONCLUSION

Information is invaluable in decision making. The ability to infer additional information from a sensor to verify other system parameters increases the reliability and safety of the whole platform. The possibility of using radar information to deduce or check other flight parameters is the focus of this study. Using a perceptual metric (SSIM) to quantify image quality degradation, especially via noise in data transmission,

transformed radar images are compared to Google vectored roadmaps or Satellite 1 SAR vertically polarized databases. All databases are transformed via one or two transformations, that assures that shape features such as roads or highways, or highly reflective objects are most visible.

To simulate possible GPS faults, new coordinates in an area around the the actual aircraft coordinates are created. From there new image candidates are proposed for comparison with the radar image. The best candidate is taken and an error based on distance from original coordinate is calculated. To attempt and analyze heading variations, the rotation of candidate images is also employed. While being heavily affected by noise via power and received echoes, one algorithm provides a high degree of accuracy within the experiments. The algorithm belonging to M-8 is especially designed to detect blood vessels in noisy radiograms within the medical field. The same algorithm was able of identifying the image corresponding to the GPS coordinate in most test cases where large shape features were present representing highways. This allows for information identification under heavy noise conditions to ascertain whether GPS coordinates are correct, as well as for heading information from the magnetic compass. This could be used in the future to make the aircraft a self contained system, with no necessary outside inputs.

VIII. FUTURE WORK

Within the boundaries of this experiment, it still remains to be seen whether computational times can be improved. The SSIM score should be increased by utilizing the algorithm to its full capability, incorporating luminance and contrast information. To achieve the transformations, it is necessary to take into account additional radar parameters, especially related to power. The SSIM can be used to discriminate image quality. This means a potential for using the SSIM to predict the amount of noise within an image and determine if it is suitable for comparison. Additionally, varying parameters within the SSIM can also provide an answer of whether there is an object to detect. Given a more in-depth implementation of the SSIM, it may be possible to filter the image without the need for additional algorithms.

As the heading was deduced from successive GPS coordinates, a more qualitative method should be employed. The overall test should verify whether the heading information is consistent with radar information and if it can be used as a secondary measurement or input to more consistently determine heading information.

For shape detection within Google vectored maps, a simple color and grayscale transform can be implemented to work aside the transform of the radar image. This should ease the calculations as well as improve the SSIM output due to a direct segmentation consisting of only highways.

Due to the lack of an extensive database, no machine learning algorithms can be employed to check coordinate information. As of this moment, the test setup can only attempt a prediction algorithm that takes aircraft parameters as inputs and attempts to find the next image in the database

that best corresponds to a future radar image. Additionally, the test setup used within this paper can be used to create a database that can train machine learning algorithms to deduce position and heading information, based on previous state information.

REFERENCES

[1] Modern Radar Detection Theory. SciTech Publishing, sixth edition, April 2016.
[2] Introduction to Modern EW Systems. Artech House Publishing, first edition, 2012.
[3] A. Meta, P. Hoogeboom and L.P. Ligthart, Range Frequency non-linearity correction for FMCW SAR, European Patent Application No. 06076057.6, May 2006.
[4] H. R. Sheikh Z. Wang, A. C. Bovik and E. P. Simoncelli. General aviation radar system fornavigation and attitude determination. IEEE Trans. Image Processing, vol. 13, no. 4, pp. 600612pril 2004.
[5] X. X. Zhu M. Schmitt, L. H. Hughes. The sen1-2 dataset for deep learning in sar-optical datafusion. Commission I, WG I/3, 2018.
[6] K. Kawamura and T. Tanaka, "Study on the improvement of measurement accuracy in GPS," 2006 SICE-ICASE International Joint Conference, Busan, 2006, pp. 1372-1375. doi: 10.1109/SICE.2006.315576
[7] Global Positioning System, Inertial Navigation, and Integration. Wiley, John Sons, Incorporated,second edition, August 2001
[8] Erik Reinhard; Wolfgang Heidrich; Paul Debevec; Sumanta Pattanaik; Greg Ward; Karol Myszkowski (2010). High Dynamic Range Imaging: Acquisition, Display, and Image-Based Lighting. Morgan Kaufmann. p. 82. ISBN 9780080957111.
[9] D. J. Ketcham, R. W. Lowe J. W. Weber: Image enhancement techniques for cockpit displays. Tech. rep., Hughes Aircraft. 1974.
[10] Lorensen, William and Harvey E. Cline. Marching Cubes: A High Resolution 3D Surface Construction Algorithm. Computer Graphics (SIGGRAPH 87 Proceedings) 21(4) July 1987, p. 163-170
[11] Ng, C. C., Yap, M. H., Costen, N., Li, B. (2014, November). Automatic wrinkle detection using hybrid Hessian filter. In Asian Conference on Computer Vision (pp. 609-622). Springer International Publishing.
[12] C. Galamhos, J. Matas and J. Kittler,Progressive probabilistic Hough transform for line detection, in IEEE Computer Society Conference on Computer Vision and Pattern Recognition, 1999.
[13] L. Bretzner and T. Lindeberg. Feature tracking with automatic selection of spatial scales. Computer Vision and Image Understanding, 71(3):385392, 1998.
[14] van der Walt, Stéfan Schönberger, Johannes Nunez-Iglesias, Juan Boulogne, François Warner, Joshua Yager, Neil Gouillart, Emmanuelle Yu, Tony contributors, the. (2014). scikit-image: Image processing in Python. PeerJ. 2. 10.7717/peerj.453.
[15] TY - K V, Lalitha .R, Amrutha Michahial, Stafford M, Dr. (2016). Implementation of Watershed Segmentation. IJARCCE. 5. 196-199. 10.17148/IJARCCE.2016.51243.
[16] C. Wang, B. Yang and Y. Liao, "Unsupervised image segmentation using convolutional autoencoder with total variation regularization as preprocessing," 2017 IEEE International Conference on Acoustics, Speech and Signal Processing (ICASSP), New Orleans, LA, 2017, pp. 1877-1881.doi: 10.1109/ICASSP.2017.7952482
[17] Leena Matikainen, Kirsi Karila, Juha Hyyppä, Paula Litkey, Eetu Puttonen, Eero Ahokas, Object-based analysis of multispectral airborne laser scanner data for land cover classification and map updating, ISPRS Journal of Photogrammetry and Remote Sensing, Volume 128, 2017, Pages 298-313, ISSN 0924-2716, https://doi.org/10.1016/j.isprsjprs.2017.04.005.
[18] Z. Wang, A. C. Bovik, H. R. Sheikh, and E. P. Simoncelli, Image quality assessment: From error visibility to structural similarity, IEEE Trans. Image Processing, vol. 13, no. 4, pp. 600612, April 2004.
[19] M. P. Sampat, Z. Wang, M. K. Markey, G. J. Whitman, T. W. Stephens, and A. C. Bovik, Measuring intra- and inter-observer agreement in identifying and localizing structures in medical images, Proc. IEEE Int. Conf. Image Processing, pp. 8184, October 2006
[20] Langley, R.B.. (2003). The magnetic compass and GPS. 14. 70-81.

3

Preliminary thesis report

3.1. Introduction

Avionics represents the sum of all available information that is presented in order to allow decision making on an informational level. Thus, the availability of information is the corner stone of efficient decision making. It is through this philosophy that the development of avionics has evolved, to present as much knowledge regarding the environment, the pilot and aircraft performing in that environment, as well as filtering that information into a package that is easily understandable under time constraints. The following report is a support document that offers additional information with regards to the research paper, with a focus on the methodology.

According to the ICAO Annex 2[7], Rules of Air, the General Aviation (GA) is represented by all the civilian aviation operations that fly under Visual Flight Rules (VFR), which are defined by certain regulations that require an aircraft to be flown in conditions of visibility and distance from clouds[7], which should be equal or greater than certain reglemented minimas. In these situations, the pilot is in charge to look out in case of collisions. This constitutes a safety hazard for aircraft flying under Visual Flight Rules and need to switch during the fight, under different circumstances, to Instrumental Meteorological Conditions (IMC). This has been statistically deemed a leading factor for fatal accidents[22]. This becomes more problematic for medium to high-speed aircraft, such as different propeller aircraft, or business jets, as it leaves little or no time to understand a hazardous situation and proceed to avoid it, in an ever increasingly populated environment.

Witih in VFR airspace, different aircraft are operated such as gliders, ultralight vehicles or balloons. Under the ICAO regulations, these type of aircraft are not required to be equipped with active transponders [8]. This leaves the pilot responsible to maintain the separation during the whole flight, based on visual reference to the ground, therefore there is no explicit distance minima stated by the regulations [7]. Consequently, efforts have been made to increase the pilot's awareness during flight [26]. This has brought the creation of airborne collision avoidance systems (ACAS). These systems are regulated in regard to ICAO ANNEX 10[8]. This system issues traffic advisories that aids the pilot in cases of possible traffic collisions, therefore it reducing the risk of collisions.

In the advent of UAVs, more specifically, commercial drones that have little to no legislation set into place, only adds to the disruption of traffic and the balance of safety[10]. Consequently, both the EU [29] and independent research facilities such as TU Delft have begun initiatives to offer new sensory capabilities for VFR flights [35]. Developments on radar techniques have made it possible to create lightweight radar systems that can be carried on board of an aircraft and are now becoming available to General Aviation [39]. When such a system is carried on board, it may be used for in-flight surveillance of neighbouring aircraft and the environment. A radar installation can alert the pilot if proximity with other participants or terrain poses a hazard to the safety of the aircraft. Additionally, radar installations are especially useful for VFR flights that might enter IMC [11], as their sensing capabilities are not infringed by adverse weather [5].

A consequence for on-board radar systems is that they may also be used to provide assistance in navigation and attitude determination. A radar system can determine the relative position of the world around the aircraft, and this information can be used to find the actual aircraft state information. Clear reflections of the ground can be observed from radar images taken mid-flight, in which structural reflections are distinguishable. These reflections originate from ground elements, such as rivers, highways, lakes, forests etc. It would be possible to determine the locations of these ground structural elements by using Direction of Arrival Estimation (DAE), algorithm which makes use of the propagating wave arriving at a certain point [39]. This allows for enough features to be recognized in order to possibly navigate using a map.

As much as humans used to navigate using a map of the roads on the route they were taking, so too it may be possible for aircraft to navigate using a satellite map, that has precise coordinates of all available locations. Selfly [20] has created a Collision Avoidance Radar (CAR) to actively aid during flight. The CAR operates on Frequency Modulated Continuous Waves (FMCW) with a relatively small size and light with the possibility to be installed on the wing [35]. It can be used as an ideal test case to obtain radar imagery that can determine the aircraft parameters.

The current proposal "Navigation through terrain recognition for on-board radar systems" has the aim to assess whether within the data provided by the on-board radar, a set of information can be derived, which leads to a strategy that analyses and confirms coordinate information of the aircraft. This brings up the question if we have the necessary computing and methodology to recognize landmarks in a radar image that can help aircraft navigate?

If such options for an on-board radar system would become a reality, the system would behave closely to current Global Positioning Systems (GPS), or Inertial Navigation Systems (INS). From an industry perspective, this will allow the aircraft to confirm location information given by GPS, but acting as a self-contained system, similar to INS [6]. A GPS system would still have several disadvantages to a radar system. First of all, a radar system does not require other participants to have one in order to conduct the separation. Secondly, and more important for this project, the radar system will be self-contained and will not rely on external inputs to navigate. This lessens the reliance on GPS or other Navigation Aids, namely Non-Directional Beacons (NDB) or VHF Omnidirectional Range (VOR) , while also providing the aircraft with a system that allows it to independently navigate around the world. Apart from the aircraft industry, airports and Air Navigation Service Providers (ANSP) would also benefit from this technology, as the navigational system is completely moved on-board the aircraft, which makes beacons obsolete in the face of a GPS/Radar navigational pair, by lessening the expensive to maintain equipment and space.

On an academic level, a breakthrough in the area of navigation by on-board radars would allow for a new field of research of navigation and aircraft parameter determination. Furthermore, research of which type of radar is preferable for on-board navigation, or which frequencies are better for landmark detection also become accessible. Research based on the methodology of radar image analysis and coordinate computation can also be undertaken to provide a comprehensive view of this new field. Finally, radar navigation will add the necessary sensors, methodology and self-reliance to allow for advancements in the field of completely autonomous aircraft.

Following the Introduction, the next chapter includes the state of the art, where multiple examples are presented from adjacent industries or completely different and somewhat unrelated other fields than aviation. The research questions along with the aims and objectives are presented in the following chapters of this thesis. Next, the methodology chosen to accomplish this research is presented. Different techniques and methodologies will be discussed. Following this the results and outcome of the experiment are depicted. This report will then end with the conclusion section.

3.2. State of the art

The first operational airborne radar was on board the Messerschmitt Me 110 G-4 in 1941, using a bulky antenna outside the aircraft that managed an approximate range of 5 km [39]. The determination of target coordinate was at the beginning, only within the aircraft body frame. Only latter, with the advent of the Navigational Aids, was this extended to a global body frame. This was the very first time when such a radar system was integrated into the aircraft and opened the path for more research in this area. On this note, Selfly B.V attempts to continue the integration of such a system in GA, by developing a Collision Avoidance Radar (CAR) that uses Doppler information to detect the surrounding

around the aircraft[20], thus aiding the pilot during IMC.

Currently, two different researches conducted at TU Delft concluded the possibility to use an FMCW radar in order to determin aircraft parameters[35]. This, however, in not a valid method for long-term navigation, as the drift becomes too large over time [1]. One of the research attempted to use the CAR radar, specifically as a Side Looking Aperture Radar (SLAR) in order to allow for navigation purposes [11]. SLAR produce high resolution images of the surroundings, being usually used in missions to map the Earth's surface. The results showed no evidence that the modification of the CAR for SLAR would bring the accuracy of the navigation below CAT I ILS navigation systems (which entails Decision height above 200ft, Runway Visual Range above 550m or runway visibility above 800 m), linking the accuracy to the wavelength of the radar signal. The possibility to process signal of FMCW synthetic apertures is further upheld by literature [33].

Further in the literature, information with regards to SLAR [39] shows that this type of radar would normally provide the necessary accuracy to create a map where landmark information can easily be distinguished. They provide information with regards to reflected objects, ranging from smooth objects such as roads or water fronts, to farm lands and trees, but also to buildings. Displaying these differences in intensities of the received echoes, allows to produce a ground map of the terrain. Miniature SAR have been successfully designed and developed to be effective in the use of drones, with limited power requirements [39]. In order to be used on a commercial multi-purpose platform, a different system is required to satisfy the transmitter power and antenna size, as well as the receiver noise [1].

What follows next is to search literature in order to find whether SARs are being used for any type of navigation. Several research have posed the question of the possibility of using SAR Navigation and map aiding [28], [40]. Some remarks can be presented with regards to the literature on SAR being used for navigation. First of all, the computational power that was used to obtain these results is not mentioned, either if it was on-board of the aircraft, or used on the ground. This is a limiting factor for the computational possibilities found on aircraft. For reference, drones and UAVs with Jetson TX2 single board chips have more computational power due to the on-board Graphical Processing Unit (GPU) [4]. Secondly, the algorithms used work once every 120 seconds, the typical time for SAR image acquisition, during which corrections to the GPS/ INS navigation system are performed [40]. This completely excludes real-time functionality, which excludes the fusion system from being a primary system used for navigation and rather a correction brought to the conventional GPS/ INS navigation system. The same observations are found in another study [38], where SAR adds to the accuracy of the GPS/ INS system. Thirdly to the aforementioned remarks is the use of machine learning, more specifically, deep learning.

The use of deep learning or machine learning algorithms in such a circumstance relates to real-time use, availability of data and advances in computational power. The present software industry is moving towards machine intelligence. Machine Learning (ML) has become a necessary tool on all technology sectors. Quite forward, ML is a set of algorithms that parse data, learn them and apply the algorithm to future, intelligent decisions. The downside of ML is that they behave still like a machine, needing plenty of domain expertise and human intervention in order to work on a designated task. Here, Deep Learning (DL) holds more promise as it is not bound by domain expertise and not substantially by human intervention [23]. Practically, DL is a subset of ML that achieves higher power and flexibility through learning the representation of a system as a nested hierarchy of concepts[23]. A key distinction of DL is through the advent of "Big Data" era, where vast amounts of data become available for the algorithms to train on and learn better representations [44]. On the other hand, DL algorithms require high-end machines, where GPUs have become an integral part of the overall system. Fortunately, hardware is now available that specifically is tailored to work with DL algorithms [4]. Furthermore, these algorithms require a longer time to train due to the large possible number of parameters, where as traditional ML take a few seconds to a few hours. This has been taken into consideration in regards to this proposal as well as any follow-up work as the expertise of the author will play a major role in the decision of the type of algorithm to be used.

Literature in adjacent industries such as satellite image object recognition or drone sensing and navigation provide valuable insights on where to begin and how to setup a DL algorithm. Of course, SAR images offer a very high resolution which can be used to train DL algorithms, however, although the FMCW provided by Selfly can work as a SAR, the high resolution of an image is not guaranteed. What is left is to either make several assumptions or train a DL algorithm to recognize landmarks in the received data. Fortunately, The Stationary Target Acquisitions and Recognition (MSTAR) study

on the resolution of SARs have proven the possibility of low resolution target acquisition using DL[21]. Furthermore, the aforementioned study provides with an algorithm that does not require data sets with targets that were preset by other MSTAR SAR databases, i.e. end-to-end.

As mentioned before, DL requires vast amounts of data to train. Fortunately, in the case of SAR images, the database exists under the name of Sentinel 1&2 (abbreviated as SEN1&2) [31]. These databases are available under request, developed by the Sentinel Application Platform (SNAP) software. The free open source nature of the software aids in obtaining a database that can be used to train and test a DL algorithm specifically for navigation. It should be mentioned that two sets of databases are needed, one to train and one to test the DL algorithm. SAR images from the ESA database are preferable also as they already come with attached coordinates. This makes for a perfect ground truth in the testing phase. Ideally, the output of a DL algorithm is a set of coordinates along with a simplified version of the captured radar image that can be used to compare with the test database.

An effective strategy on roads segmentation in SAR satellite images using DL comes from a particular study [32]. This strategy converts the drawback of a SAR image into an advantage, namely, the fact that they do not reflect very well roads and water masses, such as lakes or rivers. Their low reflective coefficient makes them ideal candidates for building a template, of rivers and roads, that can be used as features for recognition. Another strategy that can be used is to segment all detected objects as much and as best as possible. Several studies help provide with approaches towards segmenting SAR images [19]. This is done using Fully Convoluted Neural Networks (FCNN) with feature extraction during training. As the literature suggests, Convolutional Neural Networks (CNN), or various variants of it provide a feasible answer. The work within this proposal will complement the work conducted in previous researches in the field of SAR navigation.

As it can be seen from the current state of affairs that was presented above, little to no research has been conducted on the subject of navigation using radar information through deep learning algorithms. However, adjacent fields of research have provided enough pieces of the puzzle, such that when put together, they provide a coherent path that can be followed towards a suitable methodology and experimental setup.

3.3. Research Questions

The research context can be established and includes airborne radar information, terrain recognition, image processing, data matching with image database using deep learning and aircraft coordinate retrieval. Furthermore, the scope of the research can now be elaborated as follows: The role of deep learning algorithms in the navigability of aircraft under VFR using radar data. With the research context and scope, together with the discussion from Chapter 2, one can proceed towards defining the objective:"The creation of a convolutional neural network that can extract landmark information from radar data and match it to a set map with known coordinates."

In order to proceed further, a definition for performance must be given. This is the accuracy of the results for a given algorithm per the computational time and e ffort. The literature implies that if successful results will be obtained, a measure in difference will be required in order to discriminate between multiple algorithms. Therefore, to achieve the scope presented above, a traditional template matching algorithm is necessary in order to better understand the whole process, after which to bring optimization choices. Building upon this strategy, a system consisting of a convolutional neural network can be built. From this, strategies to improve performance and assure real time capability can be undertaken. Based on this research strategy, multiple secondary research questions have been established to create a road-map.

With the research objective in mind, the research questions are as follows:
- Is it possible to identify landmarks in a radar data?
  - If so, which types are easily recognizable?
  - Can landmarks be recognized consistently through multiple iterations?
- Can the landmarks detected in one radar frame compound a unique template amongst the data?
  - If not, can another assumption be made to mitigate this?
- Can the same type of landmarks be identified in SAR image databases, such as the Sentinel1&2 databases, landmarks similar to the ones identified in the second question?
- Is it possible to deduce coordinate information through template matching of the map and radar

data?
  – Can the computation be done in real-time and how accurate is the result?
  – Can metrics be defined to calculate this?
- Can the same process of identifying landmarks in a radar frame of information and matching them onto SAR images be replaced by deep learning algorithms?
  – Which steps in the whole matching process can be replaced by deep learning algorithms?
- Do the steps replaced by deep learning algorithms lead to a better performance?
  – Can metrics be defined to calculate this and afterwards to compare?
  – How reasonable are the results in comparison to the metrics?

The aforementioned research questions are a good point that ensures the advancement of the research towards its objectives as well as providing invaluable checks along the way. Up to this point the research context, scope, objective and research questions were discussed. Therefore, the research framework starts with the understanding of how image processing works and what techniques can be used to best represent the radar data.

3.4. Radar principles and technology

The following chapter introduces the basics of radar (radio detection and ranging) that are relevant to the thesis. Additionally, some aspects of using Frequency Modulated Continuous Wave radars as Synthetic Aperture Radars(SAR) will also be displayed, as well as their importance to this thesis. It is important to present within this chapter some basic aerospace radar relations. More specifically, all parameters relevant towards mapping the range-radial velocity radar image onto the earth surface, under the form of a radar map. These calculations were provided by supervisor, Ir. Jerom Maas and are presented here more in-depth. A radar system can determine the relative position of the world around the aircraft, and this information can be used to find the actual aircraft state information. The main working principle is the emission of electromagnetic energy and the analysis of the reflected energy by the environment, or echo of a reflecting object. The echo can be used to determine the direction and distance and based on the radar frequency,the Doppler speed. Based on the type of technology, radar scan be categorized into multiple sets. A focus will be given to Frequency Modulated Continuous Wave (FMCW) radars, Side Looking Airborne Radars (SLAR), as well as databases based on Synthetic Aperture Radars (SAR). This is due to the radar database being recorded in FMCW radar in SLAR conditions. Most databases that encode geographical information are captured using SAR technology and that will be used for comparison purposes.

3.4.1. Frequency Modulated Continous Wave Radar

Frequency Modulated Continuous Wave (FMCW) Radar is a type of radar where the power radiated by the emitter is continuous[1], while also being able to change the range of frequencies with which it operates, either in frequency or in phase, as shown in Figure 3.1. Within the figure, δt is the difference in time, δf is the difference in frequency and f_D is the perceived Doppler frequency. It should be noted that it is unknown whether the original radio also modulated a saw-tooth signal, and the figure is used as an example.
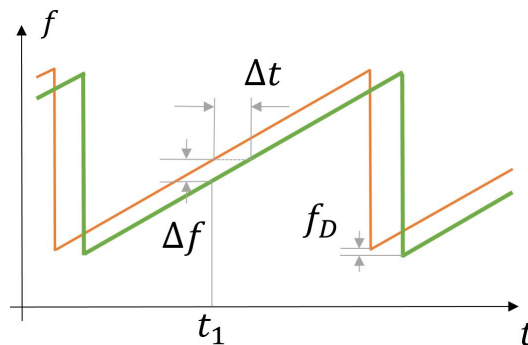

Figure 3.1: Saw-tooth modulation example of a FMCW radar with transmitted signal (orange) and received signal (green)

The main advantage of FMCW is the possibility to determine range with regards to other types of continuous wave radars[2]. Continues wave radars do not have the timing mark necessary that enables the system to have a timing function between the transmission cycle and the reception cycle. By frequency (or phase) manipulation, a time reference to measure distance towards stationary reflections is obtained. This is done by manipulating the change of frequency linearly over time. Through this, the radar behave closer to a pulse radar rather than an continuous wave radar, without measuring the run-time directly. With FMCW radars, run-time is measured by detecting the differences in frequency (or phase) between the received signals. FMCW radars have an advantage over other radars to measure relatively short distances to a reflected object. This is due to the fact that the minimal measured range is proportional to the wavelength). So far, reflected objects are considered to be stationary, however FMCW radars can measure their relative velocity with a high accuracy of range.

Principle of measurement

FMCW becomes a viable solution for measuring reflections in a pre-defined environment. Setting a pre-defined range for measurements greatly simplifies the comparison calculations further along the system, especially with regards to comparison techniques [22]. The following relation 3.1 calculates the distance R to an echo,replacing that the lack of pulse for normal radars with a change in frequency to determine range.

$$R = \frac{c_0 \cdot \mid \Delta t \mid}{2} = \frac{c_0 \cdot \mid \Delta f \mid}{2 \cdot (df/dt)} \tag{3.1}$$

Here, c_0 is defined as the speed of light (or $3 \cdot 10^8 m/s$, the time difference Δt along with Δf, the frequency difference between the when the signal is transmitted and the echo is received. And df/dt is the frequency uplift or downshift per unit of time. It can be observed that range is highly affected by the power of the radar and objects further away need to reflect more power to be detected [5].

Should the frequency change be linear over a wide range, yields a direct proportionality between the radar and the frequency comparison. In case that echo is not stationary, a Doppler frequency Δ_f that is added or subtracted from the received echo frequency, depending on the type of movement the object has in relation to the antenna.

The Doppler frequency is proportional to the speed of the aircraft as well as the wavelength of the transmitted beam [39]. Taking the radial velocity of a reflection on a earth fixed projection, it's speed is determined by $v_r = -V \cdot cos(\alpha)$, as a function of the aircraft speed V, and the flight path angle, α. This yields the previous mentioned formula for calculating Doppler frequency based on aircraft speed 3.2.

$$F = -2 \cdot \frac{v_r}{\lambda} = 2 \cdot \frac{V}{\lambda} \tag{3.2}$$

Range and Resolution Determination

The radar resolution can be determined through the deviation per unit of time. This offers an advantage over pulse radars with regards to setting a resolution as well as for the range, i.e. the longer the rising edge [1]. The bandwidth plays a critical role for determining the range resolution of an FMCW radar, as shown in the figure 3.3, shown below.

$$\Delta f_{FFT} = \frac{1}{T} = \frac{\delta(f)}{\delta(t) \cdot (f_{upshift} - f_{downshift})} \tag{3.3}$$

Where Δf_{FFT} is the smallest frequency difference that is measured, $\frac{\delta(f)}{\delta(t)}$ is the slope of the FMCW radar function and $f_{upshift} and f_{downshift}$ are the largest and smallest frequency configurations set for the radar. This equation determines the frequency at which the FMCW theoretically works as well as the linear frequency duration to achieve that [43]. With regards to the range resolution, the bandwidth is used as the chirp to determine the range. It is self contained and set to 5 km as per the experiment data, being determined by the frequency change.

3.4.2. SLAR

The concept of a Side Looking Airborne Radar assumes the transmission and antenna to be perpendicular to the flight direction [39]. The transmitted ray from the radar along the flight path detects two points in the earth fixed frame, symmetrically located along the flight path. This ambiguity is resolved by placing the radar in a SLAR configuration [39]. The radar beam illuminates a swath of land obliquely at right angles. Figure 3.2 shows a depiction of a SLAR concept, which can also be applied to a Synthetic Aperture Radar.
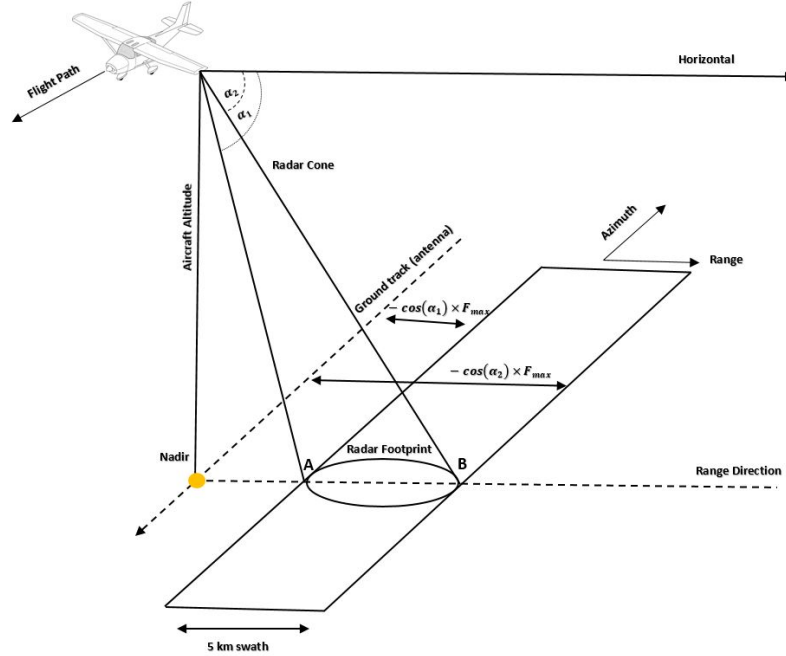

Figure 3.2: FMCW side looking radar concept

In figure 3.2, the altitude "h" is also where the first echo is detected, with its projection on the ground known as the nadir. With SLAR, specular reflection is usually very strong, adding noise to he captured reflections. As with all radars, the power of points decreases with the range at the fourth power, also being modulated by the two-way elevation characteristics of the antenna. The nadir is assumed to have no Doppler speed and can be used as a ground truth for correcting Doppler speed information. The azimuth range is defined as the dimension parallel to the flight track and calculated as a depicted in Eq. 3.4:

$$R_a = \frac{h \cdot \lambda}{L \cdot cos(\theta)} \tag{3.4}$$

Here, h is the height of the detector or antenna which is also assumed to the the height of the airplane, λ wavelength, L the total breadth of the antenna and θ overly incidence angle. It becomes obvious that increasing the altitude requires a longer antenna length to maintain the same resolution. This can be avoided with a SAR. Furthermore, the equation shows that the ground resolution is distorted towards the edge of the captured image, however within this experiment, the area is small enough to ignore.

The Swath width is defined as the part on the Earth's surface where data is collected[39]. Both the azimuth and the range are chosen within all databases to cover an area of 5 square km. The longitudinal area captured by the SLAR comes through the motion of the aircraft. SLAR have a real aperture, that normally require a fairly large antenna to record high angular resolutions. The following equation 3.5 determines the SLAR range acquisition[39].

$$R_r = \frac{c_0 \cdot \mid \Delta t \mid}{L \cdot cos(\theta)} \tag{3.5}$$

On a pulse radar, only the pulse duration is taken, however within an FMCW radar, this is simulated by difference between the two upshift and downshift frequencies [3]. 3.5 depicts the increase in resolution with regards to the azimuth in relation to the altitude. However, this can also be done via Synthetic Aperture Radars, to acquire a higher resolution.

As discussed in the previous chapter, it is possible to use FMCW radars as SLAR, relating reflected objects in a range and radial velocity matrix. This assumes that any coordinate in the earth fixed coordinate has a corresponding echo that is expressed in the range-Doppler velocity, located in the aircraft fixed frame[39]. Equation 3.6, depicts the mathematical formulation of the relation between the echo coordinate on the ground and its range and Doppler velocity. This equation was fully provided by the supervisor Jerom Maas.

$$F(x,y) = \begin{pmatrix} x \\ \pm y \end{pmatrix}(r, v_r) = \begin{pmatrix} h \cdot tan(\gamma) - \frac{v_r \cdot r_r}{V_{a/c} \cdot cos(\gamma)} \\ \pm \sqrt{r^2(1-(\frac{v_r}{V})^2) - h^2} \end{pmatrix} \tag{3.6}$$

Here, the x and y coordinate translation of a reflection are calculated using the altitude h, speed V and the flight path angle γ, as well as the Doppler speed and range of the object, v_r and r_r. This equation translates the range and Doppler velocity measurements of any reflected points to a 2D map consisting of coordinate points in a 5 square km area, using flight parameters. Due to measuring the slant range, SLAR create several distortions, with regards to elevation and range, and due to the altitude, as well as with occlusion. These conflicts are resolved when using a Synthetic Aperture Radar (SAR), that removes the dependence of the azimuth resolution on the incidence angle. By limiting the SLAR emission of radar waves sideways, it solves the problem for object ambiguity, as it can be seen in Fig. 3.3. Object ambiguity is the radar wave problem where for each range-Doppler velocity pair, two other points that are reflected on the surface with their positions being symmetric to the flight path.
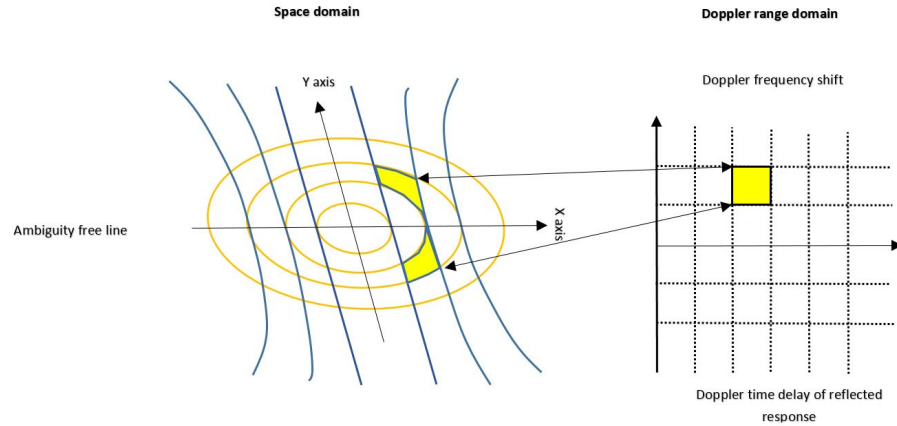

Figure 3.3: FMCW Resolving of Ambiguity

3.4.3. SAR

A Synthetic Aperture Radar (SAR), is a type of SLAR that electronically reproduces a large antenna aperture by using the aircraft flight path [2]. This generates a very high resolution imagery of the selected area. Over multiple runs at slightly different configurations, especially with regards to position, a database is being created electronically. The signal is processed from a magnitude and phase point of view and after a multiple series, the data is merged into a very high resolution image of the terrain. Figure 3.2 also depicts the same working principle for a SAR. The difference is with the SAR behaving similar to a phased array, or multiple antennas that is capable of detecting multiple transmission at different phase shifts, all incorporated in one antenna, using the movement of the aircraft to simulate the different geometric positions [2].

The returned signals are all stored in accordance to amplitudes and phases at a certain time stamp. This allows the reconstruction of the signal which normally would need an antenna of length $v \cdot T$, where is the platform speed and T is the time. A synthetic aperture is produced as the line of sight changes, which lengthens the antenna. This increase the resolution of the antenna by making T extremely large.

Any reflection from one object is recorded multiple times and as the aircraft moves forward, as long as the object is within the beam. The resolution however remains constant due to the combined expanding beam width that is synthesized and the increasing time. The azimuth resolution is proportional to half the breadth antenna has, hence multiple small slices are required over time to build an entire area[2].

Several assumptions are made in order to achieve the creation of a synthetic aperture image:

- Constant relationship between oscillations and electromagnetic waves, or coherence.
- A powerful processor that computes the different slices;
- Exact knowledge of flight parameters, such as the flight path and velocity.

3.5. Scope and limitations

The main scope of this research thesis is the investigation of feature identification or recognition within FMCW radar imagery taken in SLAR conditions as well as within SAR or Google databases. Furthermore, robustness is to be verified with a suitable comparison metric. Appendix 4.3 also presents how the Sentinel 1 [31] are polarized.

Among various research topic regarding the Navigation through terrain recognition, this MSc Thesis' scope is mainly related to computer vision applications within the aerospace industry:

- Radar systems
- Feature recognition and comparison
- Image segmentation
- Noise removal

The focus is on feature recognition techniques that can afterwards be incorporated into navigation strategies. This implies the investigation of having an on-board database that is used to identify features at a location given by GPS coordinates and compared to a 2D transpose of radar reflections, named the radar map. This radar map is constructed using certain flight parameters and as some of them were not defined, they were deduced from other available data. An example is the heading that was calculated from GPS coordinates, that does not take into consideration wind velocity and direction. As such wind is assumed to be negligible with regards to the impact of the final comparison. The flight path angle used in equation 3.6 was again calculated using altitude readings.

3.6. Comparison databases

Within this section, all comparison databases are presented as well as how they were obtained. Several examples and trade-off will be illustrated and an explanation will be provided in order to justify certain design choices.

3.6.1. Radar database

As presented in the previous chapter, it is possible to employ a FMCW radar in SLAR configuration to obtain echos of reflections within the environment and map them on a 2D translation in the aircraft reference frame [35]. This provides a 2D matrix with the X and Y coordinates as well as encapsulating the intensity of each pixel. Following is to represent this matrix under the form of the radar map. Two methods were chosen namely, 2D histogram in Fig. 3.4 as well as a scatter map, presented in Fig. 3.5. Using equation 3.6, three vectors are computed relating to the X and Y coordinate in the aircraft reference frame, encoding the third vector containing the intensities of all reflected points. This data can be visualized under the form of a 2D density plot or 2D histogram as presented in Fig. 3.4.
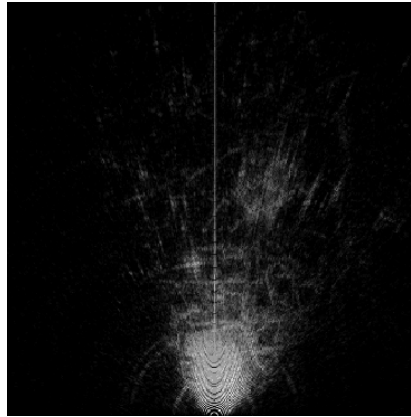
Figure 3.4: Histogram representation at second 1000 of GPS record start

A 2D histogram is a function that shows the occurrence of combination of intensities between two data sets. As a comparison, a 1D histogram display the total number of elements with a particular value occurs in the data set [37]. A 2D histogram shows the intensity relationship at each exact position between two data sets. When adding this third intensity vector as a weight factor to the function to further discriminate the intensity relation ship between the two coordinates, the 2D Histogram becomes suitable to map the radar reflected intensities in a 2D plane [37], in the aircraft reference plane as shown in Figure 3.4. Additionally, alternatives methods of mapping have been considered under the scatter function, or a graph in which the values of two vectors are plotted along two axes, similar to the 2D Histogram, using intensity to create the grayscale. It becomes clear that for the same settings, the scatter map presents more details that can be used in future image transformations. The second method was chosen as part of all other future experiments.
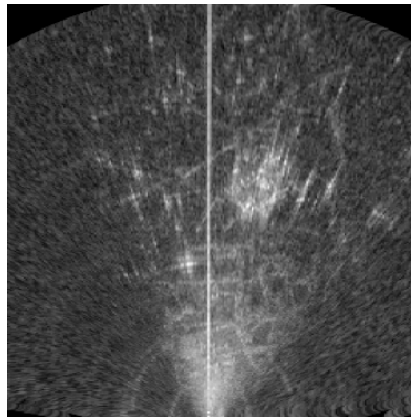

Figure 3.5: Scatter representation of the same image

3.6.2. Google maps and Sentinel 1 databases

Having computed the radar map, it becomes increasingly useful to have an equivalent map for comparison purposes. Theoretically, several features should already be visible and show similarities for roads. Google maps allows the visualization of either a satellite or a vectored depiction of the roads for a certain central coordinate. The mathematical maximum of both calculated X and Y vectors is a

distance of 5 km, which is the maximum mathematical area in which the antenna can detect reflections. The region is overlapped onto a Google image to show what the radar can detect. Within Figure 3.6, a vectored Google image along side a Sentinel 1 map are depicted for the given GPS coordinates at second 1000 from the start of the GPS reading. In future iterations, the use of a SAR database will provide additional accuracy, especially towards the intensity of the detected points, as they are proportional to the frequency and emitted power. This will provide a direct link between SAR and FMCW intensity reflections. The databases considered are the Sentinel 1&2 databases [31] for their good resolution.
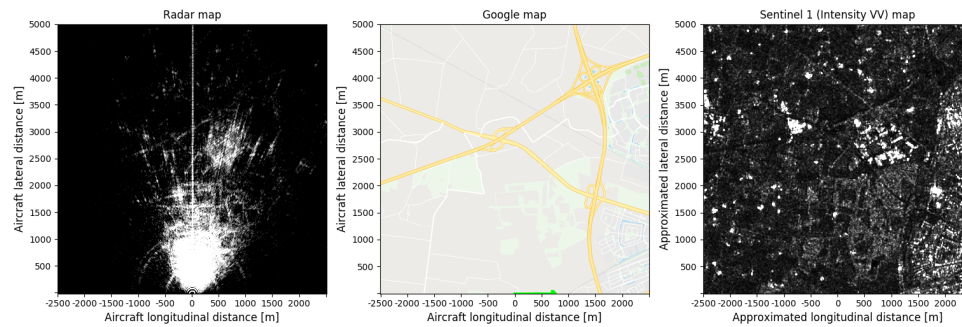
Figure 3.6: Histogram (left), Vectored road map Google (middle), Sentinel 1 (right)

3.7. Methodology

The following chapter presents the research methodology used to answer the research questions, the research approach, as well as a description of all used algorithms, along with data analysis techniques, metrics for measurement and adopted research method.

3.7.1. Hypothesis

This section introduces the hypothesis that will be tested during the research along with the resources that will be used. The first hypothesis to be tested relates to the possibility of a connection between radar information and coordinate determination. Although the literature implies that there is a connection between radar information and the landmarks identified within [32], the efficiency of deep learning algorithms on detecting coordinates information from the radar is not yet known[16]. The second hypothesis is whether a strategy can be created such that real-time performance is achieved. Therefore, the theoretical basis that will assure the research objective is set in motion. The research splits in two blocks, one that deals with image processing and one that does template matching. Ideally, both of these procedures should be done by a, modular or fixed, deep learning algorithm in real time.

The consequence for on-board radar systems is that they may also be used to provide assistance in navigation and attitude determination [6]. Clear reflections of the ground can be observed from radar images taken mid-flight, in which structural reflections are distinguishable. These reflections originate from ground elements, such as rivers, highways, lakes, forests etc. It would be possible to determine the locations of these ground structural elements by using Direction of Arrival Estimation (DAE), algorithm which makes use of the propagating wave arriving at a certain point[2]. This provides the basis for creating a new radar map, a translation from the radar distance and Doppler velocity reflections to their positions on a 2D plane depicting the distance from the antenna. Within this radar map, certain features become apparent. These features either present geometrical or intensity consistency and together can be used as a unique template. The task of image processing algorithms is to segment the image in a robust way to ensure the same template identification in both the radar and satellite databases. Due to radar noise, as well as the absence of a ground reference, the use of additional information from GPS and

flight parameters becomes of paramount importance. Furthermore, the process needs to be conducted in a timely manner and with the advances in machine learning and computer vision, more specifically with the almost complete dominance of systems built on top of Convolutional Neural Networks, deep learning will also be considered [23]. However, due to the lack of a solid database upon which a deep learning algorithms can be trained, only pre-trained algorithms will be treated. These algorithms will mainly focus on image segmentation within Synthetic Aperture Radar (SAR) imagery, in order to offer a suitable comparison for future research.

3.7.2. Noise and non-linearities

The following subsection presents the analysis with regards to noise and non-linearities present within the image. This analysis was conducted in order to cover as many techniques as possible to account for noise as well as for the intensity of reflected object that are further away, that drops in value by the range to the fourth power. The properties employed by FMCW radars in a SLAR configuration allows for feedback that supersedes normal reflections intensities, under the form of noise. Additionally, due to the fourth power rule, intensities of reflected objects further away from the antenna are not as strong as those closer. This produces a "drowning" effect of any echos further away than half the range of the area being recorded. While analyzing the histogram of the original radar image, the same non-linearity can be observed. Attempts to artificially linearity this particular non-linearity via a power of the range. Finally, a technique to linearize taken from statistical literature for non-linear statistical system based on [17] was also employed.

Fig. 3.7 shows the original histogram, followed by the histogram modified as a function of the range, as well as statistical analysis. It can be observed that the result is not completely linearized and as such, intensities that are close to the antenna are still high. As such, other techniques to account for this non-linearity are required, as presented in the research paper. Furthermore, due to system performance, or because interference between the emitter and the antenna, additional noise is being detected. With this into consideration, several de-noising techniques are taken into consideration.
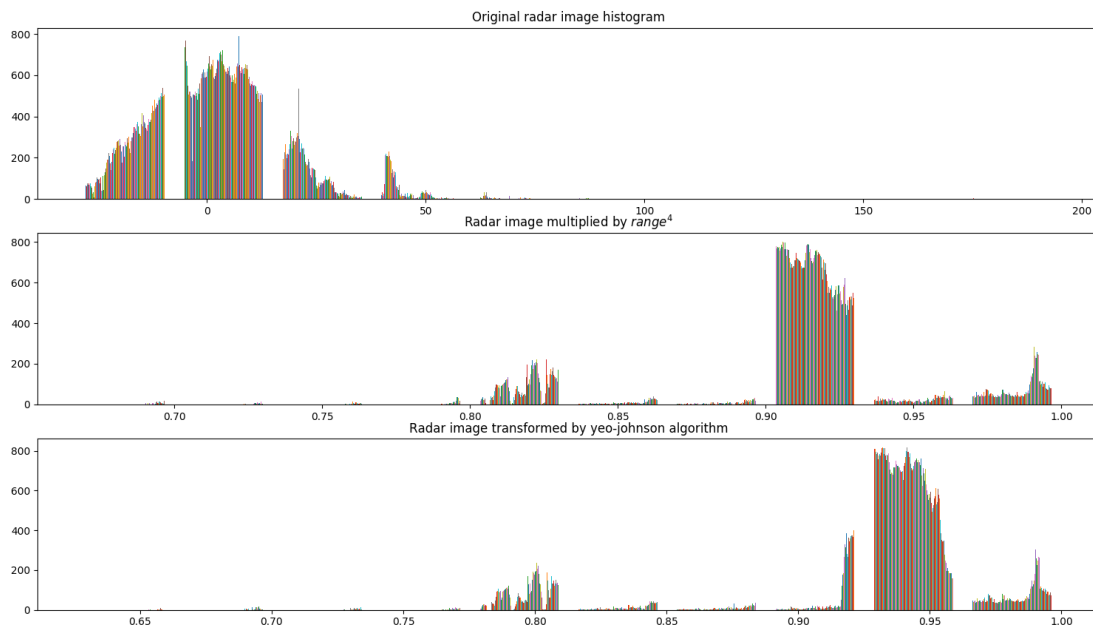

Figure 3.7: Histograms of different methods to transform non-linearities within the image

The first one was the Mean Filter (Me-F) [25]. Altough the Me-F does not remove speckle noise, it manages to reduce it to a moderate extent. Me-F works as the average around a center pixel, replacing all pixels in the selected area by the calculated average. The filter has a tendency of blurring the image and thus removing information that was considered important, especially with regards to a structural comparison. Formula 3.7 below depicts how the algorithm works:

$$h(i,j) = \frac{1}{mn} \cdot \sum_{k \in m} \sum_{l \in n} f(k,l) \tag{3.7}$$

Following, the Median Filter (Med-F) was used [25]. The center pixel is now interchanged by the median value of surrounding ones within the selected area. This technique better preserves edges, however, heavily burdens the computational speed.

The Lee Filter (LF) [25], is a very well known technique employed in the de-speckling of SAR imagery, being based on a local statistical analysis to preserve edges. The LF performs smoothing over predetermined areas that have a low variance, compared to the maximum computed within the image. This allows to preserve details within the image, even when high differences in contrast are present. The mathematical model for the Lee filter is presented below:

$$Img(i,j) = M_i + W \cdot (C_p - M_i) \tag{3.8}$$

With equation 3.8 the new image is computed via the mean pixel intensity of the filter window M_i, times the intensity of the center pixel C_p minus the mean pixel intensity over the filter window W. A distinct disadvantage for the filter is the inability to denoise the image near edges[25]. Finally, instead of focusing on each pixel within the radar image on a local level, a Non-local Means De-noising (NLMD) algorithm was chosen [cite]. This is usually employed in visual imagery and videos and was chosen with regards to the radar database. The property of noise is considered to be a random variable that has a zero mean. Constructing multiple areas and taking their average provides a better metric that reduces noise. Below, Fig. 3.8, shows the employed techniques, it can be observed that the NLMD provides the best results, however it also smooths features that are considered important in a structural context.
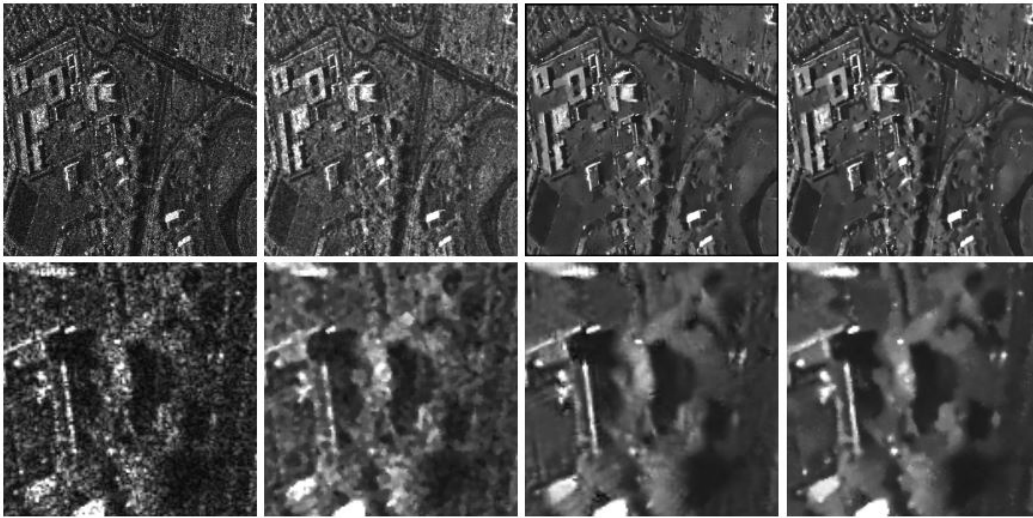

Figure 3.8: All four denoising techniques on different images with Me-F first, Med-F second, LF third and NLMD fourth

As small features such as small streets or dirt roads present within the image may have played an important part in the experiment, a higher importance to image transformation techniques that did not containing de-noising was finally decided. Additionally, some considered algorithms incorporate a form of median filtering under the form of Gaussian transformations, further motivating not using de-noising techniques. With the results of the final experiment taken into consideration where it became evident that only large features are important with regards to the comparison, applying a de-noising technique may improve results.

3.7.3. Metrics

In order to compare two templates from their designated radio or Google/SAR databases, a comparison metric is necessary. The used comparison metric is the Structural Similarity Index Measure(SSIM). Two other metric types were also chosen, namely the Mean Square Error (MSE) along with the Peak to Signal Noise Ratio (PSNR) [9]. They are introduced in the following section with a test to determine which ones should be used.

The MSE, also known as the mean square deviation is a measure of the average of the square errors [9]. One reason for employing this measure is due to its simplicity as well as being used as a measure of quality, where values that are as close as possible to zero are the best. The MSE incorporates the variance of difference alongside the bias, which would allow an estimation of the quality of a comparison as well as the actual value of the comparison. Equation 3.9 shows how the MSE is calculated:

$$MSE = \frac{1}{n} \sum_{i=1}^{n} (i_O - i_C)^2 \tag{3.9}$$

Within equation 3.9 the evaluation between the radar image value and candidate is squared and mean to yield the MSE. The Peak Signal to Noise Ratio (PSNR) represents the fraction of nois in relation to the maximum power of a signal [9]. Under nominal image transformations, the PSNR represents a good representation of the original radar image and its comparison image, identifying relevant noise within the taken radar image. The Structural Similarity Index (SSIM) The SSIM is a metric for measuring the similarity[18], based on luminance, contrast and structural correspondence, as shown in equation 3.10.

$$SSIM = \frac{(2\mu_x\mu_y + c_1)(2\sigma_{xy} + c_2)}{(\mu_x^2 + \mu_y^2 + c_1)(\sigma_x^2 + \sigma_x^2 + c_2)} \tag{3.10}$$

SSIM requires two images that are identical graphically and bounded within the same size. This is of great help with regards to the predetermined area captured by the FMCW radar during the flight [9]. When comparing the perceptual difference between the two similar images, luminance, contrast and structure is taken into consideration. Although it cannot decide which of the two images is better or the original, it can detect the difference in structural similarities of even to a 1°as shown in Fig. 3.9.
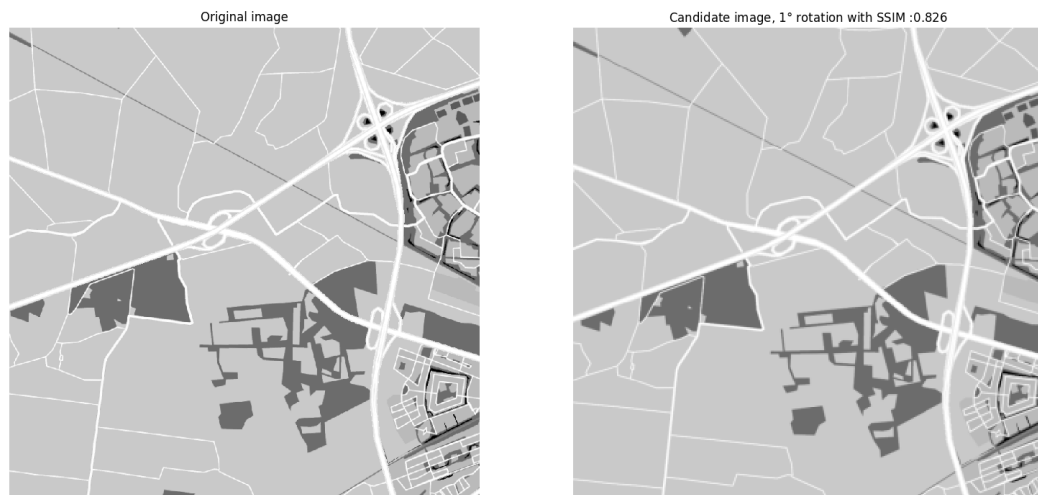

Figure 3.9: SSIM calculation for the same image with 1°of rotation

Following the introduction of the metrics used, a test was conducted to decide the final one. A total of 4 images were chosen in order to conduct the experiment from the radar database and the experiment setup was similar to the one presented in the research paper. A total of 500 random coordinate points were created and analyzed for the probability density distribution especially. Each pair had a MSE, PSNR and SSIM calculation attached for images with no transformations conducted. Although the results in table 3.1 are of poor quality in the context of the experiment, the SSIM still provided a low number of false positives, which increased with further transformations with regards to structural and luminance changes.

Table 3.1: Average results for heading deviation, position error and SSIM values over all experiments.

| Method | Average results for selected metrics | | |
	Absolute Heading Deviation	Position error	False Positive
MSE	10	108	53%
PSNR	12	120	67%
SSIM	8	80	42%

The MSE will be calculated for each pixels within every image pair. The SSIM will look for similarities in luminance, structure and contrast in each pixels[9]. This means that if the pixels have the same or similar density values, it will increase the overall calculated value. It becomes obvious that the MSE has arbitrarily high numbers and in a final examination it will be harder to standardize it, even though the higher the MSE value, the more it is indicated that the compared images are not similar. The results presented in table 3.1 that SSIM is the metric that best accommodates the needs of the results.

3.7.4. Selected algorithms

The following section presents a more in-depth view of the image transformation algorithms used within the whole experiment. A focus was given to chosen algorithms that were robust to noise. All selected algorithms attempt to segment the image and produce a mask that contains only detected objects. The targeted features that are taken as detected objects are either structural consistent features, such as roads, or highly reflective objects, such as industrial roofs. Within Fig. 3.10, an example of both is being presented for an image corresponding to second 1000 from radar start. It can be seen that the image presents both roads as well as an industrial site in the middle that is highly reflective. Ideally, an algorithm will be able to detect either of them in a consistent way.
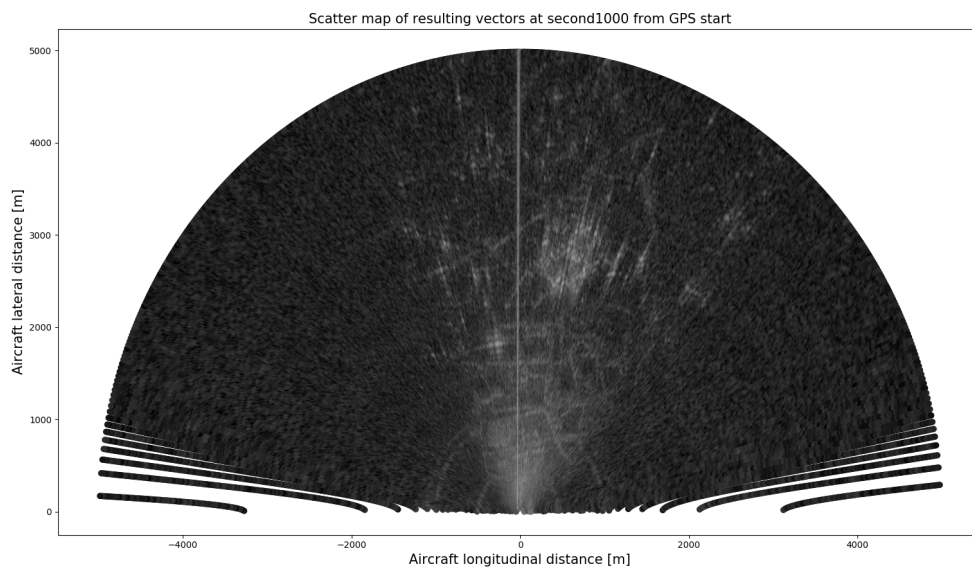

Figure 3.10: Scatter representation of the same image

Gamma Correction

Gamma Correction (GC) is a nonlinear transformation of the intensity within each pixel in a given image, based on the following equation $R_F = (R_I)^\gamma$:

Within this equation, R_F is the resulting intensity, as a function of the initial value for the intensity, R_I, raised to the power of γ [34]. As a power-law of γ, it follows that in order to bring darker parts within the image, γ needs to be less than 1. As it results in a nonlinear function of the input intensity, it was chosen as a suitable algorithm to treat the non-linearity present within the radar images. Figure 3.12, shows values for γ and how it affects the relation between the input and the output value for a grayscale input with values up to 250. This allows to set a value for γ that best fits the inverse of the linear approximation taken for the histogram of the input image. A γ value between [0.04,0.1] should provide a good approximation for future experiments [34].
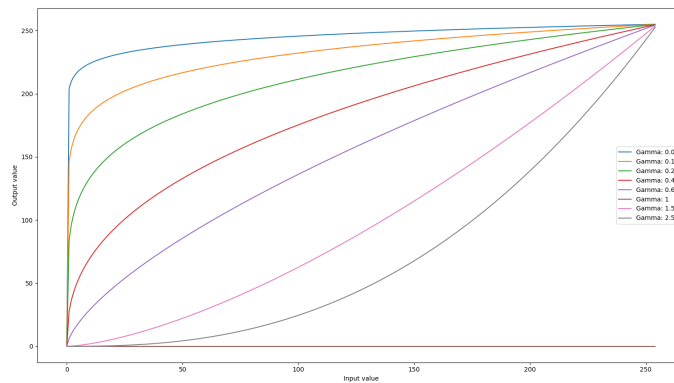
Figure 3.11: Gamma plot for different γ values.

An example of a satellite Google image at time-step 1000 is shown below in Fig. 3.12. Within the image, structures that are further away from the antenna become more apparent and allows a more robust detection for the experiment. Of course it should be noted that this image transformations brings new pixel values that need to be analyzed as part of any future transformations.
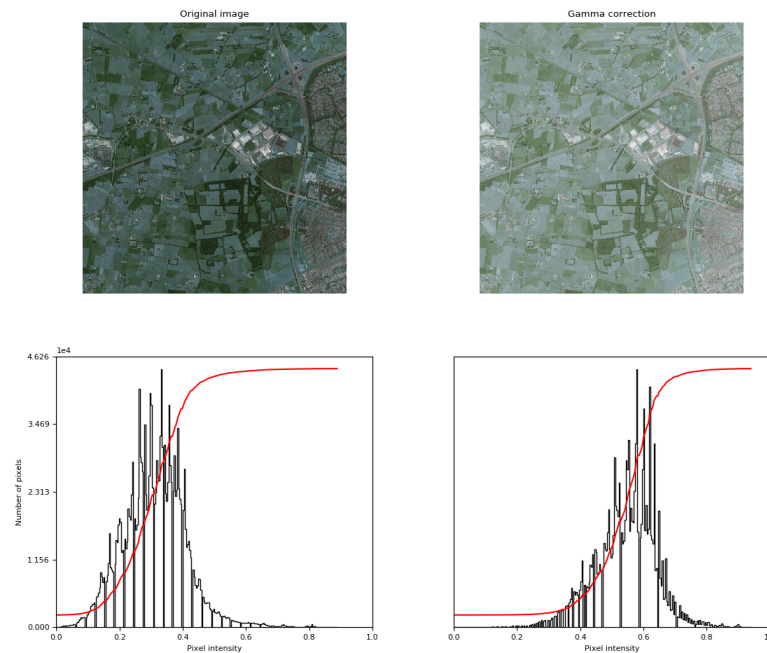

Figure 3.12: Original image (left) and gamma corrected image (right) with histograms shown below

Thersholding

Applying thresholding techniques is a simple image transformation that uses a certain value to filter the whole array of pixels. For each value, if the pixel value exceeds the threshold it will be accepted in the mask of the image, otherwise its value is set to zero. Two thresholding techniques become apparent here. One is where the thresholded pixel values are set to 1, called Binary Thresholding. The other is where the pixel value greater than the selected threshold are maintained in the mask of the image, where all values are either zero, or higher than the threshold, called Thresholding to Zero. Thresholding to Zero is advantageous when within an image a threshold is applied for unnecessary information and all other information needs to show variations. It is a good image segmentation technique, however, as both databases are captured in different wavelengths or transformed in RGB, slight variations are unnecessary. As such, the choice for Binary Thresholding becomes apparent, not only due to scope, but also due to performance. Figures 3.13 and 3.14. shows how the algorithm works for the Google and Sentinel 1 databases.
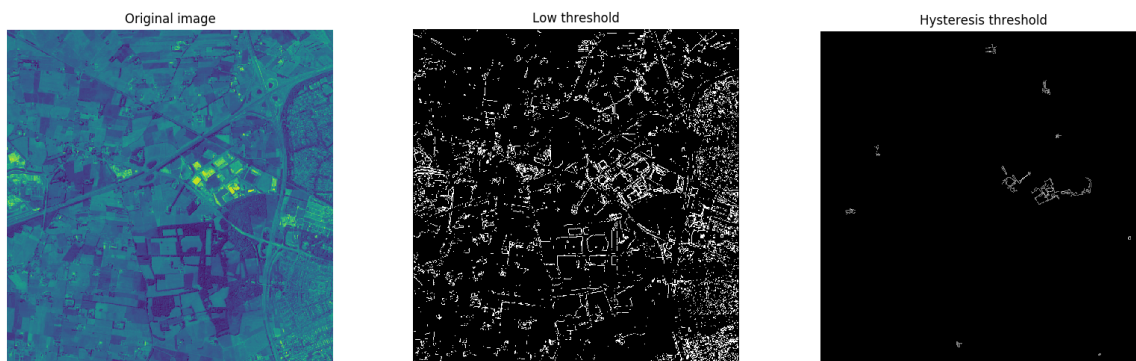
Figure 3.13: Google image for GPS at time step 1000, followed by a low binary threshold and a 80% or higher hysteresis threshold
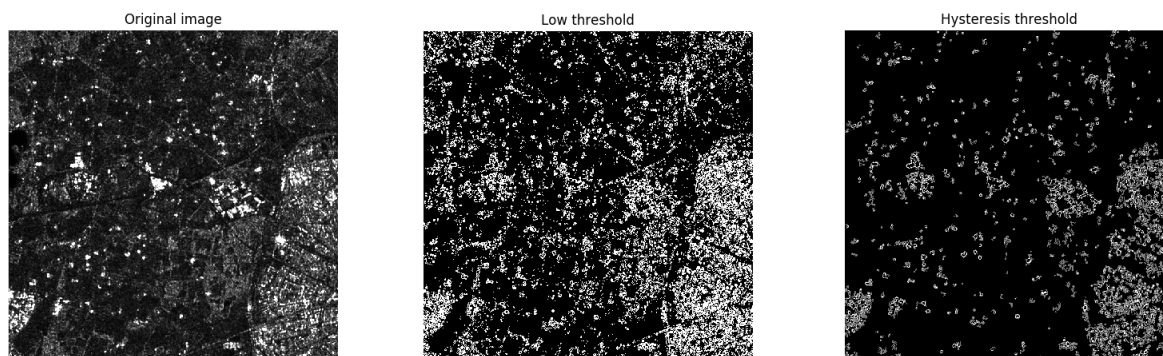

Figure 3.14: Sentinel 1 image for GPS at time step 1000, followed by a low binary threshold and a 80% or higher hysteresis threshold

Local Histogram Equalization

Histogram Equalization(HE) is a image transformation method that uses the image's histogram in order to gamma correct the image, as shown in [18]. Local Histogram Equalization (LHE) uses only a selected area within the image that equalizes the intensities within the image. An image that has an area with low contrast such as the FMCW radar database will spread out frequent intensities within the whole image, creating the effect of raising the contrast of the image [18]. This enhances many details within the image, by gray transformation. This however, produces a total modification of the image from an intensity point of view. This means that only structural features within the image can be taken into consideration. However, the modifications produced are very favourable towards structural features. In the case of the research, the equalization is done to an excellent degree the histogram of the FMCW radar image, as it linearized the non-linearity distribution. Within Fig 3.15, both equalization methods

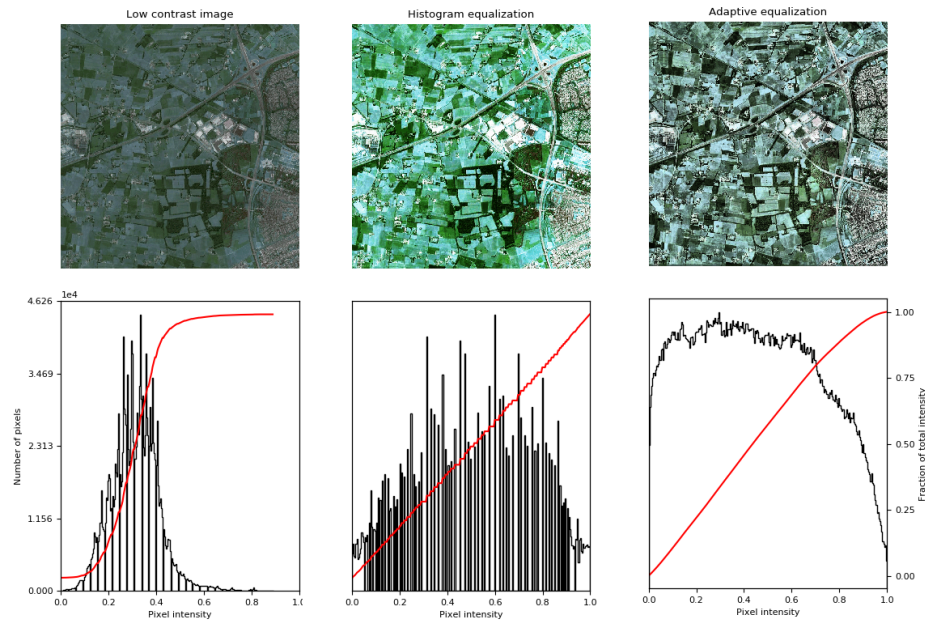are presented, with a focus on local histogram equalization.

Figure 3.15: Radar image (left) with its histogram below, global histogram equalization (middle) and adaptive local equalization (right)

Contour Finding

Contour can be defined as a curve that follows all continuous points along a boundary, that present intensity similarity. The resulting contours can be used as a the basis for object detection and recognition [30]. The accuracy of contour finding increases with binary image, being an ideal second image candidate. It should however be noted that some noise is forwarded into the final mask that will be used by SSIM for comparison. However, the process begins with a Gaussian filter that reduces noise, along with any fine details within the image that cannot be distinguished from noise. Eq. 3.11 represents the Gaussian transformation of the image, a sdepicted in [30].

$$G_\sigma = \frac{1}{\sqrt{2 \cdot \pi \cdot \sigma^2}} \cdot exp(-\frac{i^2 + j^2}{2 \cdot \sigma^2}) \tag{3.11}$$

Afterwards applying a threshold on the image, where the thresholding parameters ensures all edge elements will be forwarded, while suppressing noise. Figure 3.16 shows an example of detected edges within an image used for the experiment.

Figure 3.16: Contour identification for the vectored Google database at radar image 1000 seconds after GPS start

Ridge Operators

Ridge Detection (RD) is an image transformation that attempts to detect edges in an image. It was first introduced in the medical industry [36], in order to detect blood vessels taken by radio imagery in extremely noisy conditions. It functions similar to contour finding by applying a Gaussian filter or operating on the Hessian matrix[reference]. To define a ridge, a set of points where the local maxima of the function show a gradient for one direction. With regards to our image within, a ridge is considered over any number N of pixels if the gradient is constant for N-1 pixels. This behaves quite similar to a local minimum.

Within the image, ridges are considered to be structural features, such as roads, rivers, highways or blood vessels [36]. The algorithm works well with elongated objects within the image and extremely robust. Fig. 3.17, presents the segmentation of the image.
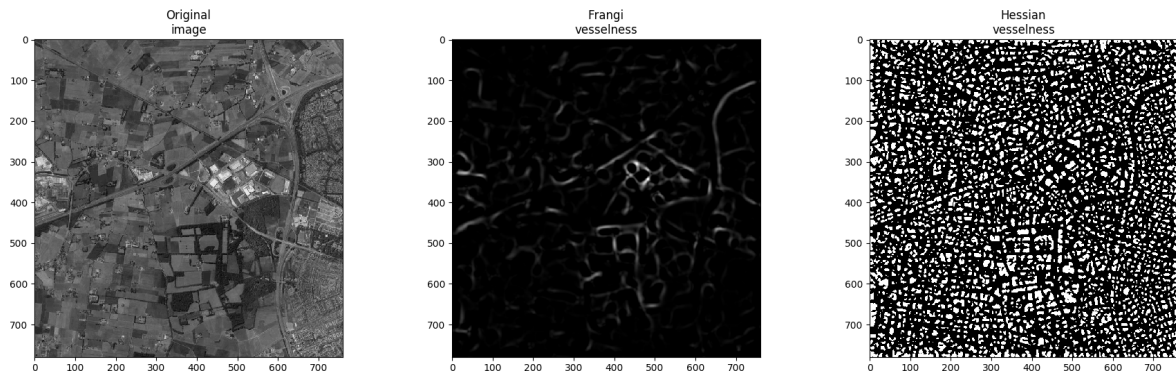
Figure 3.17: Original image next to two ridge operators: Frangi (middle) and Hessian (right)

Straight Line Hough Transfrom

The Straight Line Hough Transform (SLHT) [14] is an image transformation technique that attempts to detect lines within an image at any rotation that meet the following equation:

$$y = mx + c \tag{3.12}$$

Here, m is the gradient, y is the intercept and c is fitting constant. In order to avoid the equation to go to infinity for vertical lines, a perpendicular segment to the line is constructed that converges at the set origin. SLHT is characterized by its r as the length and an angle θ with regards to the x-axis. Lines are then saved in a histogram array that defines the parameter space, encapsulating the angle and range at which lines are detected as taken from [14]. This technique works very well with binary images, local histogram equalization also being a good candidate. A local maxima found within the calculated histogram indicates that certain ranges within it are potential candidates for lines.
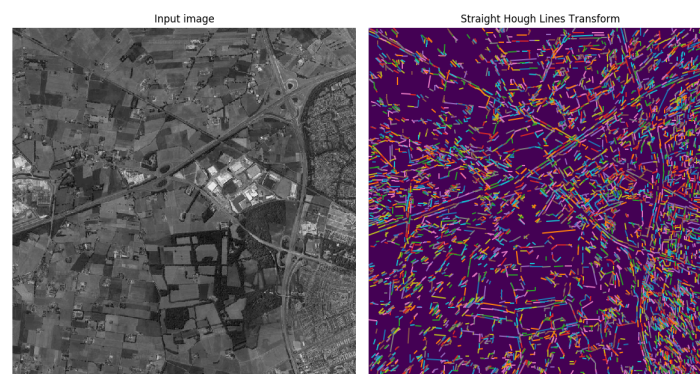

Figure 3.18: The original Google satellite image next to the the hough line transformed image

Blob Detection

Blob is a misnomer commonly accepted within the computer vision industry to define a group of pixels that share a common property. Within the constraints of the thesis, this common property is the intensity of pixels that compound a highly reflective object. The method works very well with thresholding techniques to group connected pixels in a binary image. Additionally, to ease the calculations, a center and radius calculation along close enough objects to approximate their center and radius. Blob Detection is an appealing technique to search for highly reflective points that are thresholded from background and most noise [13]. Taking the second derivative of Gaussian for a function g, or the Laplacian of the function g, in x and y coordinates is represented below inf Eq. 3.13:

$$\nabla_n orm^2 = \sigma^2 \cdot (\frac{\partial^2 g}{\partial x^2} + \frac{\partial^2 g}{\partial y^2}) \tag{3.13}$$

This provides a scale which can be used to determine the maximum of the Laplacian to $\sigma = r * \sqrt{2}$, where r becomes the approximate radius that covers the blob or group of blobs. The algorithm take the convolution of scale-normalized, or fixed length, Laplacian calculations at several different scales[13]. Finding the maxima of squared Laplacian response within the scale space ensures an approximation of the blob, as presented in Fig. 3.19 and 3.20.
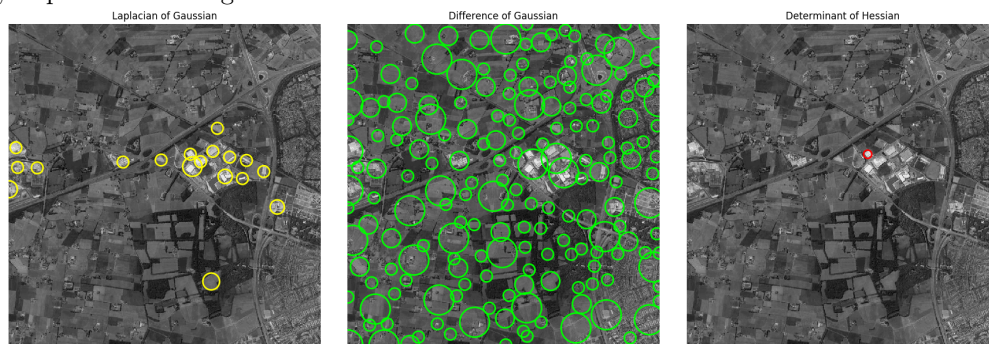

Figure 3.19: Blob Detection applied for the Google satellite map, for radar image at point 1000
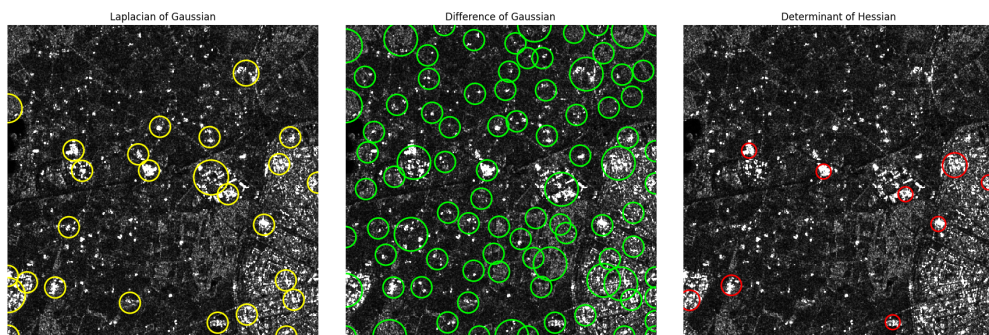

Figure 3.20: Blob Detection applied for the Sentinel 1 satellite map, for radar image at point 1000

In optimal conditions, it can be observed that the difference of Hessians, although being the fastest algorithm, does not always detect a good amount of objects. In contrast the Difference of Gaussians method for blob detection has an extremely high amount of detected blobs. This does not work very well as a more consistent method is required to avoid false positives with the radar image. Although the slowest, the Laplacian of Gaussian provided the most robust method for detecting methods overall. Furthermore, within the Sentinel 1 database, more points are detected overall and their consistency is more valuable as it is in the same or similar spectrum as reflective echos detected by the radar. Additionally, based on settings, the blob region can be increased to take into account surrounding noise and thus slightly increase the consistency.

Entropy Detection

Entropy Detection (ED) is an image transformation algorithm that relates the complexity of intensities within a given neighbourhood [42]. This complexity is defined by a structural element and can detect variations in gray level distribution.

From a computational level, ED yields and array that contains the local entropy, which is computed using a circular disk of a given radius. Different sizes will affect the overall detected entropy. The value in the image can be used for segmentation of structural features, which is helpful for the chosen metric. Entropy is defined by the equations below, through calculating a gray level co-occurrence matrix, using the described radius as a given offset as shown in Eq. 3.14.

$$-\sum_{i=0}^{n-1}\sum_{i=0}^{n-1} P(i,j) \cdot log_b \cdot P(i,j); \tag{3.14}$$

Here,we have a total number of gray scales, represented by N, while P is represents the likelihood of a pixel to have an intensity within the area with a logarithm base function b, representing the average rate at which information is produced by the stochastic source. In short, using a sliding window of a certain range to calculate the entropy within the area for each pixel[42]. Additionally, it is also possible to calculate entropy over a moving window within the image. The window moves one pixel at a time and local entropy is again estimated over a centre pixel within the selected radius as shown in the following equation, where $\sigma(X)$ represents the sliding window, in Eq. 3.15:

$$-\sum_{i=0}^{n-1}\sum_{i=0}^{n-1} p(i,j) \cdot log_b * \sigma(X); \tag{3.15}$$

The following Fig. 3.21 represents the entropy transformation of the Google image. This image transformation works very well with local histogram transform.
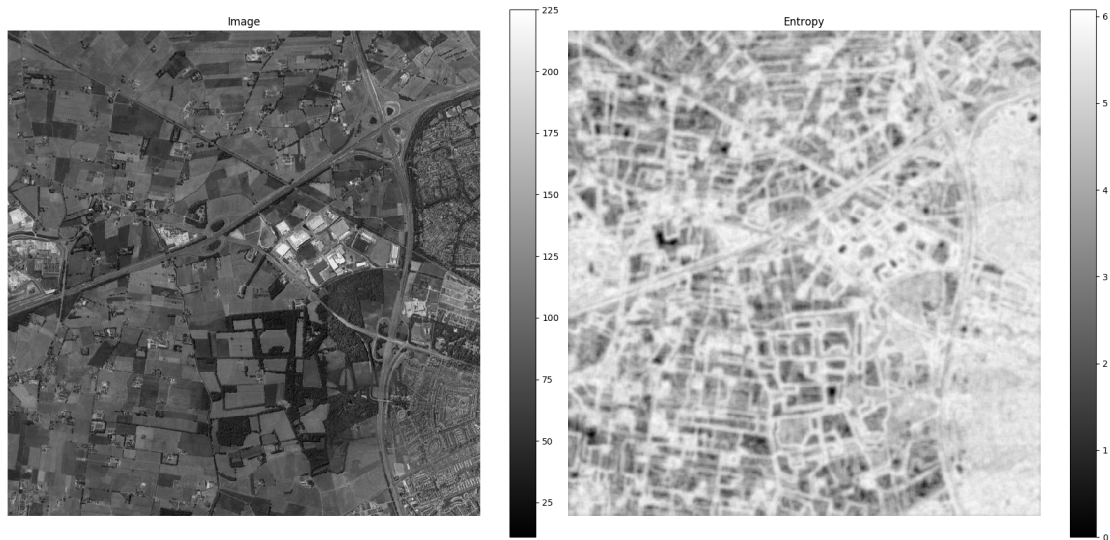

Figure 3.21: Entropy Detection applied for the Google satellite map, for radar image at point 1000

Watershed

A marker controlled Watershed is an image transformation algorithm that interacts for a grayscale image [41] and considers the image as a topographic surface, calculating the energy gradient of a higher altitude (higher intensity) towards a smaller altitude (lower intensity value), similar to how water always flows down towards a point of equilibrium. It follows that the mathematical choice is the local minima of an image gradient. Eq. 3.16 presents the definition for the topographical distance to find the local minima between two pixels q and p within the image:

$$T_f(p, q) = \inf_{\gamma} \int_f \|(\gamma(s))\| ds \tag{3.16}$$

Here, infinity symbolises going over all possibilities (smooth curves) and $\gamma(0) = p$ pixel and $\gamma(1) = q$ pixel. The minimum of T_f is taken as the overall minima. It can be observed that this techniques presents a proneness for having multiple minimas when the gray scale of the q pixel and any other candidates is close to another. This minima is segmented based on an marker, or the seed. The marker can correpond to the calculated local minima, however it can also be chosen via manual input. This offers an advantage over other algoirthms as it can be used directly via visual inspection to segment structural features. Following the marker is the mask, or a binary copy of the image that is used to restrict the area of application. For the scope of this experiment, the mask is set to the whole image or the area of the image where features are apparent via visual inspection. Fig. 3.23 offers an example of the Watershed marker being applied to a Google image.
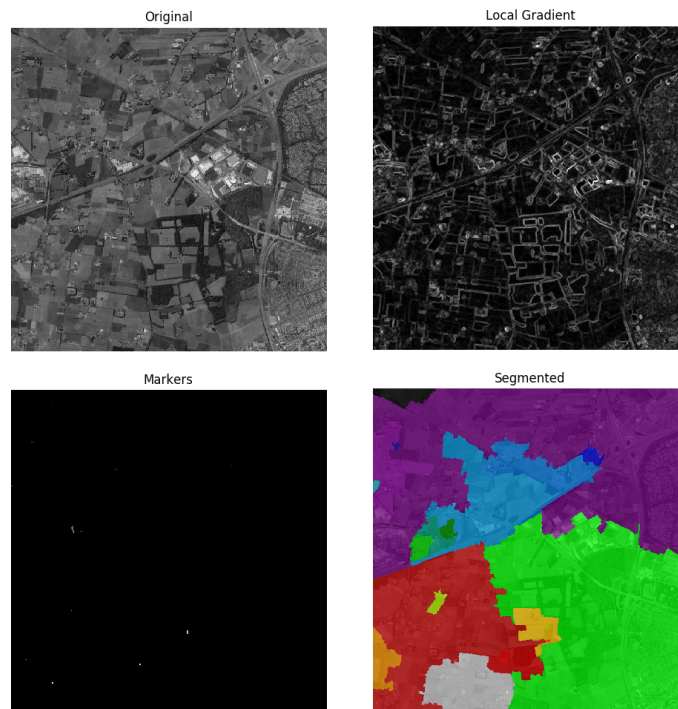

Figure 3.22: Warshed custom markers applied to a Google satellite map, for radar image at point 1000

Deep learning SAR segmentation techniques

Currently, Convolutional Neural Networks (CNN) are applied to most computer vision tasks, with results outperforming other approaches [23]. This reduces the need for feature engineering by directly leaving the network to learn suitable features. This can be used in two ways, either learning information directly from the radar and satellite data, or from their image transformation, that only shows important landmarks [12]. Of course, image transformation is resource consuming as it needs to go through the matrix multiple times.

Unfortunately, deep learning techniques require a vast database to be used as for training and validation [19]. This is not provided within the given FMCW database and forces any considered deep learning techniques to be pre-trained with very small changes to accommodate the comparison within the experiments. Furthermore, there is very little control over the setup of any deep learning techniques, due to little to no control over the features that are available within the FMCW radars [24]. As such, the techniques considered within the experiment methods were to measure the possibility of using deep learning as part of future research in regards to the chosen metric.

Within the area intersected by CNN and SAR databases is the semantic segmentation of radar images [19]. This process segments the image based on intensity values for roads, rivers, farm land, forests and cities. Each pixel in the image is classified into a class, which also includes the background. Geo Land Sensing [15] is an unsupervised learning algorithm based on hierarchical Conditional Generative Adversarial Nets (CGAN) and conditional random fields (CRF) Geo Landsensing - categorizing each pixel in satellite images with respect to the land cover of each area.

Another is [27], based on a pre-trained Convolutional Autoencoder with Total Variation Loss (CAE-TVL) for satellite image segmentation as well as generic images. Using Pytorch [44] with Fully Convolutional Networks as well as DeepLab v3, pretrained on a subset of the PASCAL VOC dataset [27]. Within Fig. 3.23 an example of a RGB segmentation is shown. The image was segmented correctly and consistently for roads and dark areas within the image that were assumed to be forests, however everything else, including dirt roads were classified as grass which is not correct. Additionally, the image was forwarded to its full resolution of 800 x 800 pixels in full RGB spectrum with a window size of 2 pixels for segmentation. This shows the potential for this algorithm to work exceptionally well under higher resolution for images in the future.

Figure 3.23: RGB Color segmented image for Google database showing roads(gray), forests (dark green) and grass(green)

Although traditional autoencoders are interlinked in order to identify mapping, the trend in computer vision is to attempt the localization of features that repeat over a given input [21]. The research paper reference attempts to replace all connected layers by convolutional layers. This helps reducing redundancy. With $W^{(l)}$ being a 4D tensor at the l-th layer containing all convolutional kernels, having two dimensions for spatial coordinates, and two dimension for the numbers of channels of the input and output layer. The algorithm was modified with regards to this experiment to mainly take into account the spatial dimensions and only have one input and output channel, due to the grayscale configuration of the radar intensity range. The convolution is defined in the equation below 3.17, with $X^{(l-1)}$ being a padding parameter to keep spatial size where needed and p,q,s,t being the dimensions of the 4D tensor:

$$(W^{(l)} * X^{(l-1)})_{mnt} = \sum_{p=1}^{P_l} \sum_{q=1}^{Q_l} \sum_{s=1}^{S_l} W_{pqst}^{(l)} X_{m+p,s}^{(l-1)} \tag{3.17}$$

This yields a 3D convolution with a time-step of 1, or stride. The activation function as well as pooling window size was kept as within the paper. The resulting output of the l-th deconvolitional layer is presented in equation 3.18

$$Z_m nt^{(l)} = \sum_{s=1}^{S_l} \sum_{p=0}^{P_l} \sum_{q=0}^{Q_l} W_{p+1,q+1,s,t}^{(l)} X_{m-p+1,n-q+1,s}^{(l-1)} \tag{3.18}$$

Within the loss function presented in the paper, the color vector $X \epsilon \Re^{MxNx1}$, with M and N being the spatial coordinates and only 1 color scale in accordance to the gray-scale. With these changes to the algorithm, the new CNN was trained using the same training objective based on the Berkley Segmentation Data Set (BSDS500)[15]. Below in Fig.3.24 the results of this attempt is shown. Once the algorithm was trained and tested, a look at time, yielded times below two seconds for the image segmentation. Although the google image was correctly segmented, the radar image included a lot of noise. This unfortunately provided a lot of false positives within the results.
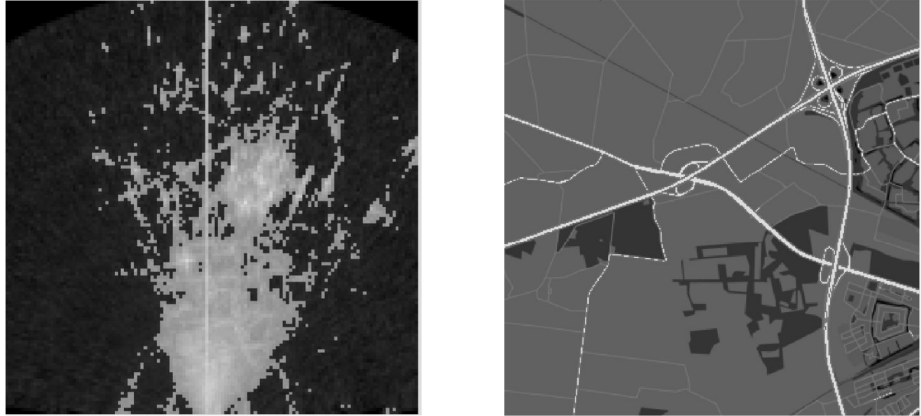

Figure 3.24: Warshed custom markers applied to a Google satellite map, for radar image at point 1000

3.7.5. Experiment setup

Having all the algorithms ready, as presented in the previous section, along with the setup metric, the experiment setup can be selected. As described in the hypothesis, the GPS coordinates provided at a certain time frame along with other flight parameters are used in order to build a radar and GPS pair. The scope is to use the radar frame to validate the GPS coordinate. Using a Google or Sentinel database, the GPS coordinate can be attributed to a set image of what the radar should detect.

Furthermore, using flight parameters, the radar map, a 2D representation of all reflections within the environment can be built. Due to the power capabilities of the radar, as presented in chapter 3.7.2, the non-linearity for all intensities was observed, that could not be fixed via multiplication with a range function. This non-linearity is kept even with different range multiplications, as presented in chapter 3.7.2. This implies that local changes in intensities are required to obtain a clear image. This can be easily obtained from using image modification algorithms such as the Gamma Correction, Threshold setting or Local Histogram Equalization. These algorithms become the corner stone for a first filter within the image to attempt a linear equalization of all intensities and assure that any transformation conducted by following algorithms would work correctly over the whole considered area. Fig. 3.25 shows how a random candidate is created for the experiment.

It can be observed that both image transformations focus on filtering certain features within the radar image. These features can be any combination between high intensity points and shape features, such as roads or highways. In order to correctly compare to a database, a one-to-one comparison is preferable. This means that vectored shape information contained in Google images can only be compared to radar images filtered by methods that focus on filtering for shapes. It is possible to compare both within the same light spectrum, however, the vertical polarized nature of the provided information, makes filtering for intensity more favourable. Only methods that use Blob Detection will compare with Sentinel 1 database [?]. As all other methods only filter mostly for geometric shapes which represent roads or highways, it is easier to use the Google database.
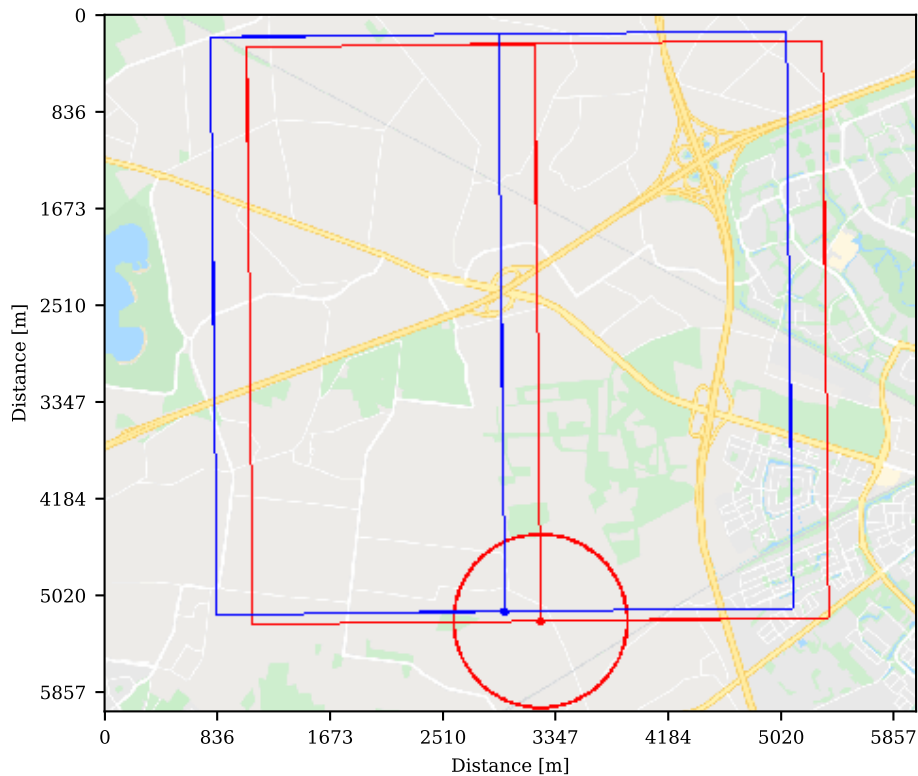

Figure 3.25: Example of experiment setup with exaggerated range of 1000 m

3.8. Results

Within the following section, additional details that was not presented in the research paper is shown. The presentation of the results starts by showing the first four images that were used for the first experiment, within Fig. 3.26. Additionally, the image transformations table is presented.
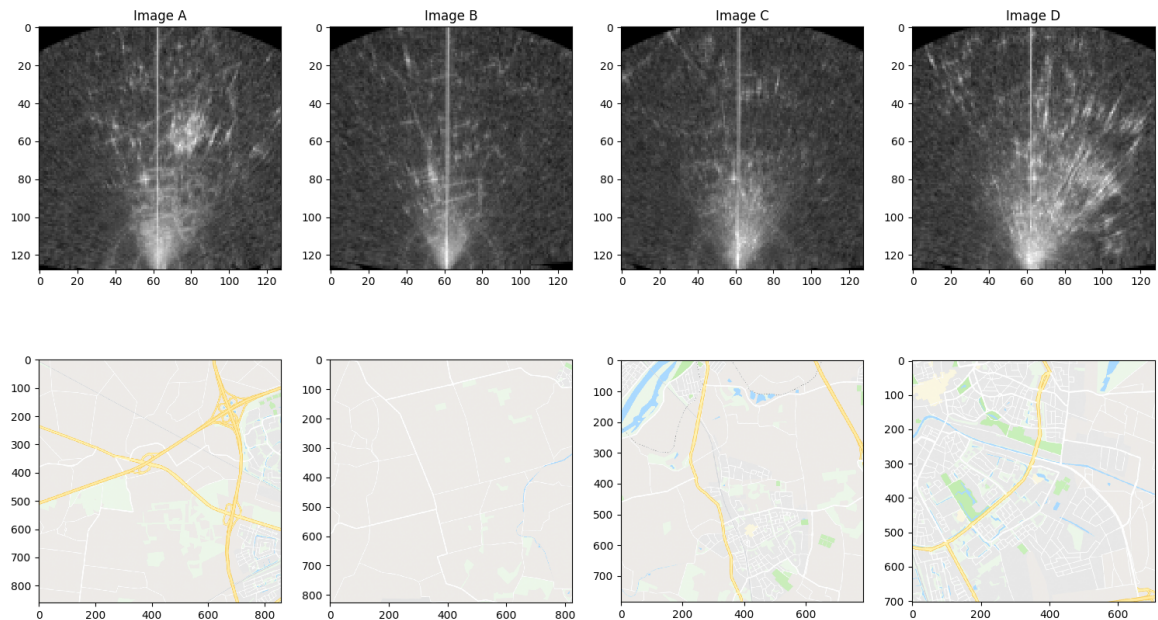

Figure 3.26: Warshed custom markers applied to a Google satellite map, for radar image at point 1000

Within table 3.2, two image transformations are employed, one to transform the image and bring most feature points and another to discriminate between either structural features such as roads or rivers and high intensity features such as industrial rooftops. Due to the power capabilities of the radar, a non-linearity for all intensities was observed, that could not be fixed via multiplication with a range function. This non-linearity is kept even with different range multiplications, whether it is with regards to range squared, cubed or fourth. This implies that local changes in intensities are required to obtain a clear image. This can be easily obtained from using image modification algorithms such as Gamma Correction, Threshold setting or Local Histogram Equalization. These algorithms become the corner stone for a first filter within the image to attempt a linear equalization of all intensities and assure that any transformation conducted by following algorithms would work correctly over the whole considered area.

It can be observed that both image transformations focus on filtering certain features within the radar image. These features can be any combination between high intensity points and shape features, such as roads or highways. In order to correctly compare to a database, a one-to-one comparison is preferable. This means that vectored shape information contained in Google images can only be compared to radar images filtered by methods that focus on filtering for shapes. It is possible to compare both within the same light spectrum, however, the vertical polarized nature of the provided information, makes filtering for intensity more favourable. Only Methods 2 and 7 that use Blob Detection will compare with Sentinel 1 database. As all other methods only filter mostly for geometric shapes which represent roads or highways, it is easier to use the Google database.

Table 3.2: Image transformation sequence

Method #	1st Image Transformation	2nd Image Transformation
1	Gamma Correction	None
2	Gamma Correction	Blob Detection
3	Gamma Correction	Threshold
4	Threshold	Contour Finding
5	Threshold	Entropy Detection
6	Threshold	Hough Line Transform
7	Threshold	Blob Detection
8	Histogram Equalization	Ridge Operators
9	Histogram Equalization	Entropy Detection
10	Histogram Equalization	Watershed marker
11	Histogram Equalization	Contour Finding
12	CGAN - CRF	None
13	CAE - TVL	None
14	Histogram Equalization	CGAN - CRF
15	Histogram Equalization	CAE - TVL

3.8.1. Results experiment A

Following a total of 15 experiments done over 4 flight radar images,the results with regards to heading deviation, position error and the percentage of SSIM that is greater than the original pair are presented in table 4.1.
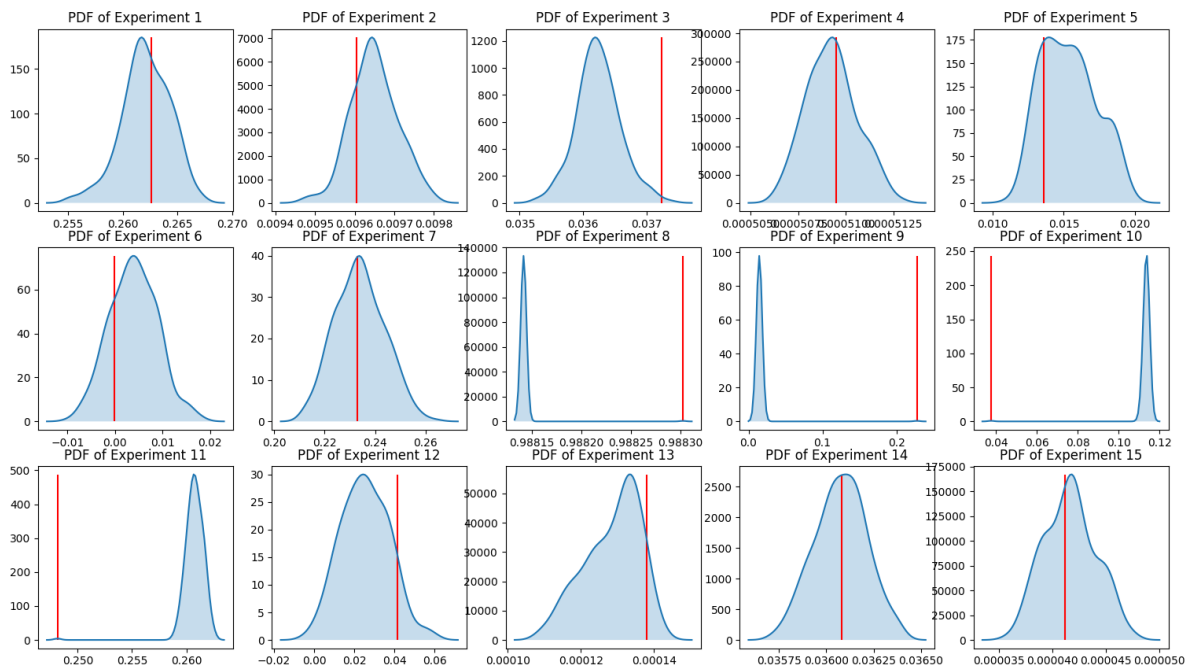
Figure 3.27: Probability distribution function over all Methods for Experiment A

The average of position error, as well as heading values is of interest to show the overall performance of the experiment, not just the best indicated value. It should be noted that the heading deviation is absolute, between calculated heading and be candidate heading. The position error is the distance from the generated coordinate to the GPS-indicated coordinate. And, finally, of the total randomized positions, a percentage above the original pair is calculated and presented in Fig. 3.28. All averages are taken as integers, calculated by summing the best candidates and dividing by the amount of total candidates. Over all parameters within the results, the lower the value, the better the performance.
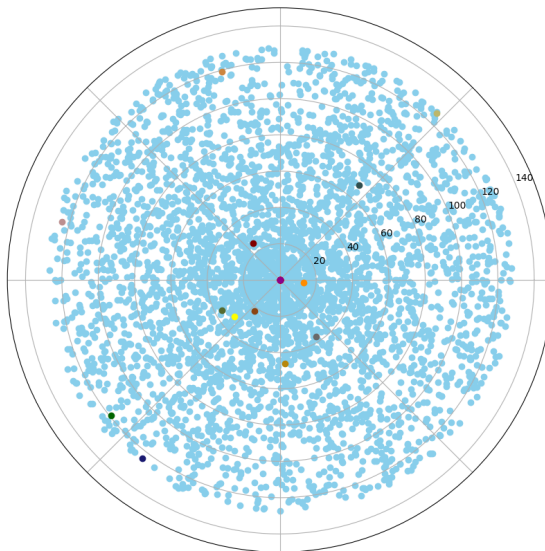
Figure 3.28: All experiment points along with best candidates per experiment

Table 3.3: Average results for heading deviation, position error and SSIM values over all experiments.

| | Results Experiment A - Average over 4 points | | |
Method	Absolute Heading Deviation	Position error	False Positive
1	7	108	53%
2	6	68	52%
3	3	75	50%
4	11	46	39%
5	5	24	23%
6	4	53	67%
7	8	35	28%
8	0	0	0%
9	0	0	0%
10	6	119	38%
11	2	37	89%
12	14	126	55%
13	12	124	53%
14	12	52	45%
15	6	112	35%

From the large amount of candidates within each method , several stand out for high results. Unfortunately, all methods employing pre-trained deep learning techniques have a poor performance, due to the noise that was forwarded to the algorithms for segmentation. Appendix secion 4.2, shows the results and short explanations for the three remaining images.

3.8.2. Results experiment B

Once the top three most performing combinations of algorithms are chosen, the second experiment can commence. This algorithms are: Method 5, Method 8 and Method 9 as taken from Table I in the research paper. This time, a more extensive representative sample is chosen, comprising a total of 20 images. In this experiment the independent variables are randomized more strictly, in two steps. The first step assumes the first randomization technique of radius and headings, applied to a larger variation of radar images during the flight as shown in Fig. 3.29. Additionally, Appendix 4.1, illustrates all used images and explains the features that can be found within.
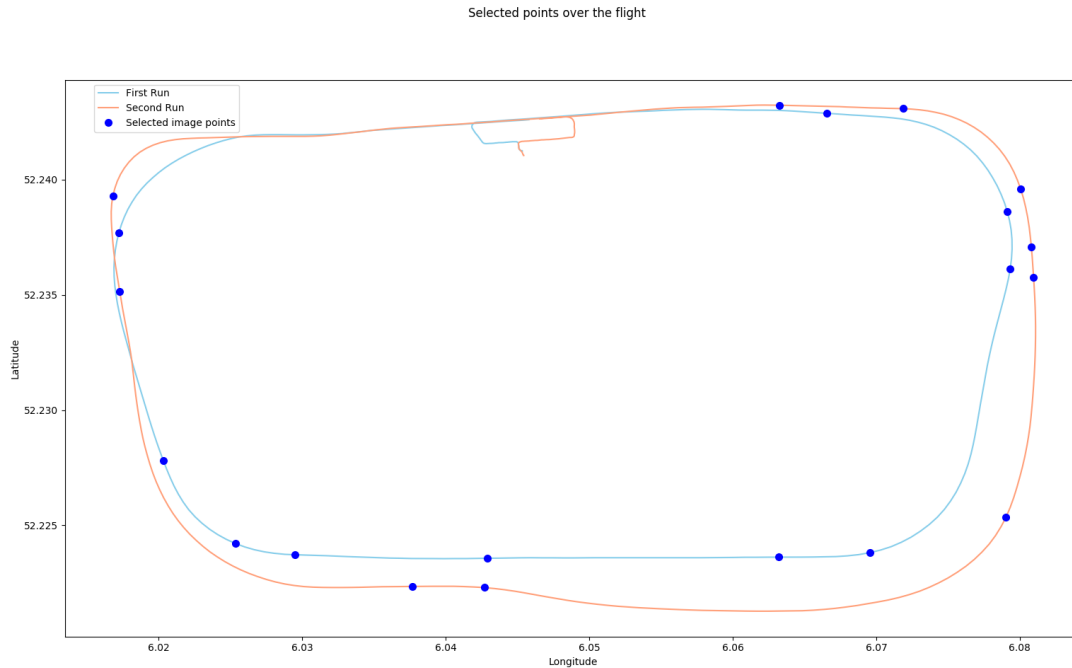
Figure 3.29: Warshed custom markers applied to a Google satellite map, for radar image at point 1000

Within Fig. 8 it can be seen that these points are chosen as far apart as possible along the two flights. During landing and take off, the altitude of the aircraft is too low to ensure a good reading of the surrounding area and proper match within the five square kilometer area. As such, only points above 100 m are taken into consideration. The second step greatly increases the realism of the experiment, only varying the heading by $+/-15\circ$ while assuming a near-perfect reading of the GPS coordinate, at 0 m.

Following this step, candidate coordinates are produced in a radius of 150 m around the original coordinate with a modification of $+/- 15\circ$ around the correct heading. The increment for creating randomized values for both radii and heading measurements is always one. The radius and heading measurements can be regarded as the independent variables within the experiment. A total of 300 candidates are created,each with their own SSIM value, which will be regarded as the dependent variable.Following the 2 experiments done over 20 flight radar images, Table 3.4 shows the average results with regards to average heading deviation, average position error and percentage better candidates with regards to the original SSIM value. The average of position error, as well as heading values is of interest to show the overall performance of the experiment, not just the best indicated value. It should be noted that the heading deviation is absolute, between calculated heading and best candidate heading. The position error is the distance from the generated coordinate to the GPS-indicated coordinate. And, finally, False positive is the percentage of candidates with a higher value for the SSIM than the one of the indicated pair. All averages are taken as integers, calculated by summing the best candidates and dividing by the amount of total candidates. Again, over all parameters, the lower the value, the better the performance and averages are taken as integers. Through a quick look at the results, it becomes obvious that the average position error is not 0, as in the previous experiment. As such, a direct representation of these variations per image is shown in Fig. 3.30 and 3.31.

Table 3.4: Average Results over Experiment B

| Method | Results with 0:150m range | | |
	Absolute Heading Deviation	Position error	Percentage Better
5	5	45	42%
8	1	1	14%
9	2	5	9%
Method	Results with 0m range		
	Absolute Heading Deviation	Position error	False Positive
5	12	N/A	51%
8	2	N/A	2%
9	9	N/A	48%

The first set of results within table 3.4 was the initial test for the final methods. It can be seen that in accordance with experiment A, Method 5 provides consistent results. The same is for Method 8 and Method 9, however, unlike showing a 0 integer as the position error, the final average result was different. This is due to some images having their candidates at different distances and averaging to small integers. Fig. 3.30 shows the best candidate for all experiment images and in order to better understand the results in the table. It can be seen that for image 10, 16, 17 and 20, all algorithms do not provide a suitable result. The same consistency is present for the deviation from the calculated heading as shown in 3.31. Within the Appendix 4.1, images 10,16 and 20 are presented in order to have a more clear view of why all methods failed to provide any meaningful accuracy. When investigating the images, it becomes clear that they do not provide any type of structural features. Additionally, the images present high amounts of noise as they are taken during turns. Although urban zones are present that show highly reflective objects, the present noise does not allow for any accuracy, regardless of the used comparison database.
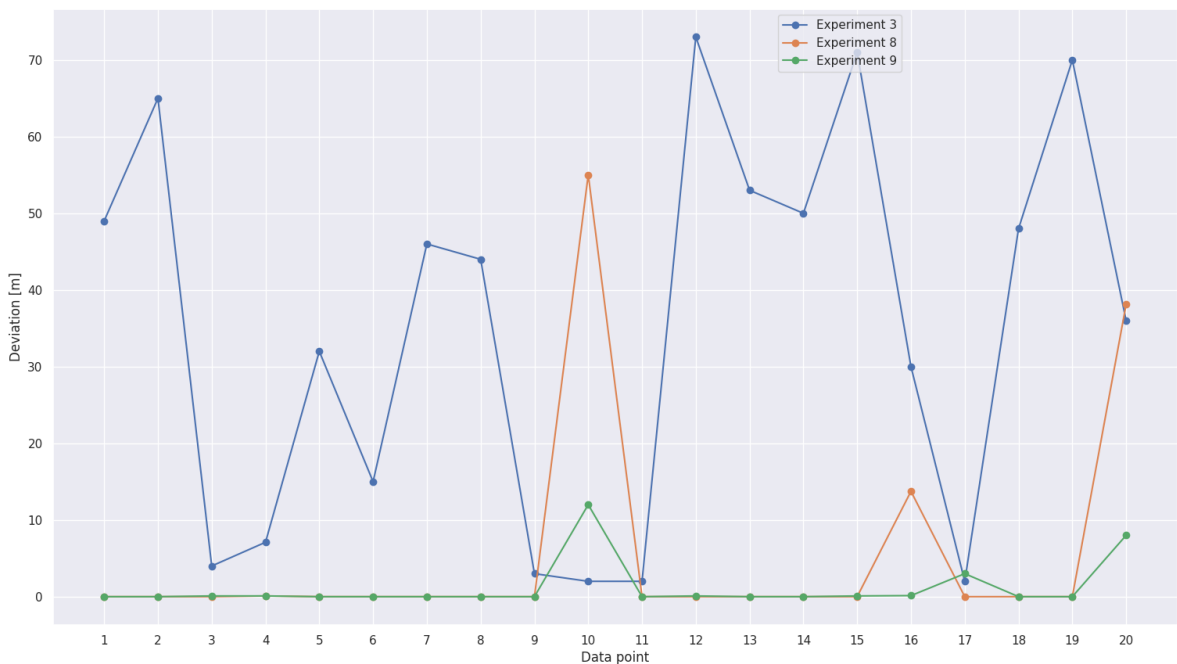
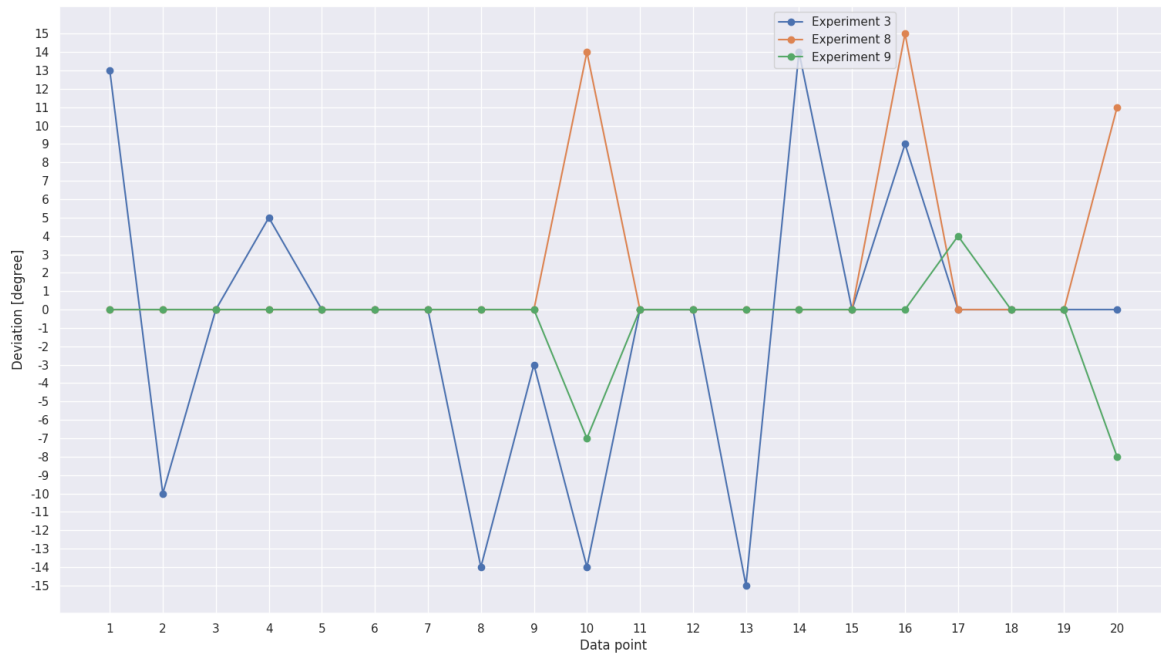Figure 3.30: Best candidate error over all images and methods up to 150m

Figure 3.31: Deviation error from calculated heading for all methods over all experiment images up to 150m

As two methods, method 8 and 9, have a high accuracy for detecting the original candidate pair, a final setup was created, where the range was kept at 0m while the heading was varied between +/- 15°. Fig. 3.32 shows the results that better explains table 3.4. Here completely different results can be observed as Method 5 and 9 completely fail with regards to accuracy. However, the consistency of Method 8 has been maintained. As shown in chapter ??, the difference of rotation even of 1°is hard to detect under visual inspection. The image transformations that are applied by Method 5 and 9 unfortunately forward too much noise to effectively let the SSIM detect rotational transformations even up to 15°.
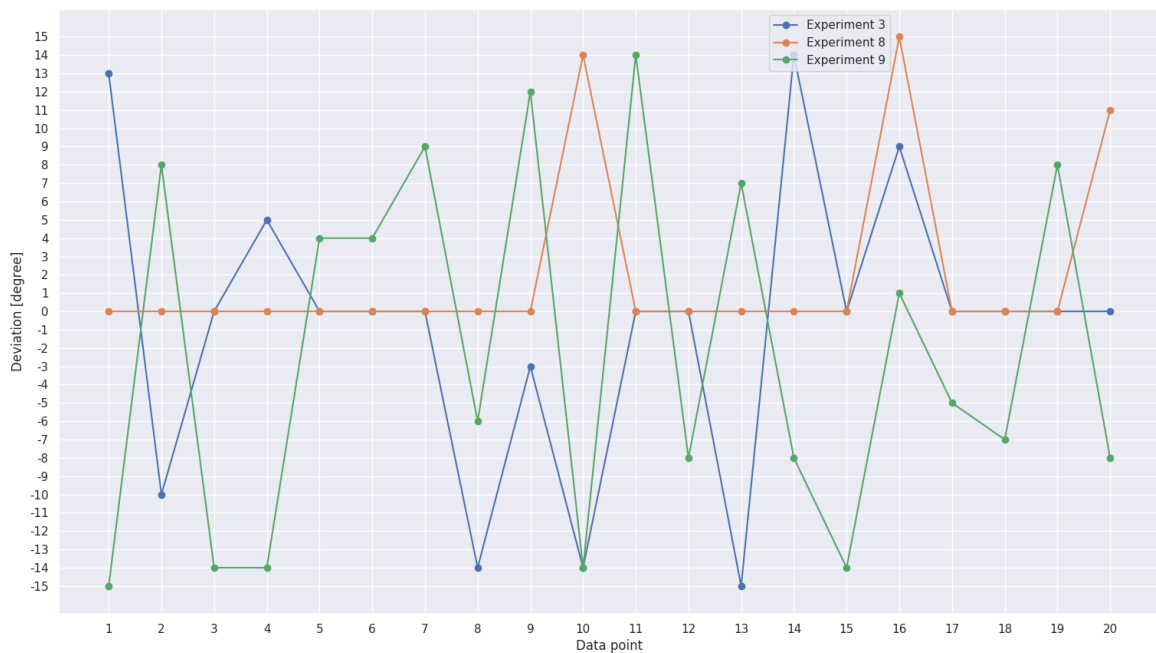
Figure 3.32: Deviation error from calculated heading for all methods over all experiment images to 0 m

Finally, a look at the computational times is considered. As it can be seen in 3.33, method 5 has the fastest time calculation. This is due to applying thresholding as a first image transformation. This was found to be the case with all thresholding techniques, as first a binary choice is made for each pixel, followed by the entropy detection algorithm searching within the created binary mask. Following is Method 8, which had times between 1.1 and 1.55 s. This is a fast time with regards all methods, mainly because ridge detection applies modification to the Gaussian of a matrix that was created by a local histogram equalization. The higher time is also explained as the final image contains every pixel. Method 9 however has a very long duration in the context of both experiments. This is explained through the fact that the local histogram for both the radio as well as the vectored Google image transform the image and makes any edges and or ridges distinct. This increases the total number of entropy calculations.
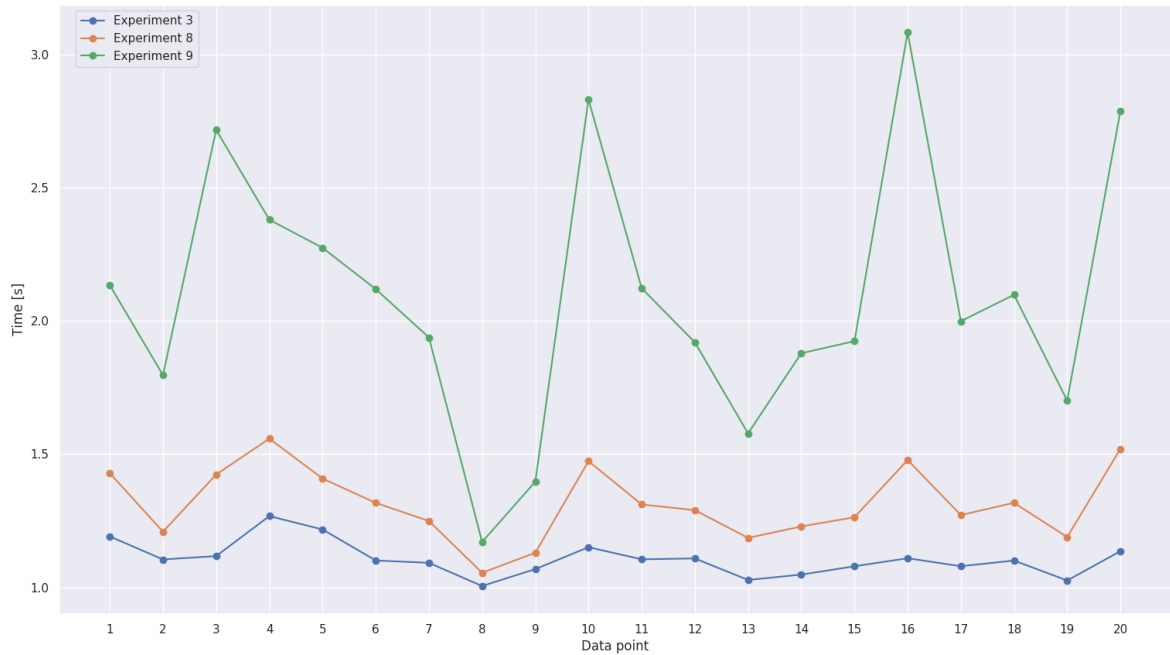
Figure 3.33: Warshed custom markers applied to a Google satellite map, for radar image at point 1000

Overall, both experiments achieved the scope of isolating candidates that provided a high accuracy in relation to proposed radar-GPS candidates. Within experiment A, the probability distributions functions (PDF) 3.27 shows curios results for methods 8, 9, 10 and 11. While methods 8 and 9 were chosen afterwards to be part of Experiment B, methods 10 and 11 were analyzed more closely. The calculated false positive metric shown in table ??, shows that for methods 10 and 11, the PDFs skew the perceived percentage of better results. Should the original candidate pair have a high percentage of false positive, additional investigation would have been requird.

Unexpectedly, Method 8 had an accuracy even at 0m when large enough structural features are presented in the image. While inspecting the participating images that can be found in Appendix ??, it can be seen that that for images 10, 16 and 20 no large structural elements were detected. As it can be seen, these images present mostly noise with very little features that can be robustly detected by any methods. Interestingly, image 19 is very similar to 20, however presents a road that is more visible and detected by the employed methods. This opens the possibility of using ridge detection and SSIM in noisy radar images to a high degree. The result will be a mechanism that verifies GPS coordinates to increase the reliability of all parameters.

3.9. Conclusion

The presented document aimed at displaying all important information as well as the process of decision making on the way to a successful research analysis. Avionics are an invaluable asset in decision making and safety practices, with their provision of environment information. Using existing sensing systems, such as FMCW radars, to provide new information for the avionics system becomes apparent when analyzing the possibility of use in a similar setting to SLAR or SAR. This may allow the identification of features and as such the placement of the aircraft within a known coordinate system. In order to do this, a synchronization between GPS and radar information, will place the radar database into a known framework, and ease the matching process. It becomes clear that the calculated frame rate constitutes an issue towards the synchronization process and only varying slightly the frequency, it matches the GPS possibility. Finally, to continue and start identifying features as well as their efficiency, a comparison experiment is proposed, concluding with an enumeration of algorithms that were used as part of the experiment as well as their results.

Using a perceptual metric (SSIM) to quantify image quality degradation, especially via noise in data transmission, transformed radar images are compared to Google vectored road maps or Satellite 1 SAR vertically polarized databases. All databases are transformed via one or two transformations, that assured that shape features such as roads or highways, or highly reflective objects are most visible. To simulate possible GPS faults, new coordinates in an area around the the actual aircraft coordinates were created. From there, new image candidates are proposed for comparison with the radar image. The best candidates are taken and an error based on distance from original coordinate is calculated. To attempt and analyze heading variations, the rotation of candidate images is also employed. Out of all the employed algorithms, several were able to produce high accurate results that required the addition of other experiments. While being heavily affected by noise via power and received echoes, one algorithm provides a high degree of accuracy within the created experiments. The algorithm belonging to M-8 is especially designed to detect blood vessels in noisy radiograms within the medical field. The same algorithm was able of identifying the image corresponding to the GPS coordinate in most test cases where large shape features were present representing highways. Using deep learning techniques, pre-trained on other databases, offered the possibility to investigate how they would work in the context of radar images that presented heavy noise.

Within the boundaries of this experiment, it still remains to be seen whether computational times can be improved. Although it is possible to determine the position using intensity features, they unfortunately contain noise that decreases the accuracy. As such, a preference for Google vectored images was chosen as well as a focus on detecting structural features. The SSIM score should be increased by utilizing the algorithm to its full capability, incorporating luminance and contrast information. To achieve the transformations, it is necessary to take into account additional radar parameters, especially related to power. The SSIM can be used to discriminate image quality. This means a potential for using the SSIM to predict the amount of noise within an image and determine if it is suitable for comparison. Additionally, varying parameters within the SSIM can also provide an answer of whether there is an object to detect. Given a more in-depth implementation of the SSIM, it may be possible to filter the image without the need for additional algorithms.

As the heading was deduced from successive GPS coordinates, a more qualitative method should be employed. The overall test should verify whether the heading information is consistent with radar information and if it can be used as a secondary measurement or input to more consistently determine heading information. For shape detection within Google vectored maps, a simple color and grayscale transform can be implemented to work aside the transform of the radar image. This should ease the calculations as well as improve the SSIM output due to a direct segmentation consisting of only highways. Due to the lack of an extensive database, no machine learning algorithms can be employed to check coordinate information. As of this moment, the test setup can only attempt a prediction algorithm that takes aircraft parameters as inputs and attempts to find the next image in the database that best corresponds to a future radar image. Additionally, the test setup used within this paper can be used to create a data base that can train machine learning algorithms to deduce position and heading information, based on previous state information. This allows for information identification under heavy noise conditions to ascertain whether GPS coordinates are correct, as well as for heading information from the magnetic compass. This could be used in the future to make the aircraft a self contained system, with no necessary outside inputs.

4

Appendix

4.1. Image pairs used from the database

Within this section, all images used in both experiments are presented as well as a short presentation of main features found in each image.
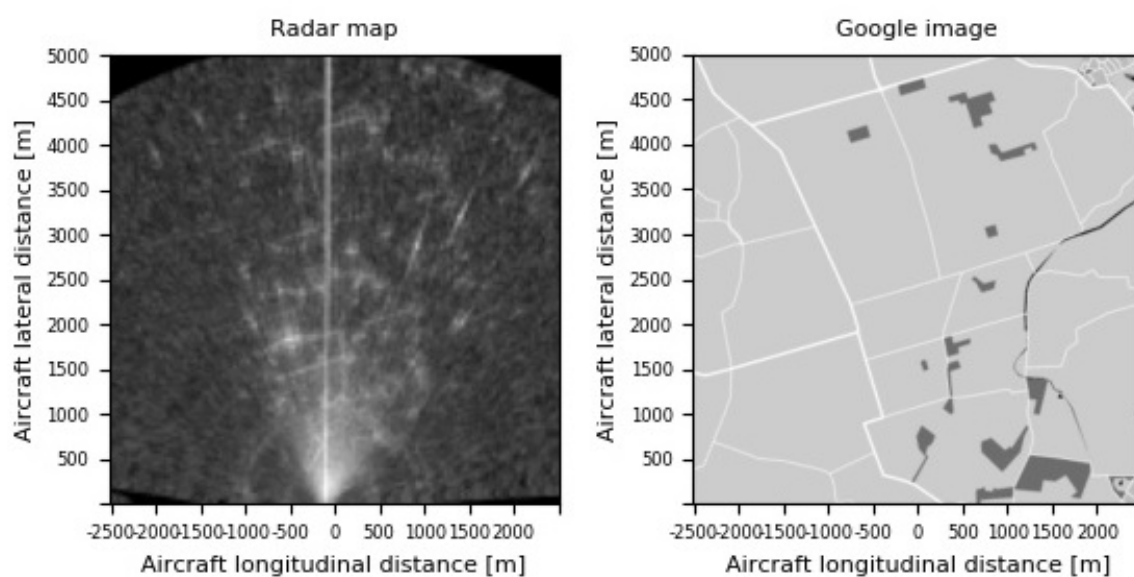

Figure 4.1: Radar image and Google maps pair at second 900 from GPS Start

Within image 4.1, taken at a lowest acceptable altitude, several large structural features can be seen along with some high reflections towards the right. This is an ideal image due to the low level of noise present in the image.
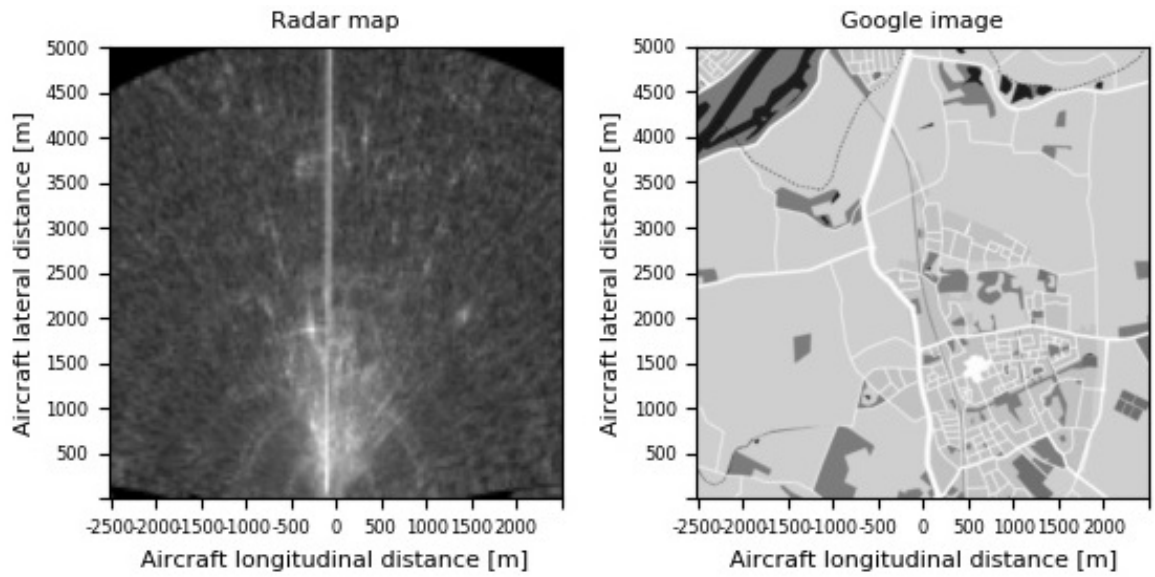
Figure 4.2: Radar image and Google maps pair at second 926 from GPS Start

Within image 4.1, taken just before a turn, the effects of high relative motion can be observed. Here the Doppler velocity is increased due to the antenna moving in two dimension, instead of one along the flight path. However, a Large structural feature can still be seen on the left of the image center.
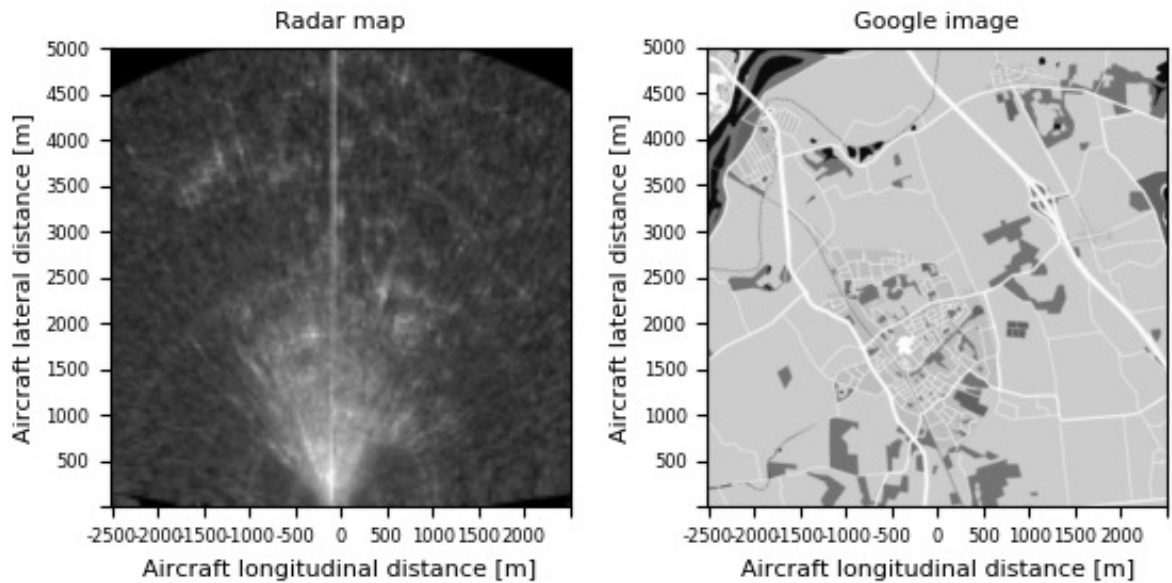
Figure 4.3: Radar image and Google maps pair at second 932 from GPS Start

Image 4.1 presents a large structure on the right of the image center, identifying a runway. In the center and lower part of the image, a city can be seen, where the high reflection along with the power of the radar mask any detectable features.
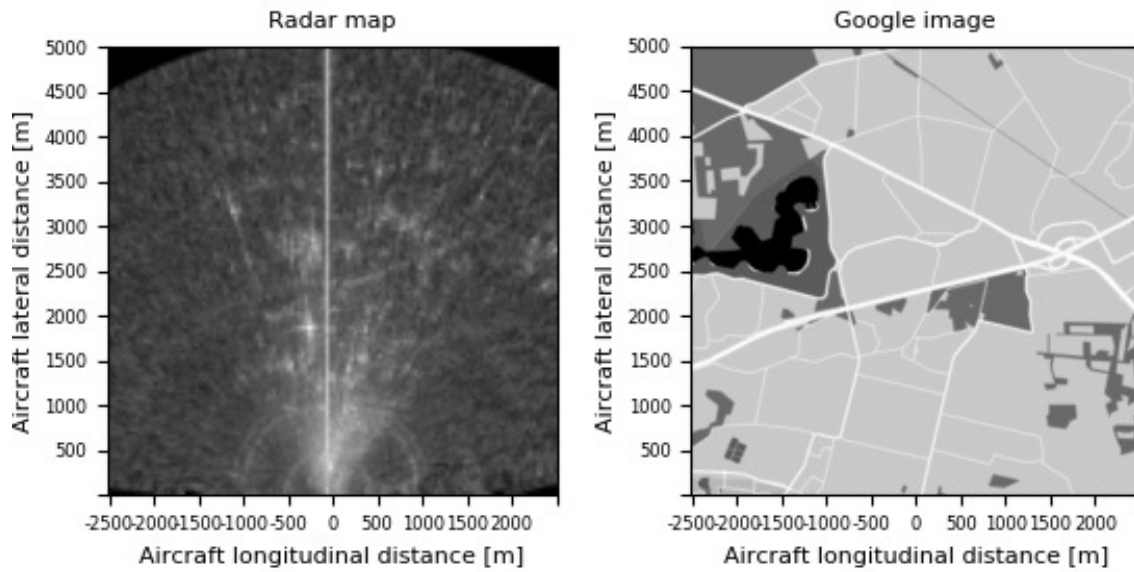
Figure 4.4: Radar image and Google maps pair at second 965 from GPS Start

Image 4.1 presents the same highway as in image 4.1, along will low level of noise due to reflections. This makes this image a good candidate for feature identification. Within the radar image, there are some high reflecting points which cannot be identified as structures or noise.
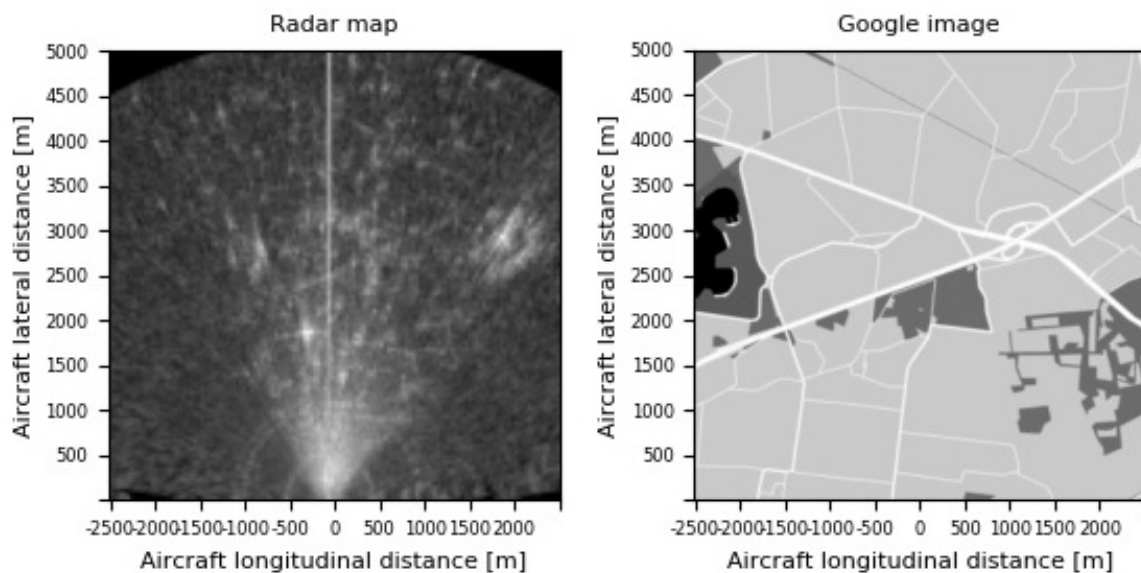
Figure 4.5: Radar image and Google maps pair at second 973 from GPS Start

Image 4.1 is a continuation of 4.1. Within this image, the altitude is close to its highest point and noise can be seen to be relatively low, allowing for smaller structural features to be observed.
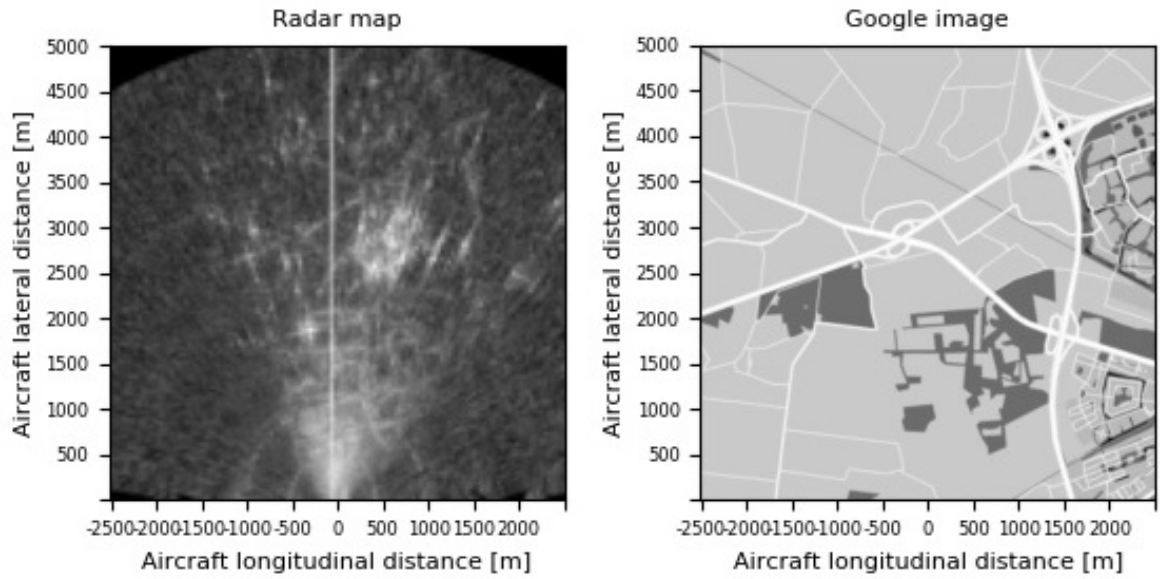
Figure 4.6: Radar image and Google maps pair at second 1000 from GPS Start

Image 4.1 is the baseline used throughout this experiment. It can be taken as the minimum ideal case for this type of radar which presents as much structural features as possible. Furthermore, in the center of the image, a set of highly reflective structures can be observed, alongside the effects of noise which mask some parts of the highway.
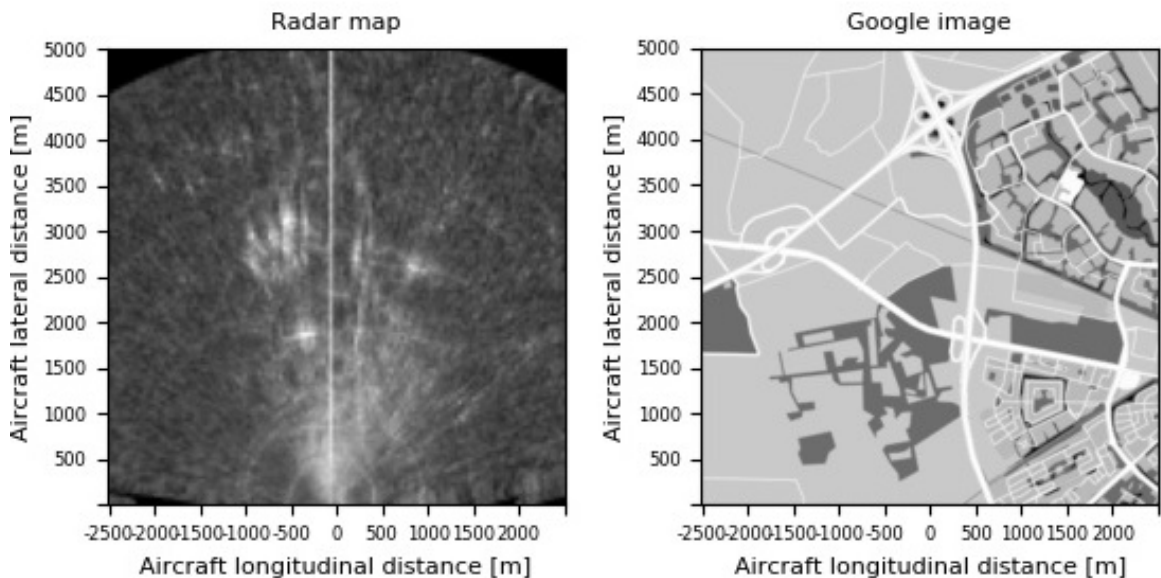
Figure 4.7: Radar image and Google maps pair at second 1018 from GPS Start

Within image 4.1, the aircraft begins a turn and the relative Doppler velocities added by the turning antenna allow for the largest structural feature to be observed. This was taken as proof for the possibility of identifying features even during turns if they are large enough.
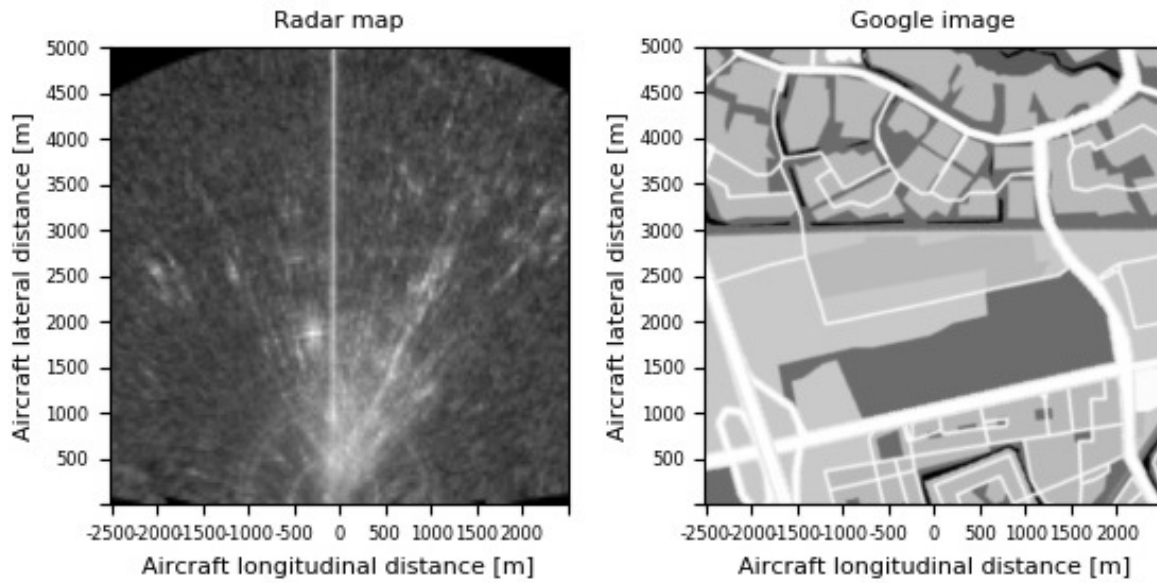
Figure 4.8: Radar image and Google maps pair at second 1024 from GPS Start

Image 4.1 is very similar to image 4.1, only taken during the turn. This image was chosen to test how the methods would behave during high noise detection. The same as with image 4.1 can be said, as a long street was detected.
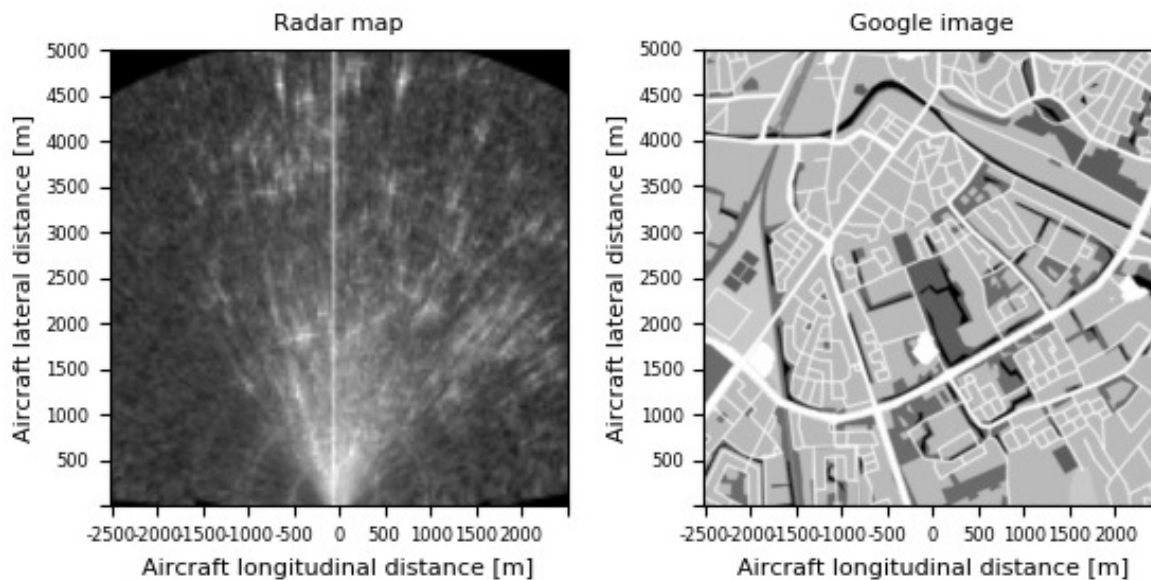

Figure 4.9: Radar image and Google maps pair at second 1036 from GPS Start

In image 4.1 a large structural feature can be observed to the right of the image center. Although one of the images that presented most noise, it still identified a road well enough to provide consistent results.
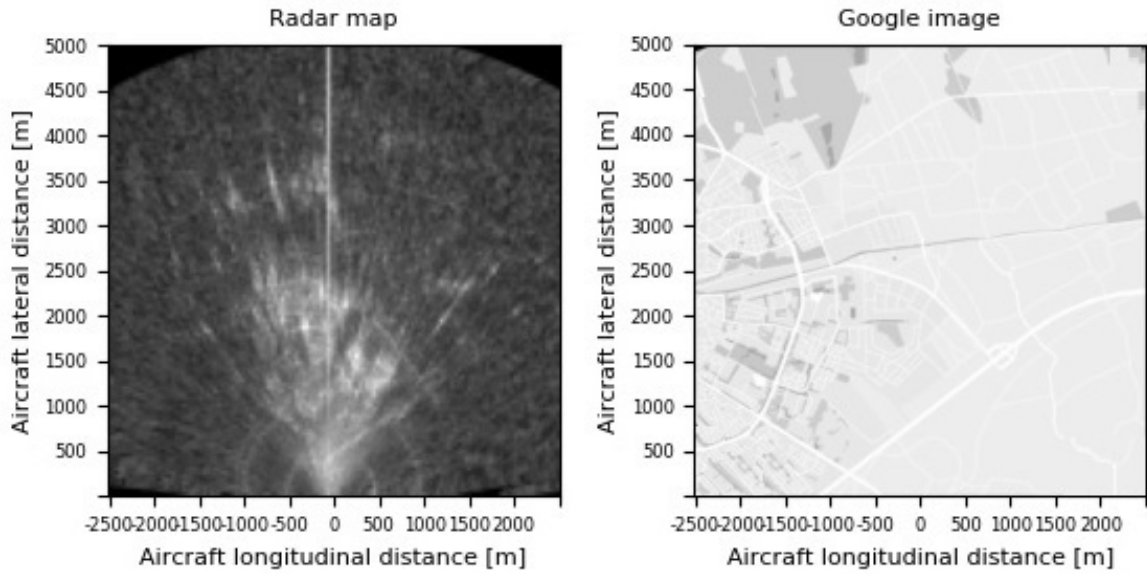
Figure 4.10: Radar image and Google maps pair at second 1062 from GPS Start

Image 4.1 was taken during a final turn of the first phase of the flight. Within this image an extremely large amount of noise can be observed. Under visual inspection, multiple features can be observed near the image center, however they do not match to any structural features in the assigned Google image.
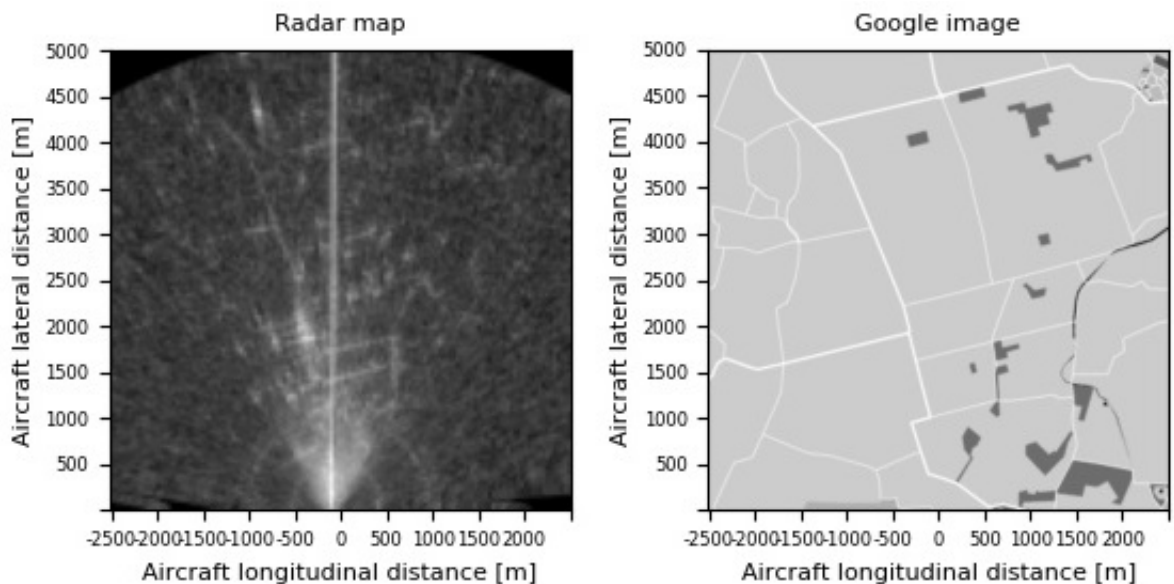

Figure 4.11: Radar image and Google maps pair at second 1155 from GPS Start

Within image 4.1 the same situation as within image 4.1 can be observed. The image was taken shortly after the second take off during the acquisition of data.
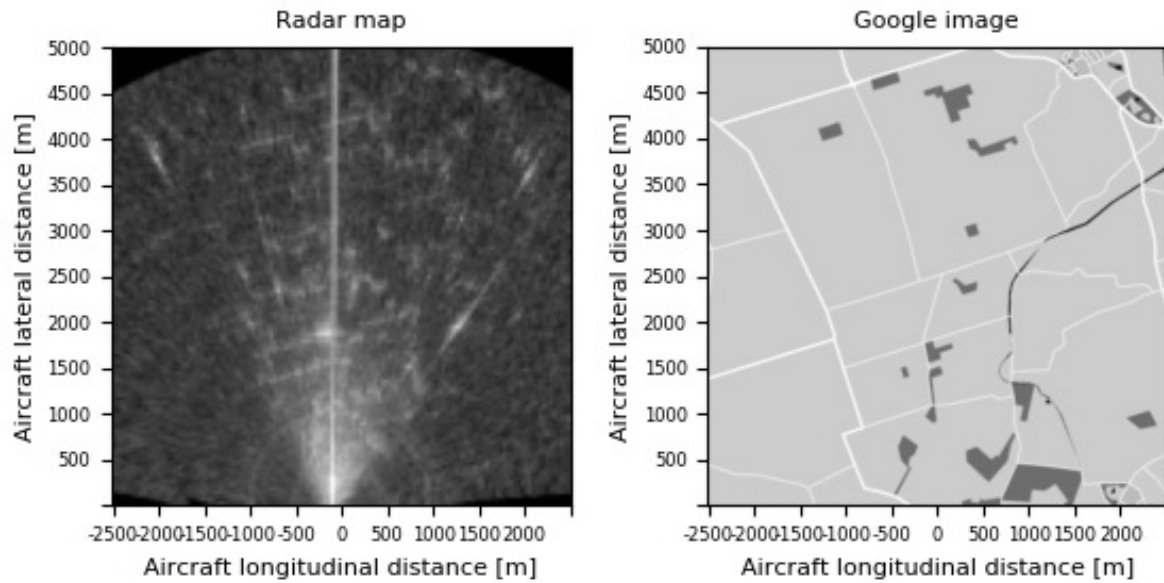
Figure 4.12: Radar image and Google maps pair at second 1171 from GPS Start

Image 4.1 was selected just before the first turn of the second take-off. This makes noise due to turning antenna apparent when compared with either image 4.1 or 4.1.
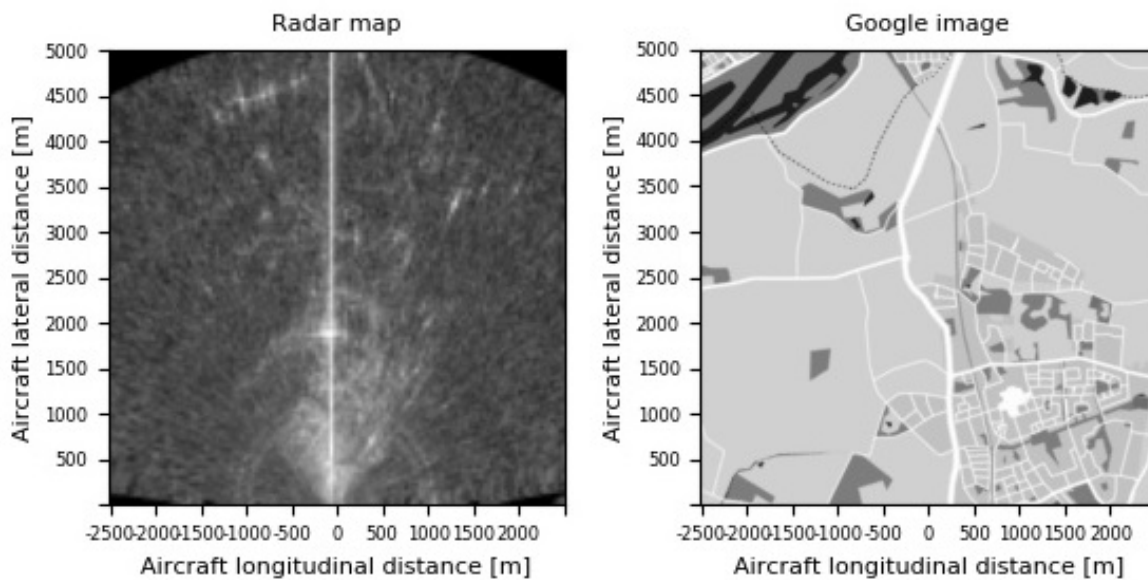

Figure 4.13: Radar image and Google maps pair at second 1189 from GPS Start

Within image 4.1 almost no features can be observed under visual inspection, apart from some intensity reflections due to the city to the right of the image center. However, a national road that is long enough is observed to the right of the image center in the upper part.
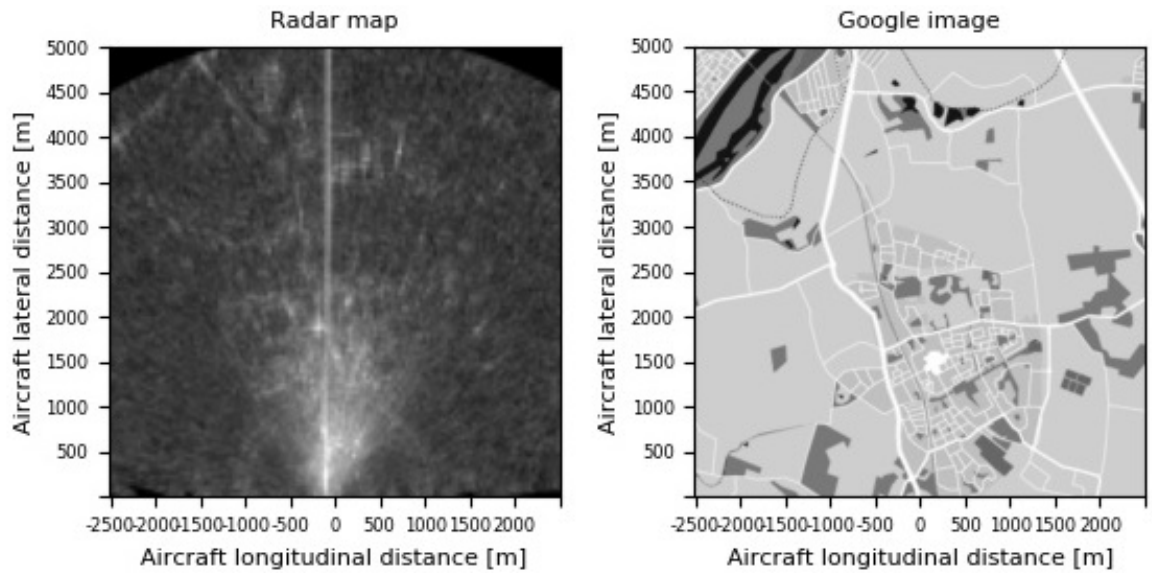
Figure 4.14: Radar image and Google maps pair at second 1195 from GPS Start

In image 4.1 the same road was detected as in image 4.1 to a more accurate degree. Again it can be seen that the reflective features caused by the city are blended in with noise, making any feature identification for intensity unreliable.
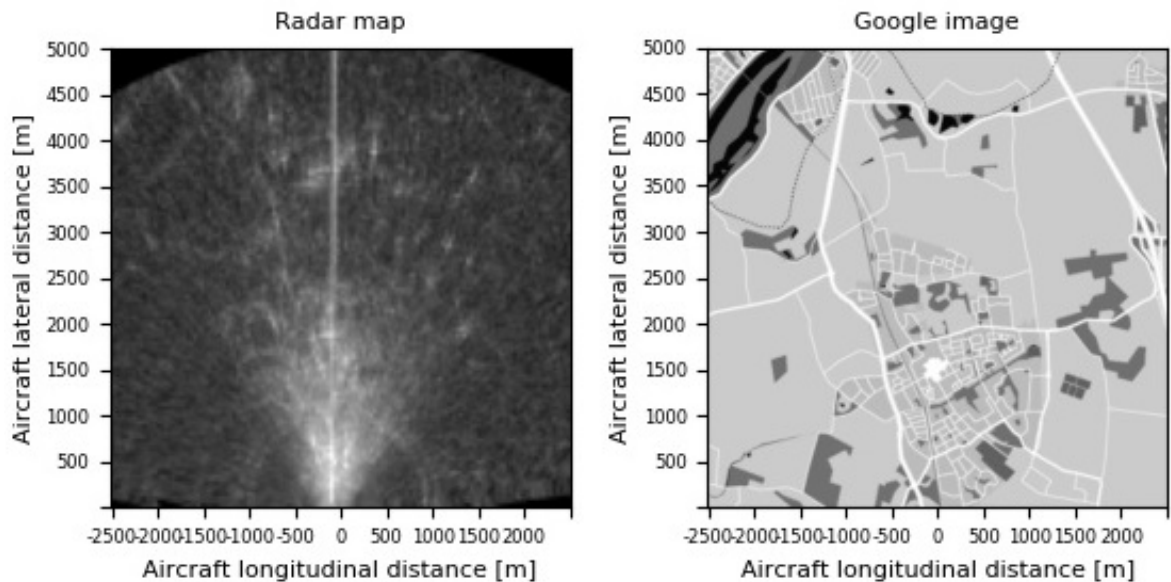

Figure 4.15: Radar image and Google maps pair at second 1198 from GPS Start

Image 4.1 was taken just as the aircraft was about to make the second turn of the second take-off. Again, this image solidifies the hypothesis that large enough structural features offer a high amount of detection accuracy.
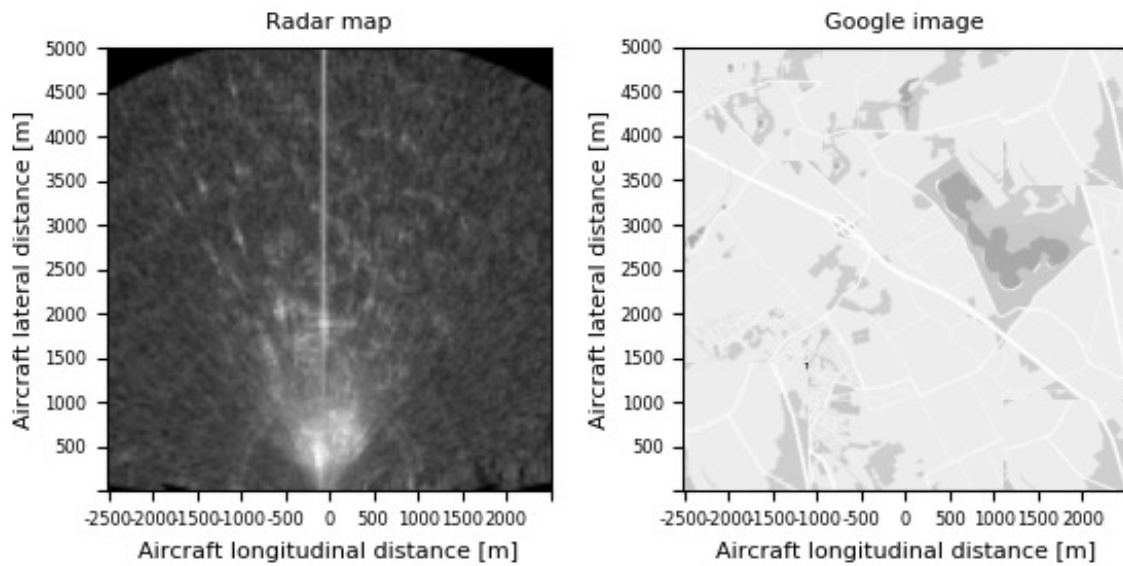
Figure 4.16: Radar image and Google maps pair at second 1222 from GPS Start

Within image 4.1 virtually no structure or intensity feature can be observed. This is due to the aircraft turning and caused all methods to provide a high procentage of false positives.
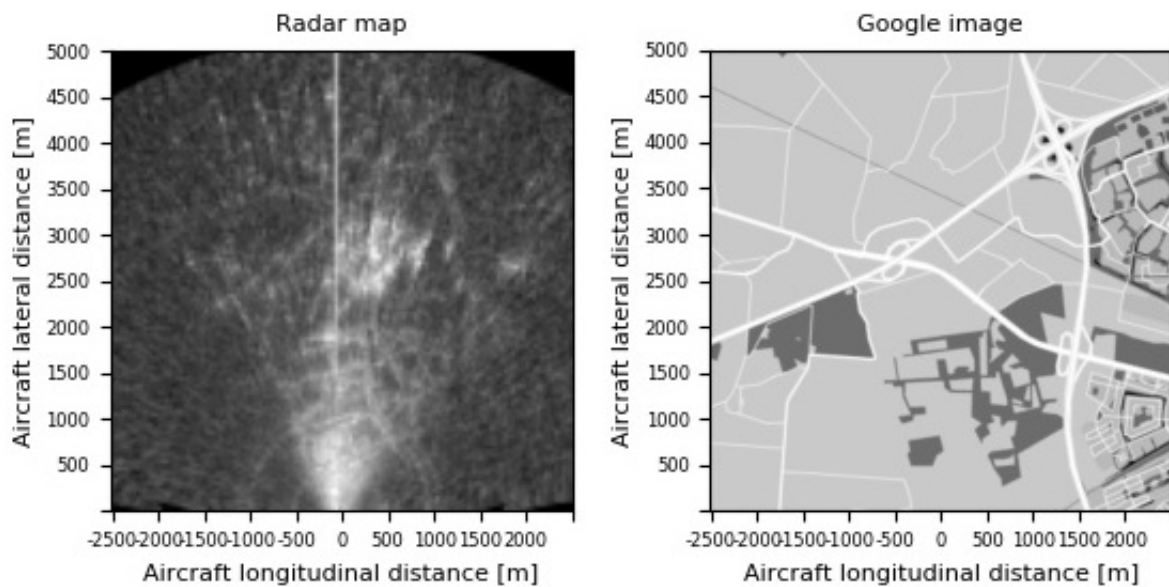

Figure 4.17: Radar image and Google maps pair at second 1274 from GPS Start

Images 4.1 and 4.1 are the equivalent of image 4.1 during the second flight, proving that the high altitude offers the best resolution for image recognition and identification.
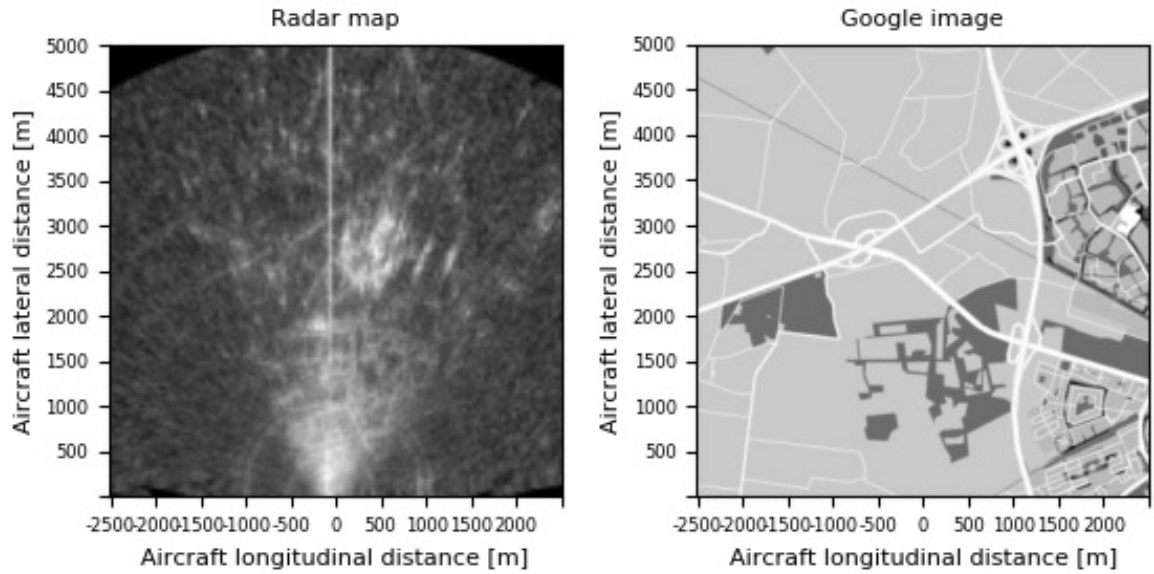
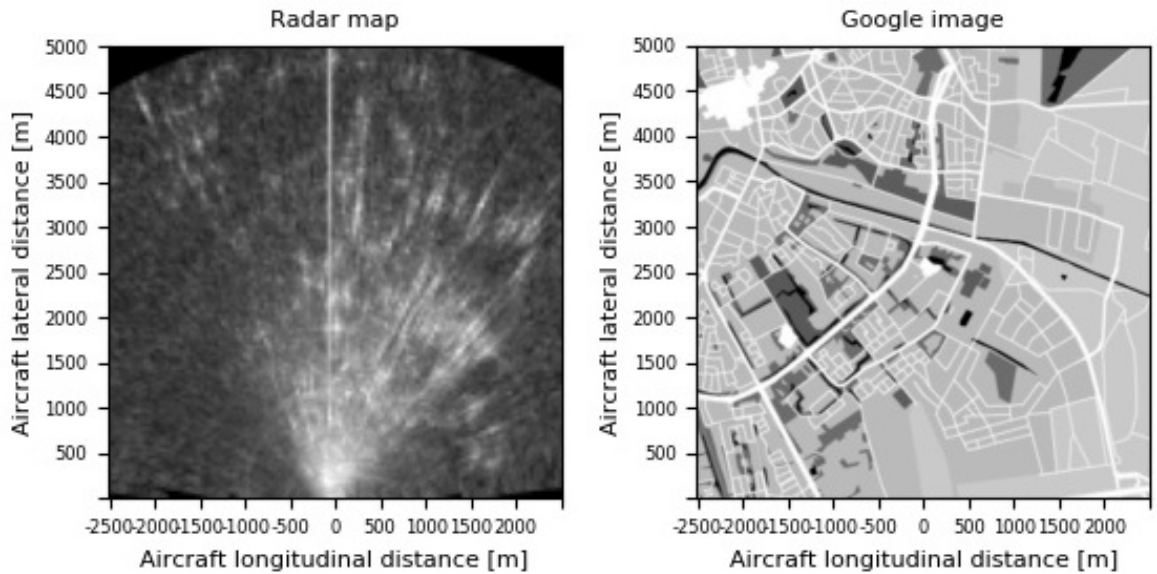Figure 4.18: Radar image and Google maps pair at second 1281 from GPS Start

Figure 4.19: Radar image and Google maps pair at second 1335 from GPS Start

Image 4.1 was taken during the third turn of the second take-off. A large street in the city of Appledorn can be observed, although surrounded by intensity features and noise.
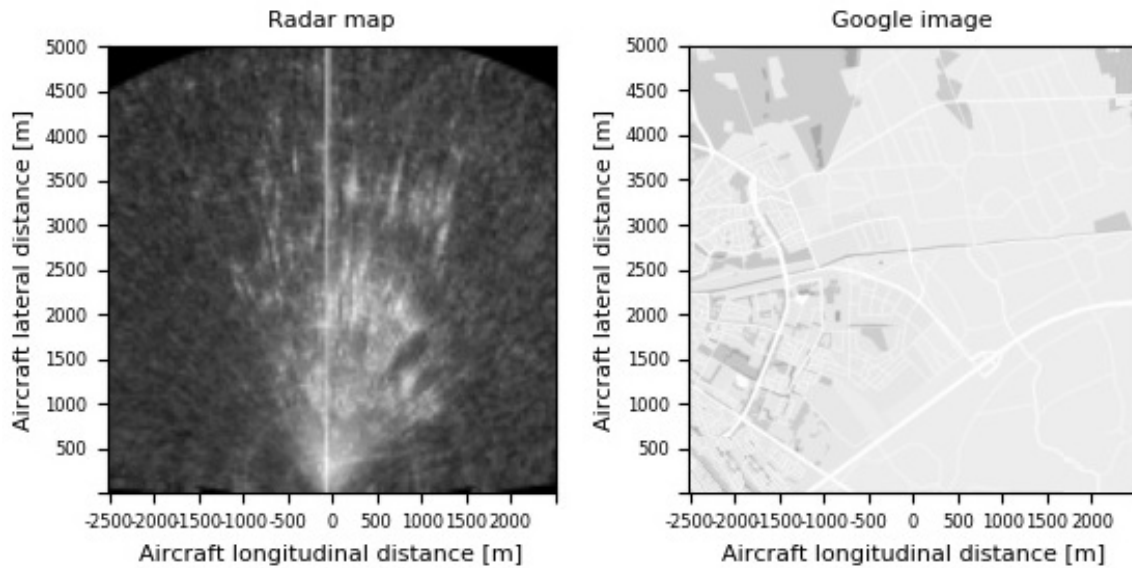
Figure 4.20: Radar image and Google maps pair at second 1347 from GPS Start

Finally, image 4.1 was taken during the end of the fourth turn of the second take-off. Again no features are observed. This is explained by the turning of the aircraft coupled with the highly reflective surfaces of the urban environment that does not allow for any structural features to be detected.

4.2. Results Experiment A

Within this section, results for experiment A for all images are presented. The section starts with the PDFs of the experiment. Overall the PDFs ??, 4.22 and 4.23 show consistency, with extra attention to Methods 3,5,8,9,10,11. As explained in the Results chapter, Methods 10 and 11 hide additional information, while Methods 3,5,8,9 provide a very low number of False Positives. This enforces the use of these Methods under higher image resolutions or lower noise through image denoising techniques as presented in the previous chapter.
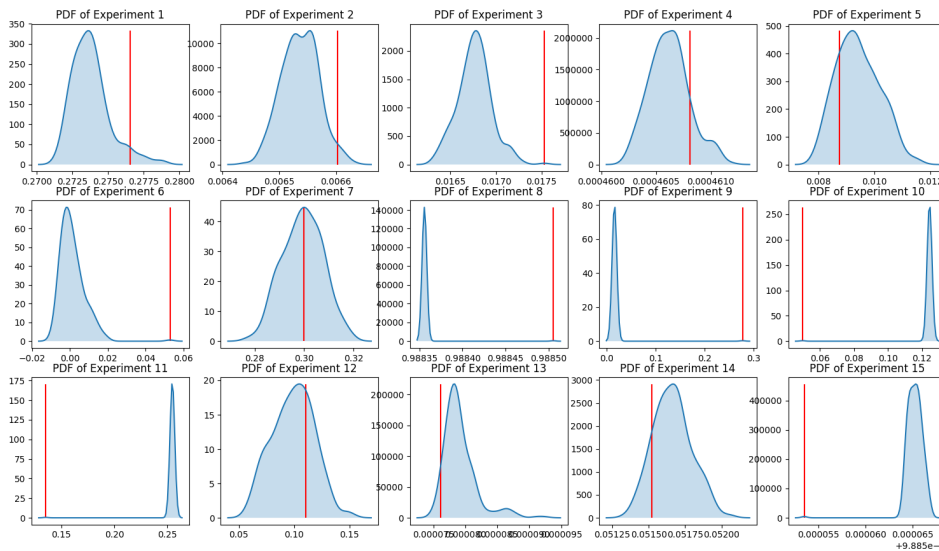

Figure 4.21: Probability distribution results for Experiment A, second image
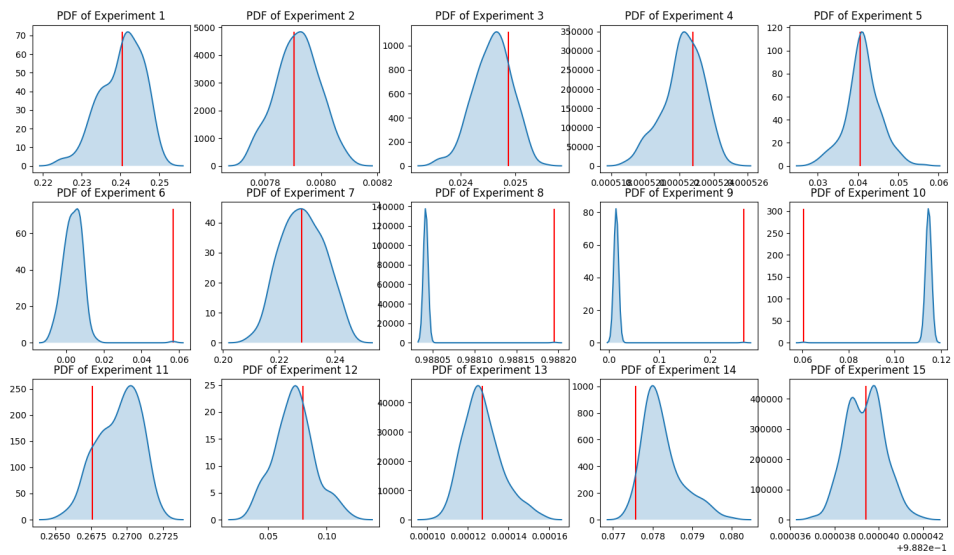
Figure 4.22: Probability distribution results for Experiment A, third image
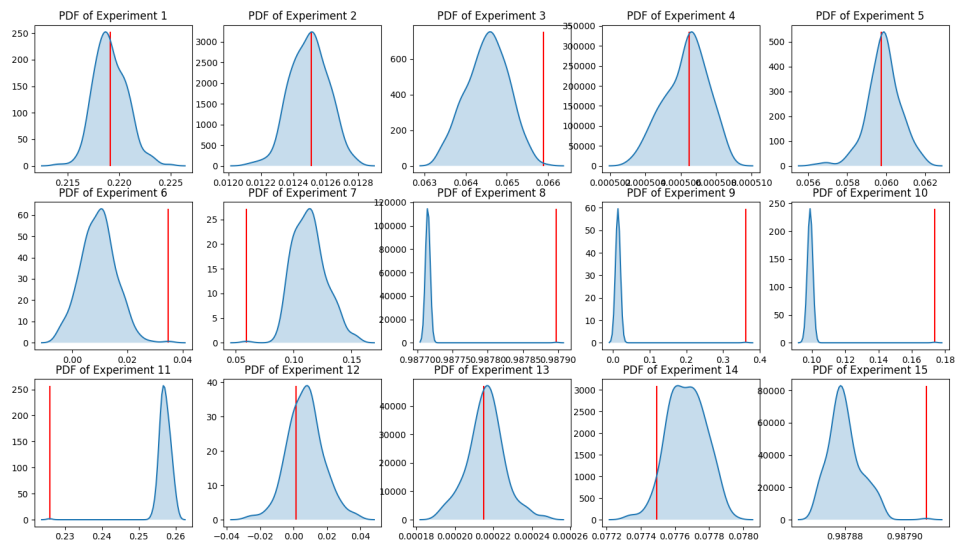
Figure 4.23: Probability distribution results for Experiment A, fourth image

Following are examples of Polar scattering for possible candidates, within figures 4.24, 4.25, 4.26. This is to check and show the randomness of the experiment overall. It should be noted that the polar configuration of the graph, makes all candidate points near the center to be greater than those towards the outer edges. This is not to be confused with the PDF. Furthermore, best candidates are presented in color within the image

All experiment points for Image B
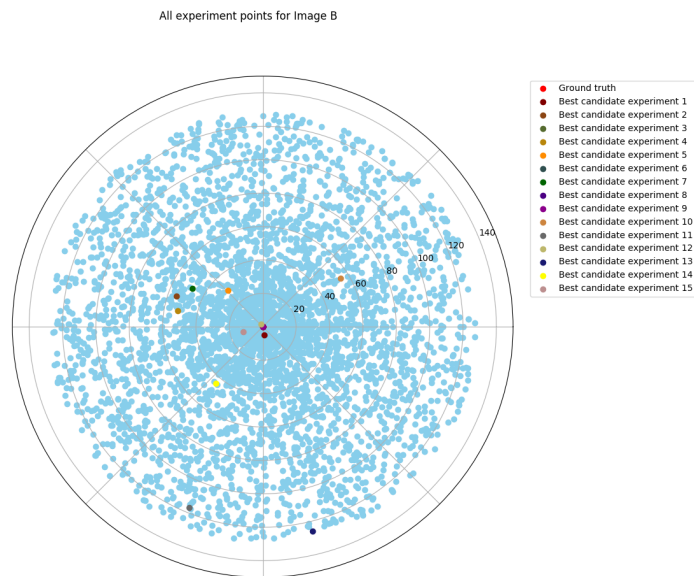
Figure 4.24: Polar scattering of best candidate per each experiment for Experiment A, second image

It can be seen within all figures that the distribution is equal indicating a successful implementation. Although there is no indication of the heading deviation, this can be found in Tables 4.1, 4.2, 4.3. It also becomes clear that most methods did not provide a consistent accuracy for all experiments, except 4.

All experiment points for Image C
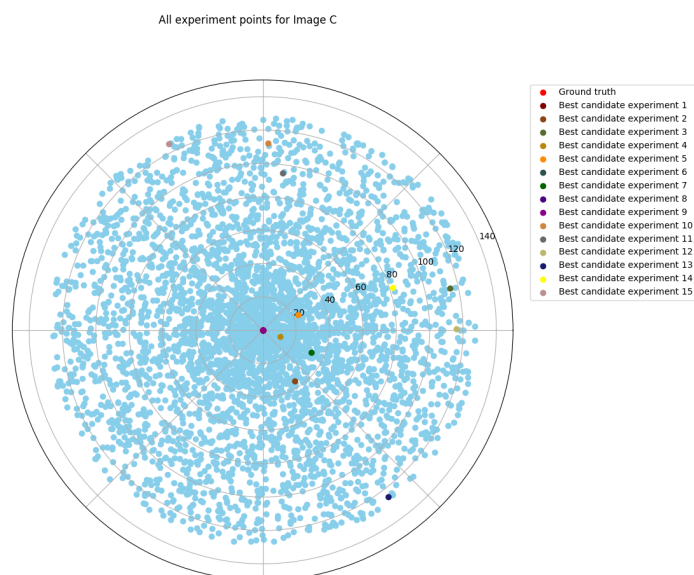
Figure 4.25: Polar scattering of best candidate per each experiment for Experiment A, third image

All experiment points for Image D
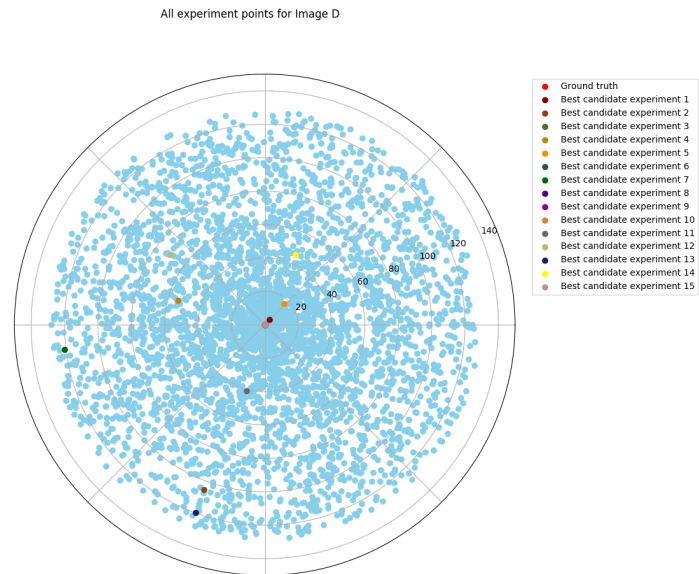
Figure 4.26: Polar scattering of best candidate per each experiment for Experiment A, fourth image
Finally, the results in tabular form show the results of each method in detail. Again Methods 5,8 and 9 had very good results.

Table 4.1: Average results for heading deviation, position error and SSIM values over all experiments, experiment A, second image

Method	Results Experiment A Image 2 - Average over 4 points		
	Absolute Heading Deviation	Position error	False Positive
1	8	7	41%
2	6	48	28%
3	5	52	8%
4	11	6	48%
5	4	0	4%
6	11	125	67%
7	8	45	52%
8	0	0	0%
9	0	0	0%
10	6	119	96%
11	9	37	98%
12	14	126	34%
13	12	124	86%
14	12	41	72%
15	6	117	99%

Table 4.2: Average results for heading deviation, position error and SSIM values over all experiments, experiment A, third image

	Results Experiment A Image 3- Average over 4 points		
Method	Absolute Heading Deviation	Position error	False Positive
1	7	108	50%
2	6	68	55%
3	5	117	37%
4	9	11	39%
5	3	22	4%
6	4	57	55%
7	8	35	52%
8	0	0	0%
9	0	0	0%
10	7	14	96%
11	11	114	80%
12	14	119	45%
13	12	124	48%
14	10	82	87%
15	6	112	51%

Table 4.3: Average results for heading deviation, position error and SSIM values over all experiments, experiment A, fourth image

	Results Experiment A Image 4 - Average over 4 points		
Method	Absolute Heading Deviation	Position error	False Positive
1	7	108	49%
2	6	68	51%
3	3	75	7%
4	11	46	55%
5	7	18	57%
6	4	53	3%
7	8	135	94%
8	0	0	0%
9	0	0	0%
10	6	119	1%
11	2	41	98%
12	14	126	65%
13	12	124	53%
14	12	52	82%
15	6	2	4%

4.3. Radar signal polarization

The following section presents how the radar signal is polarized and which of the Sentinel 1 databases were chosen to best fit the data that was provided by the FMCW radar. Polarization is a denomination of the wave orientation in an electromagnetic field. It is categorized in two basis types, vertical (V) and horizontal (H). It follows that a vertical receiver will only detect vertically polarized waves. Radar systems are usually created in such a way that they match the polarization of both the receiver (antenna) and the transmitter. However, it is also possible to use of different signals.

As the scatter can change the frequency of the emitted radar wave, the antenna is designed to receive

different components of the electromagnetic wave at the same time. However, for simplified systems, that is unnecessary. It is also possible for a radar system to have multiple level of polarization such as (HH) for the antenna and (VV) for the receiver.

The Sentinel 1 databases acquires radar data in multiple combinations of vertical (V) and horizontal (H). Additionally, the polarization is with regards to the wave intensity or amplitude. It should be noted that either intensity or amplitude is polarized in either (VH) or (VV) configuration and no other combinations with regards to wave properties. Image 4.27 depicts the results of each. Starting from the top left, Intensity (VH) polarization, top right, Amplitude (VH) polarization, bottom left, Intensity (VV) polarization, bottom right, Amplitude (VV) polarization. The top images are referred to as cross-polarized, while the bottom images are like-polarized.
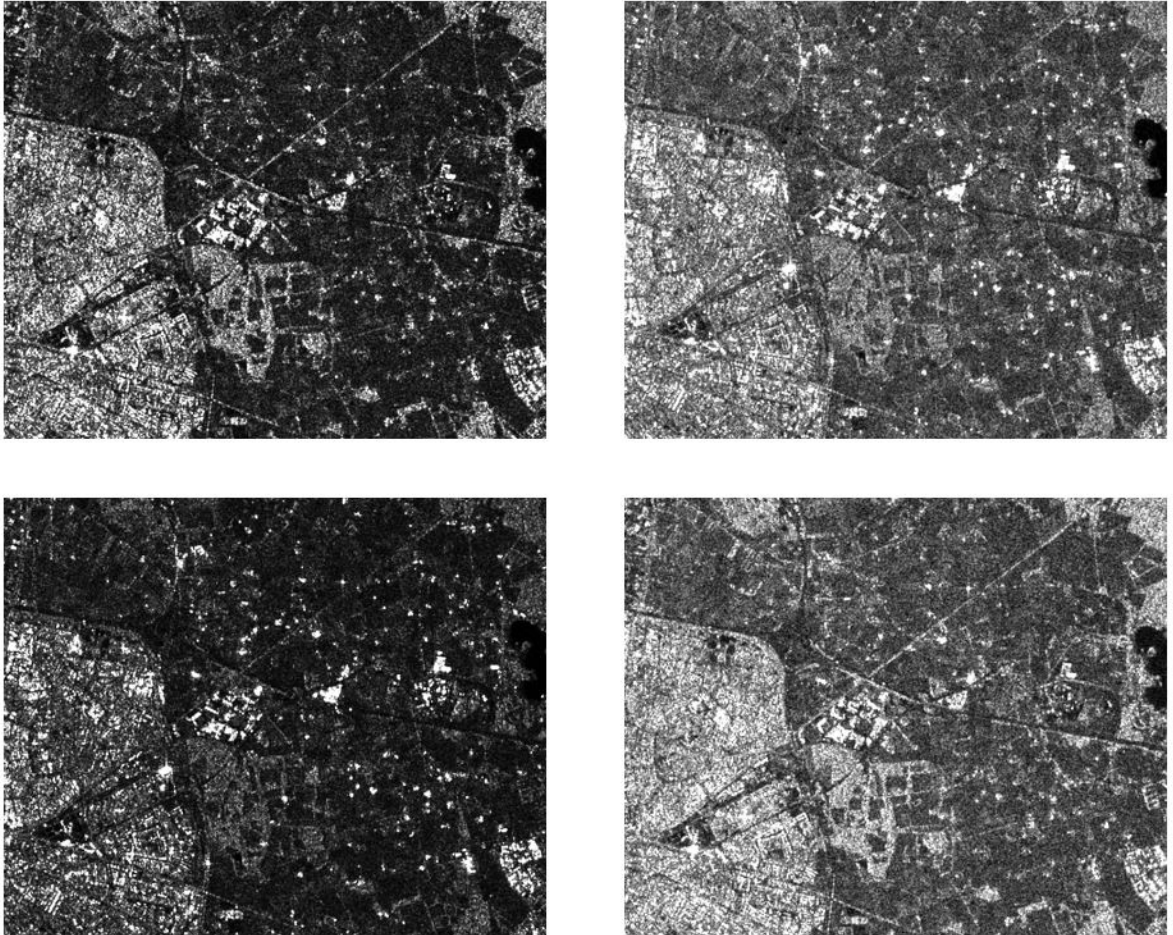

Figure 4.27: Polarization of Sentinel 1 database for the same region,
Intensity VV (bottom left), Intensity VH(top left), Amplitude VV(bottom-right), Amplitude VH(top-right)

It is observed that Amplitude polarisation offers behaves similarly to gamma correction, increasing the level of structural detail presented within the image, while intensity polarization emphasizes highly reflective objects. As vectored Google images are available of the same coordinate setting, the decision was made to use the Sentinel intensity (VV) polarized database as it is the same as the FMCW radar polarization and most usefull towards an analysis for methods that detect intensity-based features.

Bibliography

[1] Radar Principles. Wiley, first edition, 1998.

[2] Introduction to Modern EW Systems. Artech House Publishing, first edition, 2012.

[3] Pulse Doppler Radar. SciTech Publishing, second edition, 2012.

[4] Jetson tx2 website - sepcification sheets, 2018. URL `https://www.docdroid.net/yGXIxZu/data-sheet-nvidia-jetson-tx2-system-on-module.pdf`.

[5] Modern Radar Detection Theory. SciTech Publishing, sixth edition, April 2016.

[6] Global Positioning System,Inertial Navigation, and Integration. Wiley, John Sons, Incorporated, second edition, August 2001.

[7] Annex 2 to the Convention on International Civil Aviation, Aeronautical Information Service. ICAO, tenth edition, July 2005.

[8] Annex 10 to the Convention on International Civil Aviation, Aeronautical Information Service. ICAO, sixth edition, October 2001.

[9] H. R. Sheikh . Wang, A. C. Bovik and E. P. Simoncelli. Image quality assessment: From error visibility to structural similarity. IEEE Trans. Image Processing, vol. 13, no. 4, pp. 600–612, April, 2014.

[10] The Military Aviation Authority and British Airline Pilots' Association. Small remotely piloted aircraft systems (drones) mid-air collision study. The Department for Transport, 2016.

[11] L. Baardman. Radar-based landing system for uncontrolled flights. Available on Brightspace, 2016.

[12] Nikolai Smolyanskiy Alexey Kamenev Jeffrey Smith Stan Birchfield. Toward low-flying autonomous mav trail navigation using deep neural networks for environmental awareness. xArhiv, 2017.

[13] L. Bretzner and T. Lindeberg. Feature tracking with automatic selection of spatial scales. Computer Vision and Image Understanding,71(3):385–392, 1998.

[14] J. Matas C. Galamhos and J. Kittler. Progressive probabilistic hough transform for line detection. in IEEE Computer Society Conference on Computer Vision and Pattern Recognition, 1999.

[15] B. Yang C. Wang and Y. Liao. "unsupervised image segmentation using convolutional autoencoder with total variation regularization as preprocessing,". 2017 IEEE International Conference on Acoustics, Speech and Signal Processing (ICASSP), pp. 1877-1881, New Orleans, LA,, 2017.

[16] Kushwaha N. Samal A. Chaudhuri, D. Semi-automated road detection from high resolution satellite images by directional morphological enhancement and segmentation techniques. IEEE J. Sel. Topics Appl. Earth Observ. Remote Sens. 5, 1538–1544., 2012.

[17] Holt A. Scarborough J. Yan L. Gong P. Clinton, N. Accuracy assessment measures for object-based image segmentation goodness. Photogramm. Eng. Remote Sens. 76, 289–299., 2010.

[18] R. W. Lowe J. W. Weber: D. J. Ketcham. Image enhancement techniques for cockpit displays. Tech. rep., Hughes Aircraft., 1974.

[19] J. D. Wegnera S. Gallianib K. Schindlerb M. Datcuc U. Stillad D. Marmanisa, d. Semantic segmentation of aerial images with an ensemble of cnns. IEEE Geoscience and Remote Sensing Letters, 2018.

[20] Selfly EDA. Selfly - electronic detect and avoid, 2019. URL `http://selfly.nl/`.

[21] Hidetoshi Furukawa. Deep learning for end-to-end automatic target recognition from synthetic aperture radar imagery. IEICE Technical Report, 2018.

[22] Juliana Goh and Dr. Douglas Wiegmann. Visual flight rules (vfr) flight into instrument meteorological conditions (imc): A review of the accident data. https://www.researchgate.net/publication/252217964, 2014.

[23] Ian Goodfellow, Yoshua Bengio, and Aaron Courville. Deep Learning. MIT Press, 2016. `http://www.deeplearningbook.org`.

[24] Zhang L. Huang, X. Road centreline extraction from high-resolution imagery based on multiscale structural features. IEEE J. Sel. Top. Appl. Earth Observ. Remote Sens. 8, 1830–1838, 2009.

[25] Jyoti Jaybhay and Rajveer Shastri. A study of speckle noise reduction filters. Signal Image Processing : An International Journal (SIPIJ) Vol.6, No.3, , June 2015.

[26] Niklas Peinecke ; Patrizia Knabl ; René Küppers. Onboard radar display for vfr collision avoidance. 2015 IEEE/AIAA 34th Digital Avionics Systems Conference (DASC), 2015.

[27] Juha Hyyppä Paula Litkey Eetu Puttonen Eero Ahokas Leena Matikainen, Kirsi Karila. Object-based analysis of multispectral airborne laser scanner data for land cover classification and map updating. ISPRS Journal of Photogrammetry and Remote Sensing, Volume 128, 2017, Pages 298-313, ISSN 0924-2716, 2017.

[28] Adriano Meta ; Peter Hoogeboom ; Leo P. Ligthart. Navigation and sar focusing with map aiding. IEEE Transactions on Geoscience and Remote Sensing (Volume: 45 , Issue: 11 , Nov.), 2007.

[29] P.J. van der Geest L.J.P. Speijker, J.G. Verstraeten C.G. Kranenburg. Scoping improvements to 'see and avoid' for general aviation (sisa). EASA, 2012.

[30] William Lorensen and Harvey E. Cline. Marching cubes: A high resolution 3d surface construction algorithm. Computer Graphics (SIGGRAPH 87 Proceedings) 21(4) p. 163-170, July 1987.

[31] X. X. Zhu M. Schmitt, L. H. Hughes. The sen1-2 dataset for deep learning in sar-optical data fusion. Commission I, WG I/3, 2018.

[32] Corentin Henry Seyedmajid Azimi Nina Merkle. Road segmentation in sar satellite images with deep fully convolutional neural networks. IEEE Geoscience and Remote Sensing Letters, 2018.

[33] A. Meta. Signal processing of fmcw synthetic aperture radar data. Available on Brightspace, 2006.

[34] Erik Reinhard; Wolfgang Heidrich; Paul Debevec; Sumanta Pattanaik; Greg Ward; Karol Myszkowski. High dynamic range imaging: Acquisition, display, and image-based lighting. Morgan Kaufmann. p. 82. ISBN 9780080957111, 2010.

[35] C. Naulais. General aviation radar system for navigation and attitude determination. Available on Brightspace, 2015.

[36] Yap M. H. Costen N. Li B. Ng, C. C. Automatic wrinkle detection using hybrid hessian filter. n Asian Conference on Computer Vision (pp. 609-622). Springer International Publishing., 2014, November.

[37] David W. Scott. Averaged shifted histogram. Wiley Interdisciplinary Reviews: Computational Statistics. 2:2 (2): 160–164. doi:10.1002/wics.54., December 2009.

[38] Xueyuan Zhang Bijan Shirinzadeh Shesheng Gao, Yongmin Zhong. Multi-sensor optimal data fusion for ins/gps/sar integrated navigation system. Aerospace Science and Technology, 13 May 2009.

[39] G.W. Stimson. Introduction to airborne radar. The Institution of Engineering and Technology,IE3E Radar Series, 1998.

[40] Patrik Dammert Tomas Toss and Zoran Sjanic. Navigation with sar and 3d-map aiding. Saab AB, 2012.

[41] Amrutha Michahial Stafford M Dr. TY K V, Lalitha .R. Implementation of watershed segmentation. IJARCCE. 5. 196-199. 10.17148/IJARCCE.2016.51243, 2016.

[42] Johannes Nunez-Iglesias Juan Boulogne François Warner Joshua Yager Neil Gouillart Emmanuelle Yu Tony contributors van der Walt, Stéfan Schönberger. Image processing in python:scikit-image. PeerJ. 2. 10.7717/peerj.453, 2014.

[43] H. R. Sheikh Z. Wang, A. C. Bovik and E. P. Simoncelli. General aviation radar system for navigation and attitude determination. IEEE Trans. Image Processing, vol. 13, no. 4, pp. 600–612,, pril 2004.

[44] Matthew D. Zeiler and Rob Fergus. Visualizing and understanding convolutional networks. Dept. of Computer Science, New York University, USA, 2014.